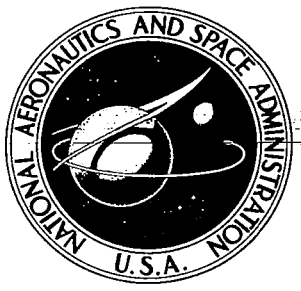

NASA CONTRACTOR REPORT

NASA CR-1369

ANALYSIS OF OSCILLATIONS IN PULSE-MODULATED SATELLITE ATTITUDE CONTROL SYSTEMS

by Robert Newhall Clark

Prepared by
STANFORD UNIVERSITY
Stanford, Calif.
for

NATIONAL AERONAUTICS AND SPACE ADMINISTRATION • WASHINGTON, D. C. • JUNE 1969

NASA CR-1369

ANALYSIS OF OSCILLATIONS IN PULSE-MODULATED SATELLITE ATTITUDE CONTROL SYSTEMS

By Robert Newhall Clark

Issued by Originator as SUDAAR No. 361

Prepared under Grant No. NGR-05-020-007 by
STANFORD UNIVERSITY
Stanford, Calif.

for

NATIONAL AERONAUTICS AND SPACE ADMINISTRATION

For sale by the Clearinghouse for Federal Scientific and Technical Information
Springfield, Virginia 22151 – CFSTI price $3.00

ABSTRACT

This study reveals the relationship between the physical parameters and the principal limit cycle oscillation of a pulse-modulated feedback system of the type used for attitude control in satellites. Explicit relationships, derived analytically as they are here, have previously been known only for a simpler class of system, and those relationships were derived by analytical methods other than the one developed here.

The pulse actuation used in this system implies there will be a limit cycle oscillation about the equilibrium point. A two-pulse limit cycle is the most efficient and most accurate one possible. Therefore, the principal goal of this work is to establish the necessary and sufficient conditions on the various physical parameters in the system to insure the existence and stability of the two-pulse limit cycle oscillation.

An integral-pulse-frequency modulator is established as having the requisite steady-state dynamic characteristics for the existence of the two-pulse limit cycle. The stability of the limit cycle is then determined from a transient analysis of the system, using a method based on the geometrical properties of the state transition equations. Previously, stability analysis of this nature has been approached using Lyapunov-like methods or conventional frequency domain techniques.

The conditions under which four-pulse, six-pulse, and higher order limit cycle oscillations can occur are also determined, and their existence is verified experimentally, using digital simulation.

CONTENTS

CONTENTS (cont)

TABLES

ILLUSTRATIONS

SYMBOLS

a	rate circuit lead ratio, seconds
A	nominal threshold of integrator output, $K_I K\mu a^2/4J$ volts
$(1+\gamma)A$	actual threshold of integrator output, volts
B_j	curves separating the R_i, j=1,2,3,4 and 5
e	input voltage of integrator, volts
e_N	input voltage to dead zone element, volts
e_o	output voltage of integrator, a state variable, volts
e_s	input voltage to rate circuit
F	state transition function, $z_{k+1} = F(z_k, \delta_k)$
F_i	state transition function for $z_k \in R_i$, i = 1,2,3,4,5, and 6
h	duration of thruster pulse, seconds
J	moment of inertia of vehicle about the controlled axis, kilogram $(\text{meter})^2$
K	attitude sensor gain, volts/radian
K_I	integrator gain, $(\text{seconds})^{-1}$, $K_I = 1$
ℓ	normalized lead ratio, $a\mu/J\theta_d$, dimensionless
m	torque on controlled body about the controlled axis, newton-meters
M	torque level of thruster, newton-meters
R_i	regions in the state plane, i = 1,2,3,4,5, and 6
R_5^+	a subset of region R_5
t	time, seconds
t_k	instant of torque pulse emission, k = 0,1,2,...
T	period of symmetrical two-pulse limit cycle, seconds
$u(t-t_j)$	unit impulse occuring at $t = t_j$

x	normalized state variable θ/θ_d, dimensionless
x_k	$x(t)$ for $t = t_k^+$
y	normalized state variable $\frac{\dot{\theta}}{\mu/J}$, dimensionless
y_k	$y(t)$ for $t = t_k^+$
y_k^-	$y(t)$ for $t = t_k^-$
z	state vector (x,y)
z_k	state vector for $t = t_k^+$, (x_k, y_k)
z_k^-	state vector for $t = t_k^-$, (x_k, y_k^-)

γ	fractional error in integrator threshold setting, dimensionless
δ_k	$-\text{sgn}[e_o(t)]$ for $t = t_{k+1}^-$
Δ_k	time interval between pulse emissions, $(t_{k+1}-t_k)$, seconds
θ	attitude displacement of controlled body from desired null position, a state variable, radians
$\dot{\theta}$	angular velocity of controlled body, a state variable, radians/second
θ_d	permissible attitude error attributable to dead zone
$\theta(t_k)$	θ for $t = t_k^+$
$\dot{\theta}(t_k)$	$\dot{\theta}$ for $t = t_k^+$
μ	strength of thruster pulse, Mh, newton-meter-seconds

I	the region in the state plane for which $e > 0$
II	the region in the state plane for which $e < 0$
III	the region in the state plane for which $e = 0$

ACKNOWLEDGMENTS

The author wishes to thank his many Stanford associates for their efforts in behalf of the completion of this work. In particular, he expresses his deepest appreciation to

Professor Gene F. Franklin, in general for the pleasant and effective manner in which he supervised the author's entire program during the 1966-68 period, and in particular for suggesting the approach to the modulator design.

Professor John V. Breakwell, for suggesting the approach to the convergence proof and for several other suggestions he made for improving the dissertation.

Professor Hugh H. Skilling, for his many enlightening discussions and for finding several ways to make this dissertation more nearly correct.

Dr. Daniel B. DeBra, for suggesting that the investigation of the existence and stability of two-pulse limit cycles might prove to be interesting, and for many helpful discussions during the course of this work, including the idea that a non-zero γ should be considered.

Dr. Rodney W. Edwards, for his interest in this problem and for the numerous informal talks which gave the author both information and inspiration that proved to be essential for the completion of this work.

Mr. Anthony J. Maran and Mr. Robert H. Whiting, for their help in computer programming which proved to be as timely as it was expert.

In addition, several institutions have provided the author with support. He is especially grateful to

The National Science Foundation, for its support under the Science Faculty Fellowship program.

The University of Washington, for its support while the author was on sabbatical leave, for an extended period.

Stanford University, for several forms of support, including that given to the author under NASA Grant NGR-05-020-007

Chapter I

INTRODUCTION

A. Attitude Control of Rigid Body Satellites

It has been shown that the angular position, or attitude, of an orbiting satellite is controlled efficiently and reliably by torquing devices which operate in an on-off fashion [1,2,3,4,5]. An important class of on-off torquing devices is the pulsed type. In a control system using a pulsed torquer, the controller (or pulse modulator) emits signals to the torquing device, which is commonly a cold gas expulsion valve, at discrete instants of time. In response to the controller signal, the valve opens rapidly, remains open for a short time, and then closes rapidly. As a result of the expulsion of this small amount of gas, the controlled body acquires a small change in its angular momentum. In a rigid body that is not spinning, this is manifested in a small change in angular velocity about the controlled axis. A block diagram for a typical attitude control system is shown in Fig. 1.

The controlled body is taken here to be rigid and to spin at a low enough rate that the torque applied about the controlled axis can produce motion essentially about that axis only [2]. The change in mass, due to the loss of gas, is neglected. Thus the dynamic behavior of the body about the controlled axis is described by Eq. (1.1) where J is the moment of inertia

$$J\ddot{\theta}(t) = m(t) \tag{1.1}$$

of the body and $m(t)$ is the torque on the body. $m(t)$ includes both the torque produced by the expelled gas and any external torques such as those due to the gradient of the gravitational field, unbalanced solar radiation pressure, unbalanced aerodynamic drag, and micrometeorite impact. All of these external torques are neglected here.

The angular position sensor, which is typically a gyroscope, a star tracker, or a horizon sensor, produces a signal proportional to θ, the angular displacement of the body from its equilibrium position. The sensor signal $e_s(t)$ is contaminated with noise, the influence of which is diminished by the use of a "dead-zone element" as shown in Fig. 1.

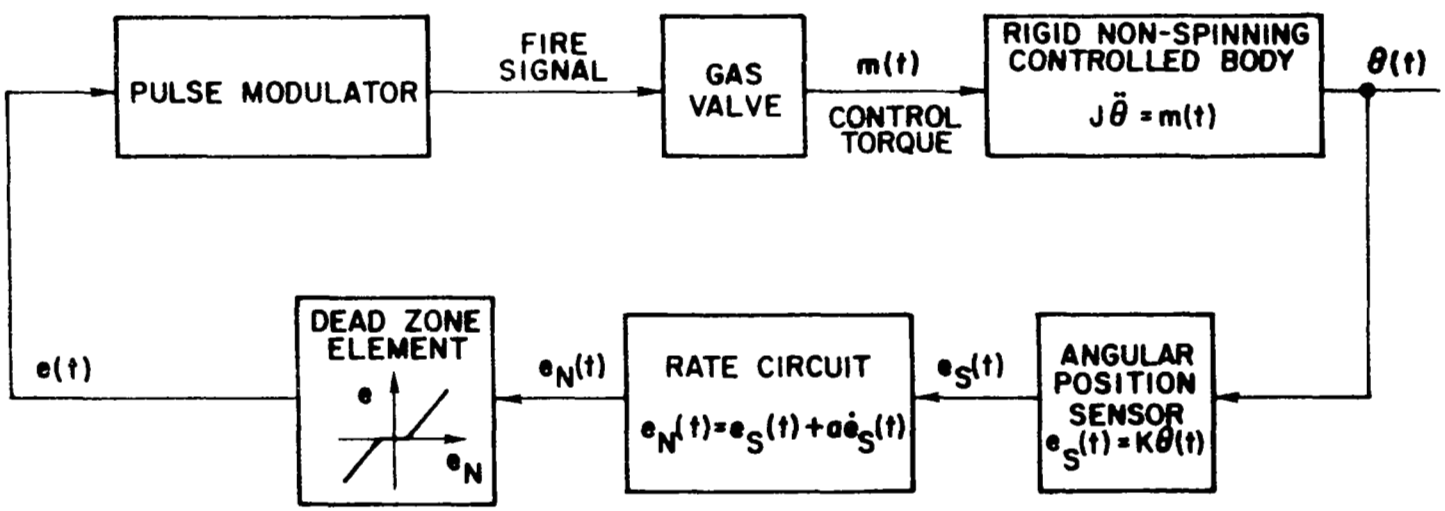

Fig. 1. PULSE-MODULATED ATTITUDE CONTROL SYSTEM.

Although the noise content of $e_s(t)$ is neglected here, the dead-zone element is included.

No external torque dependent on the angular velocity $\dot{\theta}$ is available, so it is necessary to provide a "damping" torque through the control valve. This is accomplished in much the same way as it is in a servomechanism, i.e., by a rate circuit installed in the feedback path, having the dynamic properties described by Eq. (1.2). a is called the

$$e_N(t) = K[\theta(t) + a\dot{\theta}(t)] \tag{1.2}$$

lead ratio of the rate circuit, and K is the sensitivity of the position sensor.

Pulse modulators which operate solely upon the input signal e(t), in accordance with a preset logic carried inside the modulator, are in common use in modern satellites and in many other control systems. Some of these modulate the pulse strength (or pulse duration), some the interval between successive "firing signals," and some modulate both of these quantities together. Common names for these modulation schemes are pulsewidth (PW), pulse frequency (PF), and pulsewidth-pulse frequency (PWPF). Substantial literature on various aspects of the dynamic behavior of control systems employing such devices exists [6,7,8,9,10].

In satellite attitude control systems, reliable modulation of the pulse duration is not possible for durations less than a given amount, which is typically 10 to 50 ms for gas valves. Because of this minimum pulse duration, the angular velocity of the controlled body cannot be changed by an amount less than μ/J, where μ is the strength of the minimum pulse. Therefore, when the controlled body is near its equilibrium position, it will oscillate in a limit cycle, except, of course, in the unlikely situation where $e = 0$, $\dot{\theta} = 0$ and no disturbing torques are present. These limit cycle oscillations are the subject of the studies described in this dissertation.

It is well-known from previous work [2,7] that attitude control systems similar to that described in Fig. 1 can exhibit limit cycle oscillations about the equilibrium point having two pulses of torque per cycle, four pulses per cycle, six pulses, and so forth, depending upon the initial

values of θ and $\dot{\theta}$. It is ordinarily assumed that the two-pulse limit cycle is the most desirable because for a given maximum excursion of θ the period of the limit cycle is maximized and therefore the fuel expended for control in a lengthy mission is minimized.

It has not been precisely known how the physical parameters of the system, J, μ, a, K, θ_d, and the modulator scheme are related to the limit cycle behavior of the system. In particular, it has not been known how these system characteristics can be combined to guarantee that no limit cycle except the two-pulse limit cycle will exist. Farrenkopf, Sabroff, and Wheeler, in 1963 [2] made essentially this determination for a system similar to that in Fig. 1 but without the nonlinear dead-zone element. They used a modified Lyapunov theorem [11] to establish the existence of limit cycles in a given region near the equilibrium position and investigated the stability of the limit cycles by point transformation techniques [12].

In engineering practice, the determination of the limit cycle behavior of attitude control systems is ordinarily done empirically, using simulators. This approach results in practical solutions to specific design problems but does not contribute very much to an understanding of the general nature of the dynamic behavior of such systems. An analytical study, such as that presented here, even though it is done on a simple, idealized system which is devoid of many of the features found in practical systems, provides a foundation for understanding experimental results and, further, for making design modifications to improve the performance of the system.

B. Statement of Research Problem

Figure 1 describes the system studied here. Several significant practical features of attitude control systems have been suppressed in this work to make analysis possible. Noise in the sensor signal $e_s(t)$ is not considered. External disturbance torques are not considered. It is assumed that the feedback channel transmission characteristics are symmetrical although nonlinear. The valve is also assumed to produce pulses in the positive sense which are equal in strength to those in the negative sense. It is further assumed that the pulses are of uniform

strength (corresponding to the minimum possible pulse duration) and that their duration is short enough compared to the interval between pulses that the pulse can be represented mathematically as an impulse. Thus, $m(t)$ is a sequence of impulses of uniform strength occurring at instants of time t_k, and with algebraic signs which are determined by the logical scheme in the pulse modulator. Pulsewidth-pulse-frequency modulators approximate this behavior near the equilibrium point. Because the torque pulses are approximated by impulses, the angular velocity $\dot{\theta}(t)$ is discontinuous at each firing instant.

The specific research tasks which were accomplished and which are described in this dissertation are defined as:

(1) Modulator. It is necessary to find a modulation scheme that will produce a sequence of produce a sequence of pulses in response to $e(t)$ which will move the body in a two-pulse limit cycle mode of oscillation, having an acceptable amplitude. A modulation scheme, determined on the basis of the steady-state limit cycle behavior of the system, guarantees the existence of the two-pulse limit cycle, but it does not determine the transient properties of the system. The transient behavior could exhibit higher order limit cycle oscillations, depending upon the initial conditions, or it could show the two-pulse limit cycle to be unstable.

(2) Stability of Two-Pulse Limit Cycles. The primary goal of this work is to establish the precise relationship between the system parameters and the stability of the two-pulse limit cycle. This problem is approached in such a way that the existence and stability of the two-pulse limit cycle are established for initial conditions of the state vector in a region containing the equilibrium point.

(3) Convergence of the State Trajectory. It is essential to determine the conditions under which the state trajectory, which describes the motion of the controlled body, will converge with time to the stable two-pulse limit cycle. Initial conditions for the state vector must be arbitrary.

(4) Existence of Higher Order Limit Cycles. If the conditions for the existence and stability of two-pulse limit cycles are not met, then perhaps stable higher order limit cycles exist. The existence of such limit cycles and the conditions under which they occur are established experimentally as a natural extension of the work on the two-pulse limit cycle.

The resolultion of these questions is described in Chapters II, III, IV, and V, and a summary of the significant features of the work is in

Chapter VI. Chapter VII outlines several research problems for future work which might extend the usefulness of the stability analysis technique developed here.

Chapter II

THE MODULATOR

A. Necessary Input-Output Characteristic

The terminal characteristics of the modulator necessary for the existence of a two-pulse limit cycle are determined here, using a scheme somewhat like the describing function method in elementary control theory [13,14]. The method employed is an exact one, however, whereas the describing function method is an approximate one.

It is assumed that the system is in a steady-state limit cycle oscillation of the desired amplitude, so that $m(t)$ consists of a sequence of pulses of alternating sign occurring at the required instants. The resultant feedback signal $e(t)$ is calculated, and this is the input of the modulator.

Figure 2 shows the approximate torque pulse applied to the controlled body by the gas jets in response to a firing signal occurring at time t_k. A "dead-time" occurs right after t_k because some time is required for the valve to open and for gas flow to be established in the conduit leading from the valve to the exhaust orifice. For the study of limit cycle behavior, this dead-time can usually be neglected and the actual pulse approximated by a rectangular pulse M newton-meters in amplitude and h seconds in duration, as shown in Fig. 3. The strength of the pulse Mh is taken to be the area under the $m(t)$ curve in Fig. 2. It is further assumed that h is very small compared to the interval between pulses,

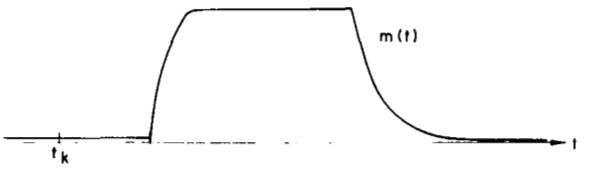

Fig. 2. TORQUE PULSE OCCURRING AT $t = t_k$.

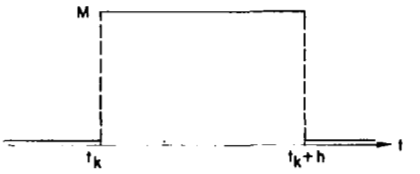

Fig. 3. FIRST APPROXIMATION TO TORQUE PULSE.

so that $m(t)$ may be represented by a series of impulses having strength $\mu = Mh$, as shown in Fig. 4. Here, it is assumed that the interval between pulses is uniform, so the limit cycle is symmetrical about the equilibrium position with a period $T = (t_{k+2} - t_k)$.

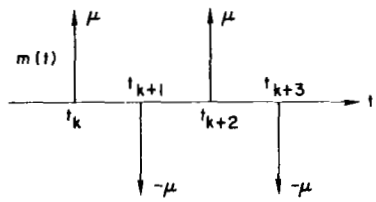

Fig. 4. SECOND APPROXIMATION TO PULSE TRAIN $m(t)$.

With $m(t)$ as shown in Fig. 4, the angular velocity of the controlled body will be discontinuous at the firing instants and constant between them, as shown in Fig. 5. The corresponding $\theta(t)$ has the triangular waveform shown in Fig. 6. At this point, it is possible to choose the amplitude of $\theta(t)$ to satisfy the performance requirements of the attitude control system. This is an arbitrary choice, but it would likely be made on the basis of the dead-zone width. For this study, the amplitude is taken to be equal to the allowable static position error θ_d. Thus we have

$$\frac{\mu T}{8J} = \theta_d \qquad (2.1)$$

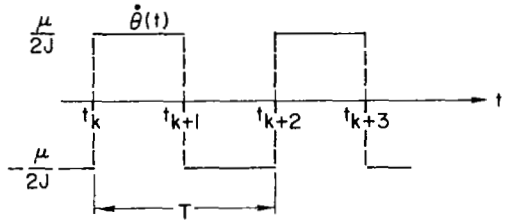

Fig. 5. $\dot{\theta}(t)$ FOR SYMMETRICAL LIMIT CYCLE OSCILLATION.

In what follows, it turns out that this is not a crucial assumption, but it is a convenient one to make at this point because it defines the period T in terms of the parameters μ, J, and θ_d.

$e_N(t)$ is just a linear combination of $\theta(t)$ and $\dot{\theta}(t)$. Its waveform is shown in Fig. 7. $e_N(t)$ is the input to the dead-zone element, so $e(t)$ may be determined from $e_N(t)$ if the characteristics of the dead-zone element are known. The width of the dead zone is chosen to correspond to the allowable static error, so it is $2K\theta_d$, the half-width

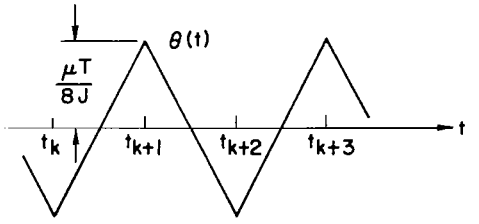

Fig. 6. $\theta(t)$ FOR SYMMETRICAL LIMIT CYCLE OSCILLATION.

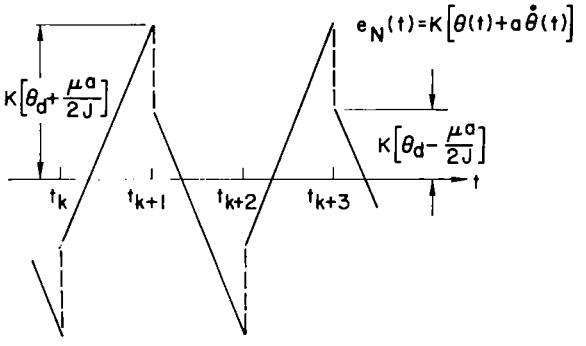

Fig. 7. $e_N(t)$ FOR SYMMETRICAL LIMIT CYCLE OSCILLATION.

being $K\theta_d$. The slope of the straight portions of the e, e_N characteristic curve is taken to be 1. The mathematical description of the dead-zone element is

$$\begin{aligned} e(t) &= e_N(t) - K\theta_d \qquad \text{for} \quad e_N > K\theta_d \\ e(t) &= 0 \qquad\qquad\quad \text{for} \quad -K\theta_d \leq e_N \leq K\theta_d \\ e(t) &= e_N(t) + K\theta_d \qquad \text{for} \quad e_N < -K\theta_d \end{aligned} \tag{2.2}$$

If the waveform of $e_N(t)$ is used in (2.2), the resultant waveform for e(t) is that shown in Fig. 8. The input-output behavior of the modulator for steady-state, symmetrical, two-pulse limit cycle oscillations is thus defined by Figs. 8 [the input e(t)] and 4 [the output m(t)]. The internal mechanism of the modulator must be such that it will produce

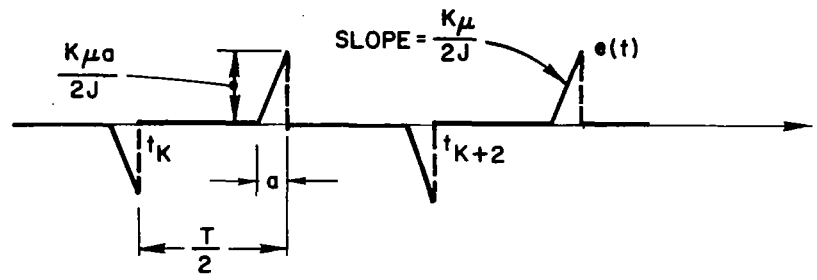

Fig. 8. e(t) FOR SYMMETRICAL LIMIT CYCLE OSCILLATION.

this specific input-output behavior, whatever its behavior might be for different input signals. The selection of a specific modulation scheme is described in the following section.

B. The Integral Pulse Frequency Modulator

There is no unique modulation scheme that will satisfy the required input-output characteristic described in Section II.A. A simple timing device, emitting pulses of alternating signs at uniform intervals of $4J\theta_d/\mu$ sec would have the required behavior even if e(t) were in no way connected to the timing device. A threshold detector that would emit a pulse whenever e(t) reached a level of $K\mu a/2J$ V would also exhibit the same behavior. In choosing a modulation scheme, the behavior of the modulator under operating conditions other than limit cycle oscillation must also be considered. The timing device suggested above would clearly be unsuitable if the controlled body should be displaced from its equilibrium position, because that device would be insensitive to the actual motion of the controlled body. The threshold detector would emit pulses if a short but large amplitude pulse of noise should appear on e(t). For these reasons those two modulation schemes are unsatisfactory.

A modulation scheme, known to have some desirable attributes in practical systems, is the integral pulse frequency (IPF) modulator--so named, apparently, because a constant voltage applied to its input will produce a sequence of pulses at uniform intervals, the frequency of the sequence being proportional to the constant applied voltage [2,6,7]. Of course, if e(t) is <u>not</u> held constant, then m(t) may <u>not</u> be periodic.

The diagram in Fig. 9 illustrates the operation of the IPF modulator. In between firing instants, $e_o(t)$ is proportional to the integral of $e(t)$

$$e_o(t) = K_I \int e(t)\, dt \tag{2.3}$$

Here K_I is the integrator gain having the dimension $(sec)^{-1}$. K_I may be set equal to unity with the loss of no essential feature of the subsequent analysis. When the magnitude of $e_o(t)$ reaches the threshold value A, a fire signal is sent to the gas valve, and the integrator output voltage e_o is reset to zero. The instant the valve fires is $t = t_k$, and here it is assumed to coincide with the instant e_o reaches A. Thus, $|e_o(t_k^-)| = A$ and $e_o(t_k^+) = 0$.

The IPF modulator is selected for study here because it is simple, because it is a device used in many existing control systems, and because it is representative of a larger class of modulators, at least in its limit cycle behavior. For example, a PWPF modulator will behave approximately the same as the IPF modulator when $e(t)$ is small, as is the case when the system is in a limit cycle oscillation.

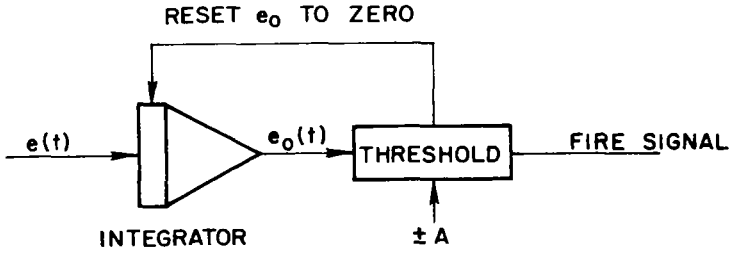

Fig. 9. SCHEMATIC DIAGRAM OF IPF MODULATOR.

C. Integrator Threshold Setting

It is apparent from Fig. 8 that the threshold value A must be

$$A = \frac{K_I K \mu a^2}{4J} = \frac{K \mu a^2}{4J} \qquad \text{for} \quad K_I = 1 \tag{2.4}$$

since this is the integral of $e(t)$ over the time interval between pulses. The modulator must also provide the algebraic sign of the required pulse of torque. It is apparent from a comparison of Figs. 4 and 8 that the sign of the impulse must be opposite to that of $e_o(t_k^-)$. δ_k denotes the sign of the pulse which occurs at $t = t_{k+1}$; therefore

$$\delta_k = -\text{sgn}\left[\int_{t_k}^{t_{k+1}} e(t)\, dt\right] \tag{2.5}$$

and $m(t)$ has the form

$$m(t) = \mu\left[\delta_k u(t - t_{k+1}) + \delta_{k+1}\, u(t - t_{k+2}) + \ldots\right] \tag{2.6}$$

where μ is the strength of each pulse and $u(t-t_j)$ is the unit impulse occurring at $t = t_j$.

A is a combination of the four parameters K, μ, a, and J. If it were to be assumed that the integrator threshold is exactly A, then there could be no allowance in the analysis for a threshold setting which is variable independently from the other system parameters. Because it is important to know what the effect of the threshold setting is on the limit cycle behavior of the system, the threshold setting will be taken to be $(1 + \gamma)A$, where γ may be considered to be the fractional error in the threshold setting. For $\gamma = 0$, the threshold value will be that determined here to be necessary for the existence of a two-pulse limit cycle.

The analysis in this chapter has established that the IPF modulator with threshold setting A and with the appropriate logic elements for determining δ_k will sustain the system in a steady-state two-pulse limit cycle oscillation having an amplitude θ_d, provided that the system is started with appropriate initial conditions. One set of these conditions is $e_o(0) = 0$, $\theta(0) = 0$, $\dot{\theta}(0) = \mu/2J$. However, up to this point the analysis is valid only for this steady-state oscillating condition, and because the system is nonlinear (by virtue of both the dead-zone element and the threshold-reset mechanism in the modulator). A complete dynamic

analysis must be made to determine the transient dynamic properties of this system. The following questions must be answered:

(1) If the steady-state two-pulse limit cycle oscillation is perturbed slightly by a small disturbance torque, for example, will the system continue in a two-pulse limit cycle oscillation or will it become unstable in some sense?

(2) If the system is started at initial conditions for e_o, θ, and $\dot{\theta}$ not corresponding to the values on a two-pulse limit cycle trajectory, will the system settle eventually to a two-pulse limit cycle?

(3) Under what conditions, if any, will four-pulse, six-pulse, or higher order limit cycles occur?

(4) How are the answers to the above three questions dependent upon the six system parameters μ, J, a, K, θ_d, and γ?

To answer these questions, a mathematical model for the complete system, using arbitrary initial conditions, is derived in Chapter III. In Chapters IV and V these four questions are resolved through analytical studies of the mathematical model and by experimental means through the use of a digital simulator of the system.

Chapter III

MATHEMATICAL DESCRIPTION OF ATTITUDE CONTROL SYSTEM

A. The Basic Difference Equations

It is assumed that the torque pulses delivered by the gas valve are impulses occurring at instants denoted by t_k, and therefore $\dot{\theta}(t)$ changes abruptly by $\delta_{k-1}(\mu/J)$ at those instants. $\dot{\theta}(t)$ is constant between firing instants because of the lack of any external torque. $\theta(t)$ is continuous for all t. Figure 10 shows the typical behavior of $\dot{\theta}(t)$ and $\theta(t)$ for $\theta > \theta_d$, outside the limit cycle region. The interval $(t_{k+1}-t_k)$ is here called Δ_k, and because of the discontinuity in $\dot{\theta}(t)$ it is necessary to define $\dot{\theta}$ for $t = t_k$ to avoid confusion in the analysis. Following an established practice [16], this is defined as

$$\begin{aligned} \dot{\theta}(t_k) &= \dot{\theta}(t_k^+) \\ &= \dot{\theta}(t) \qquad \text{for} \quad t \in \Delta_k \end{aligned} \tag{3.1}$$

A simplification of notation, introduced at this point and carried throughout the sequel, is convenient. Let

$$\begin{aligned} \theta(t_k) &= \theta_k \\ \text{and} \qquad \dot{\theta}(t_k) &= \dot{\theta}_k \end{aligned} \tag{3.2}$$

θ_k and $\dot{\theta}_k$ are sometimes expressed also as $\theta(k)$ and $\dot{\theta}(k)$. It is clear from Fig. 10 that the functions $\theta(t)$ and $\dot{\theta}(t)$ are defined by their values at the firing instants, together with the intervals Δ_k. The relationship which defines the successive values of θ and $\dot{\theta}$ at the firing instants is the following set of difference equations. These equations

$$\begin{aligned} \theta_{k+1} &= \theta_k + \dot{\theta}_k \Delta_k \\ \dot{\theta}_{k+1} &= \dot{\theta}_k + \delta_k\left(\frac{\mu}{J}\right) \end{aligned} \tag{3.3}$$

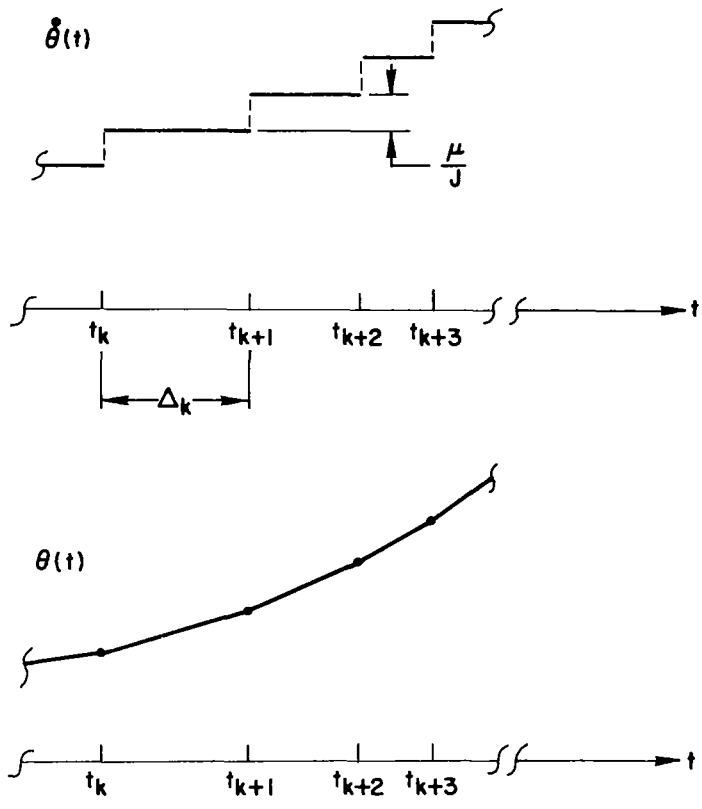

Fig. 10. THE NATURE OF $\dot{\theta}(t)$ AND $\theta(t)$.

constitute the basic mathematical model for all of the following analysis. It is shown in Section III.B that both Δ_k and δ_k, quantities which depend upon the modulator design [and threshold setting $A(1 + \gamma)$], can be determined from θ_k and $\dot{\theta}_k$. When Δ_k and δ_k are so represented, the dynamic properties of the modulator are suppressed from the analysis so that the basic equations (3.3) turn out to be second order difference equations, even though the system itself is of the third order. the three state variables being θ, $\dot{\theta}$, and e_o. Because of the logical operations inside the modulator, e_o is a "degenerate" state variable,

and dynamic analysis of the system may be accomplished in a two-dimensional state space, the $(\theta,\dot{\theta})$ plane [2,15]. Figure 11 shows a portion of a typical state trajectory on the $(\theta,\dot{\theta})$ plane. The dots on the trajectory represent the locations of θ and $\dot{\theta}$ at $t = t_k^+$, so the coordinates of the dot are θ_k, $\dot{\theta}_k$. Note that the continuity of $\theta(t)$ and the discreteness of $\dot{\theta}(t)$ are as apparent here as they are in Fig. 10. The uniform discrete changes in $\dot{\theta}$ are called $\Delta\dot{\theta}$ in Fig. 11.

It may also be deduced, from a comparison of Figs. 10 and 11, that Fig. 10, which shows θ and $\dot{\theta}$ both increasing with time, depicts behavior in the second quadrant of the $(\theta,\dot{\theta})$ plane.

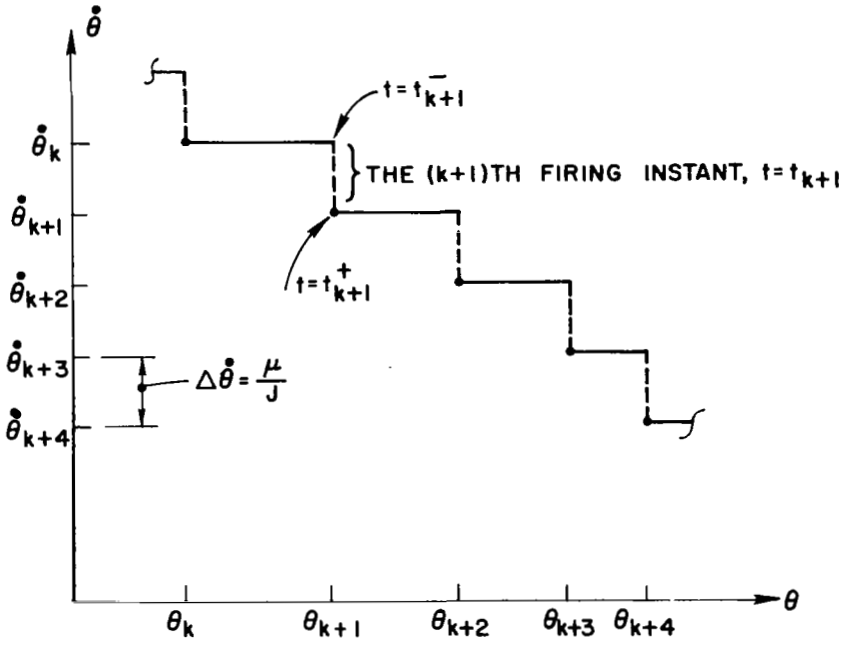

Fig. 11. A TYPICAL STATE TRAJECTORY ON THE STATE PLANE (OR PHASE PLANE).

B. State Transition Equations

Equations (3.3) are essentially state transition equations in that they express the state $(\theta,\dot{\theta})$ at t_{k+1} as functions of the state at t_k. However, the equations of (3.3) contain the quantities Δ_k and δ_k, so they are not in a convenient form for calculations or for analysis. Here (3.3) is reduced to such a convenient form. The first step in this

development is to define certain characteristic regions in the $(\theta,\dot{\theta})$ plane; within each region the system operates in a distinct manner.

The dead-zone element defines three regions, each of which is identified by the sign of $e(t)$. Equations (2.2), which defined the dead-zone characteristics, show that $e(t)$ is positive, zero, or negative depending upon $e_N(t)$. $e_N(t)$ is a linear combination of the two state variables $\theta(t)$ and $\dot{\theta}(t)$ [Eq. (1.2)]. The dead zone in the phase plane may be established by combining Eqs. (1.2) and (2.2); this combination yields

$$\begin{aligned} &\text{(I)} \quad e(t) = K[\theta + a\dot{\theta} - \theta_d] && \text{for} \quad \theta + a\dot{\theta} > \theta_d \\ &\text{(II)} \quad e(t) = K[\theta + a\dot{\theta} + \theta_d] && \text{for} \quad \theta + a\dot{\theta} < -\theta_d \\ &\text{(III)} \quad e(t) = 0 && \text{for} \quad -\theta_d \leq (\theta + a\dot{\theta}) \leq \theta_d \end{aligned} \tag{3.4}$$

For $(\theta,\dot{\theta})$ satisfying (I), $e(t)$ is positive; for $(\theta,\dot{\theta})$ satisfying (II), $e(t)$ is negative; and for $(\theta,\dot{\theta})$ satisfying (III), $e(t)$ is zero. Therefore, the state plane can be separated into three regions, each corresponding to one of the situations described by I, II, or III. Figure 12 shows the three regions drawn for $a > 0$. (It is shown later, that a must be greater than zero to have a stable system. This condition corresponds roughly to "positive damping" in a linear system.)

The boundary lines of the dead zone are called B_1 and B_2. A mathematical representation of these, using standard set theoretical notation and considering the tuple $(\theta,\dot{\theta})$ as a vector, is

$$\begin{aligned} B_1 &= \left\{(\theta,\dot{\theta}): \quad \theta = \theta_d - a\dot{\theta}\right\} \\ B_2 &= \left\{(\theta,\dot{\theta}): \quad \theta = -\theta_d - a\dot{\theta}\right\} \end{aligned} \tag{3.5}$$

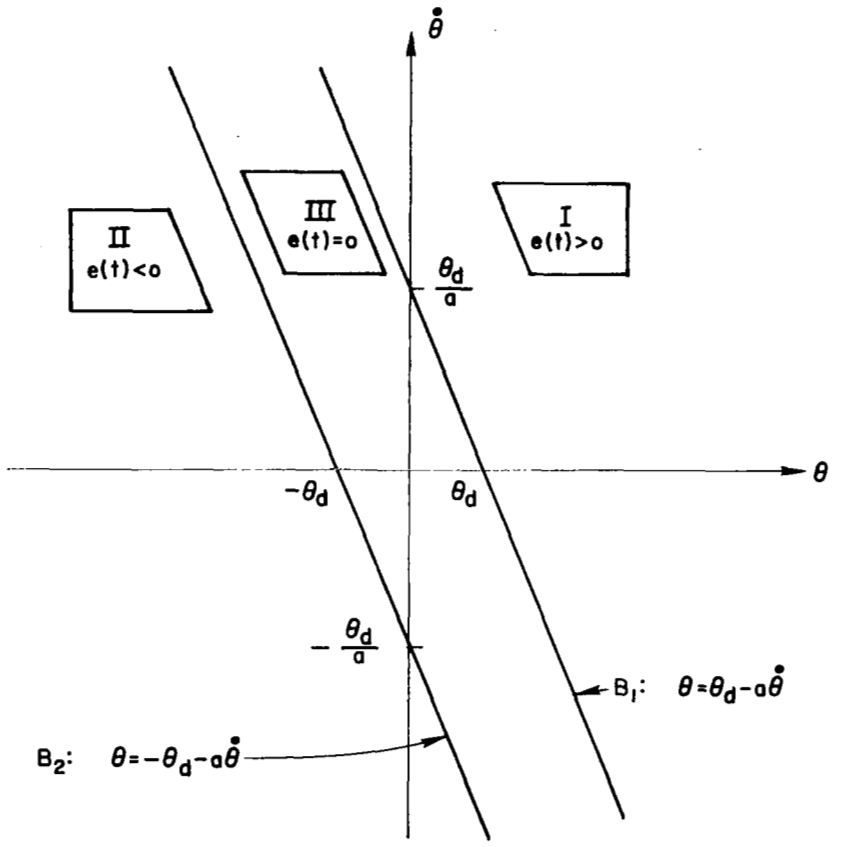

Fig. 12. THREE BASIC REGIONS OF THE STATE PLANE.

The three regions, I, II, and III, may also be represented as

$$\begin{aligned} \text{I} &= \left\{(\theta,\dot{\theta}):\quad \theta > \theta_d - a\dot{\theta}\right\} \\ \text{II} &= \left\{(\theta,\dot{\theta}):\quad \theta < -\theta_d - a\dot{\theta}\right\} \\ \text{III} &= \left\{(\theta,\dot{\theta}):\ -\theta_d - a\dot{\theta} \leq \theta \leq \theta_d - a\dot{\theta}\right\} \end{aligned} \tag{3.6}$$

It is now possible to calculate Δ_k and δ_k for trajectories that begin inside the dead zone, in Region III, at $t = t_k^+$. In this case, the dynamic behavior of the system is depicted in Fig. 13 which shows the state trajectory during the interval, Δ_k, the modulator input signal, e(t), and the output of the integrator, $e_o(t)$. The controlled

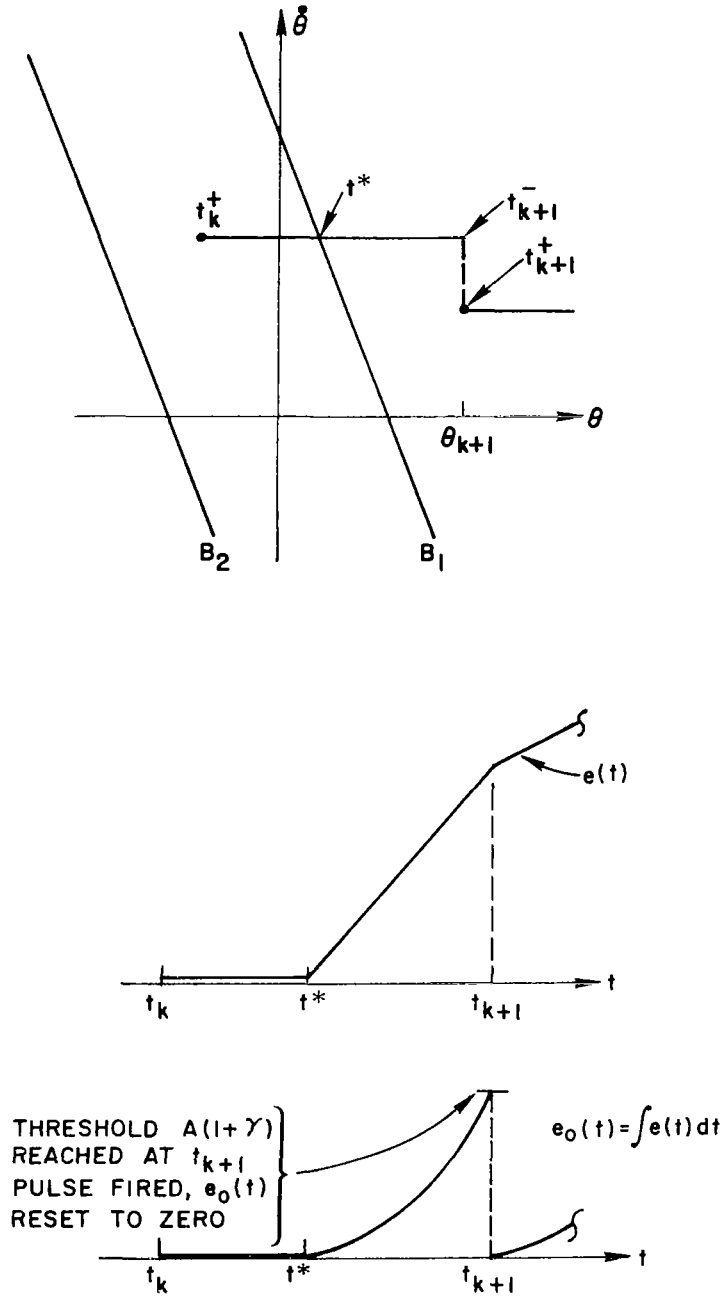

Fig. 13. e(t) AND $e_o(t)$ WITH THE CORRESPONDING TRAJECTORY ON THE STATE PLANE.

body moves at a constant velocity $\dot{\theta}_k$ during the entire interval $(t_{k+1}-t_k)$, having acquired that velocity as a result of the pulse fired at $t = t_k$, or possibly as a result of some other agent which presents us with the dynamic state $(\theta_k,\dot{\theta}_k)$ at time t_k. For $t_k < t < t^*$, the system is coasting in the dead zone so that $e(t) = 0$ during this initial interval. At $t = t^*$, the system leaves the dead zone, still coasting, but with $e(t)$ increasing linearly according to the following expression

$$e(\tau) = K\dot{\theta}_k \tau \qquad \text{for} \quad 0 \leq \tau \leq (t_{k+1} - t^*) \tag{3.7}$$

where $\tau = (t-t^*)$. The integrator output is therefore

$$e_o(\tau) = \frac{K\dot{\theta}_k \tau^2}{2} \tag{3.8}$$

The threshold $A(1 + \gamma)$ is reached when the following relationship is satisfied

$$e_o(\tau_f) = \frac{K\dot{\theta}_k \tau_f^2}{2} = (A)(1 + \gamma) = \frac{K\mu a^2}{4J}(1 + \gamma) \tag{3.9}$$

where τ_f is the instant of firing $(t = t_{k+1})$. From (3.8), τ_f is found to be

$$\tau_f = \sqrt{\frac{\mu a^2 (1 + \gamma)}{2J\,\dot{\theta}_k}} \tag{3.10}$$

From this, it is clear that the positive root of (3.9) corresponds to the physical situation. Now the sign of $e_o(t)$ is positive at $t = t_{k+1}^-$ so $\delta_k = -1$ and one of the state transition equations (3.3) can now be determined

$$\dot{\theta}_{k+1} = \dot{\theta}_k - \frac{\mu}{J} \qquad \left\{ \begin{array}{l} (\theta_k,\dot{\theta}_k) \in \text{III} \\ \\ \dot{\theta}_k > 0 \end{array} \right\} \tag{3.11}$$

The other equation is obtained by noting that the firing instant t_{k+1} is determined solely by that portion of the trajectory lying within I. As long as it puts the state $(\theta_k, \dot{\theta}_k)$ anywhere in the dead zone, the θ_k coordinate has no effect on θ_{k+1}. The θ coordinate at $t = t^*$ depends upon $\dot{\theta}_k$, of course, and this coordinate is found from the equation for B_1.

$$\theta(t^*) = \theta_* = \theta_d - a\dot{\theta}_k \tag{3.12}$$

Since the time of travel from θ_* to θ_{k+1} is τ_f, our second state transition equation is

$$\begin{aligned} \theta_{k+1} &= \theta_* + \tau_f \dot{\theta}_k \\ &= \theta_d - a\dot{\theta}_k + \sqrt{\frac{\mu a^2 (1 + \gamma)\dot{\theta}_k}{2J}} \end{aligned} \qquad \left\{ \begin{matrix} (\theta_k, \dot{\theta}_k) \in \text{III} \\ \dot{\theta}_k > 0 \end{matrix} \right\} \tag{3.13}$$

Equations (3.13) and (3.11), taken together, constitute the state transition equations for $(\theta_k, \dot{\theta}_k) \in$ III and for $\dot{\theta}_k > 0$.

If $\dot{\theta}_k = 0$, then any state in the dead zone will remain there (on the θ axis) indefinitely. If $(\theta_k, \dot{\theta}_k)$ is in III but in the lower half plane $(\dot{\theta}_k < 0)$, then, because of the symmetry of the system, the derivation of the state transition equations is similar to that given here with $-\theta_k$ and $-\dot{\theta}_k$ playing the roles of θ_k and $\dot{\theta}_k$ in the above analysis. The results of that derivation are

$$\begin{aligned} \dot{\theta}_{k+1} &= \dot{\theta}_k + \frac{\mu}{J} \\ \theta_{k+1} &= -\theta_d - a\dot{\theta}_k - \sqrt{\frac{-\mu a^2 (1 + \gamma)\dot{\theta}_k}{2J}} \end{aligned} \qquad \left\{ \begin{matrix} (\theta_k, \dot{\theta}_k) \in \text{III} \\ \dot{\theta}_k < 0 \end{matrix} \right\} \tag{3.14}$$

Next, the state transition equations for $(\theta_k, \dot{\theta}_k)$ in Regions I and II must be derived. Again, because of the symmetry of the system, it is

necessary to consider only one of these regions, say I, in detail; the behavior for Region II will be similar. One of two distinctly different modes of state transition occur, depending upon the location of $(\theta_k, \dot{\theta}_k)$ in I. These are illustrated in Fig. 14 as Modes A and B.

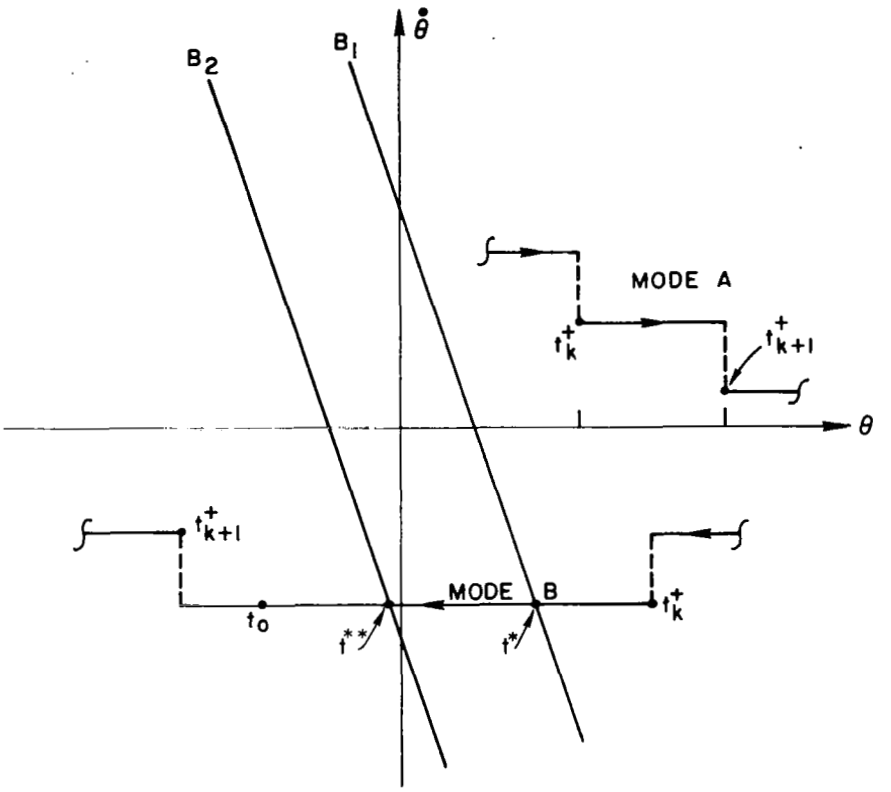

Fig. 14. MODES A AND B--STATE TRANSITIONS.

In Mode A, $e(t)$ is greater than zero during the entire interval $t_{k+1} - t_k = \Delta_k$, as is shown in Fig. 15. During this interval,

$$e(\tau) = K[\theta_k + \dot{\theta}_k \tau + a\dot{\theta}_k - \theta_d] \tag{3.15}$$

where $\tau = t - t_k$. $e_o(\tau)$ for $t \in \Delta_k$ is

$$e_o(\tau) = K \int_0^{\tau} [\theta_k + \dot{\theta}_k t + a\dot{\theta}_k - \theta_d] \, dt \tag{3.16}$$

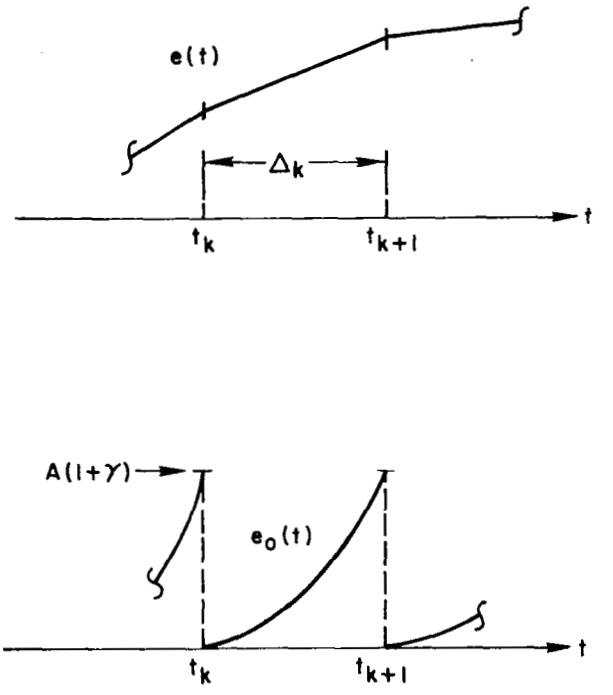

Fig. 15. e(t) AND $e_o(t)$ IN MODE A BEHAVIOR.

Δ_k is defined by t_{k+1}, the instant at which $e_o(\tau)$ reaches the threshold; therefore it is computed by setting $e_o(\tau) = A(1 + \gamma)$ for $\tau = \Delta_k$. From (3.16), this gives

$$A(1 + \gamma) = K \int_0^{\Delta_k} [\theta_k + \dot{\theta}_k t + a\dot{\theta}_k - \theta_d] \, dt \qquad (3.17)$$

The desired expression for Δ_k is obtained by evaluating the integral and using (2.4)

$$\Delta_k^2 + \left[\frac{2(\theta_k + a\dot{\theta}_k - \theta_d)}{\dot{\theta}_k}\right] \Delta_k - \left[\frac{\mu a^2 (1 + \gamma)}{2J \dot{\theta}_k}\right] = 0 \qquad (3.18)$$

By using the quadratic formula to find the least positive value for Δ_k, we obtain

$$\Delta_k = \sqrt{\left(\frac{\theta_k + a\dot{\theta}_k - \theta_d}{\dot{\theta}_k}\right)^2 + \left(\frac{\mu a^2(1+\gamma)}{2J\,\dot{\theta}_k}\right)} - \left(\frac{\theta_k + a\dot{\theta}_k - \theta_d}{\dot{\theta}_k}\right) \qquad (3.19)$$

And by substituting this expression into the basic difference equation (3.3), the state transition equation

$$\theta_{k+1} = \theta_d - a\dot{\theta}_k + \sqrt{(\theta_k + a\dot{\theta}_k - \theta_d)^2 + \frac{\mu a^2(1+\gamma)}{2J}\,\dot{\theta}_k} \qquad (3.20)$$

is obtained. $e_o(t_{k+1}^-)$ is positive in this case, therefore $\delta_k = -1$. The second state transition equation is

$$\dot{\theta}_{k+1} = \dot{\theta}_k - \frac{\mu}{J} \qquad (3.21)$$

Equations (3.20) and (3.21) are the state transition equations that hold whenever $(\theta_k, \dot{\theta}_k) \in I$ and the system operates in Mode A.

Now, if $(\theta_k, \dot{\theta}_k) \in I$, but at a point such that the integrator output does not reach the threshold value before the trajectory enters the dead-zone, the system is in Mode B and the behavior is that described by Figs. 14 and 16. Here the trajectory reaches the edge of the dead zone at $t = t^*$, $e(t^*)$ is zero, and $e_o(t)$ reaches a level less than that required to fire the valve. $e_o(t)$ remains at $e_o(t^*)$ as the trajectory coasts across the dead-zone (because $e = 0$ during this interval), reaching the edge at $t = t^{**}$. For $t > t^{**}$, the trajectory is in Region II, so $e(t)$ is negative, decreasing at the same rate as in the interval $(t^* - t_k)$. Since $e(t)$ is negative, $e_o(t)$ begins to <u>decrease</u> from its positive value of $e_o(t^*)$, and it reaches zero at $t = t_o$. At $t = t_o$, $e(t)$ has reached the same magnitude that it had at $t = t_k$, but it is negative. Apparently the intervals $(t^* - t_k)$ and $(t_o - t^{**})$ are equal. During the final interval $(t_{k+1} - t_o)$, $e_o(t)$ decreases at a rate more rapid than before (in this Δ_k interval) because $e(t)$ has a higher magnitude than before. $e_o(t)$ reaches the negative threshold at t_{k+1}, as shown. Thus Δ_k is the sum of four intervals

$$\Delta_k = (t^* - t_k) + (t^{**} - t^*) + (t_o - t^{**}) + (t_{k+1} - t_o) \qquad (3.22)$$

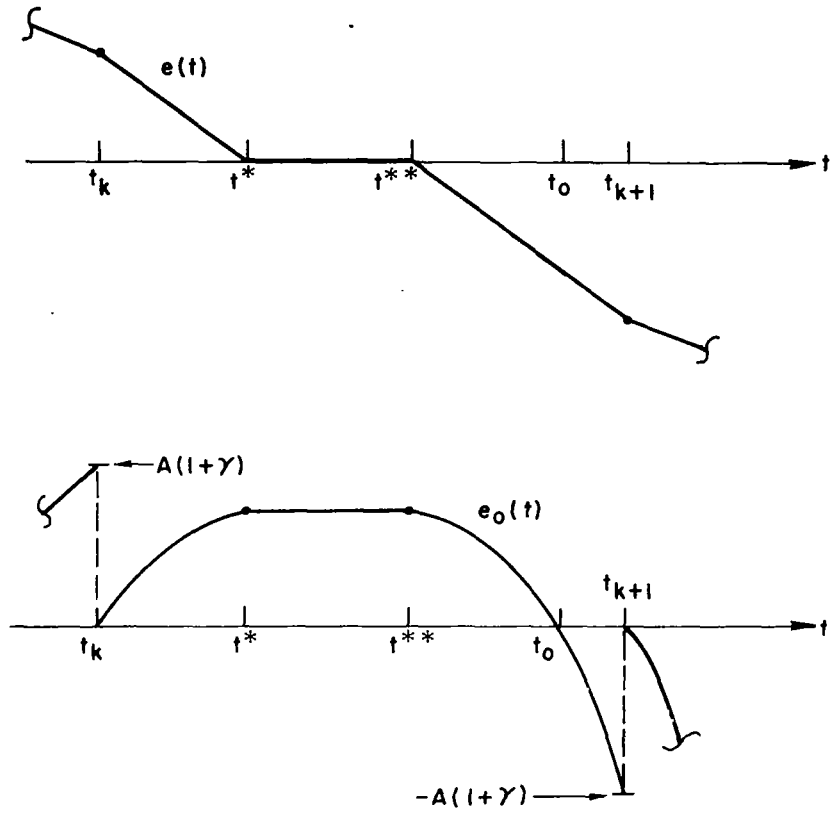

Fig. 16. e(t) AND $e_o(t)$ IN MODE B BEHAVIOR.

Two of these are equal; the interval corresponding to the dead-zone travel is

$$(t^{**} - t^*) = \frac{2\theta_d}{-\dot{\theta}_k} \tag{3.23}$$

The negative sign is required in the denominator because $\dot{\theta}_k$ is negative in the situation depicted here. Δ_k may therefore be written as

$$\Delta_k = 2(t^* - t_k) - \frac{2\theta_d}{\dot{\theta}_k} + (t_{k+1} - t_o) \tag{3.24}$$

The interval (t^*-t_k) is simply the time required for the system to move from $\theta = \theta_k$ to $\theta = \theta(t^*)$ at the constant rate $\dot{\theta}_k$. $\theta(t^*)$

may be expressed in terms of $\dot{\theta}_k$ because $(\theta_*, \dot{\theta}_*) \in B_1$. From (3.5)

$$\theta_* = \theta_d - a\dot{\theta}_k \tag{3.25}$$

so (t^*-t_k) is given by

$$(t^* - t_k) = \frac{\theta_k - \theta_*}{-\dot{\theta}_k} = \frac{\theta_d - \theta_k - a\dot{\theta}_k}{\dot{\theta}_k} \tag{3.26}$$

The interval $(t_{k+1}-t_o)$--call it Δ_f--is now calculated in much the same way that Δ_k was found in (3.16) to (3.19). During this interval, $e(t)$ is given by

$$e(\tau) = K[\theta_d - \theta_k - a\dot{\theta}_k + \dot{\theta}_k\tau] \tag{3.27}$$

where $\tau = (t-t_o)$. Integrating this from 0 to Δ_f to give $e_o(t^-_{k+1})$ and setting that equal to $-A(1+\gamma)$, yields an expression for Δ_f

$$\int_0^{\Delta_f} e(\tau)\, d\tau = K\left[(\theta_d - \theta_k - a\dot{\theta}_k)\Delta_f + \frac{\dot{\theta}_k}{2}\Delta_f^2\right] = -A(1+\gamma) \tag{3.28}$$

$$\Delta_f^2 + \left[\frac{2(\theta_d - \theta_k - a\dot{\theta}_k)}{\dot{\theta}_k}\right]\Delta_f + \left[\frac{\mu a^2(1+\gamma)}{2J\,\dot{\theta}_k}\right] = 0 \tag{3.29}$$

Using the quadratic formula with $\dot{\theta}_k < 0$ and selecting the least positive root of (3.29), yields

$$\Delta_f = \frac{-(\theta_d - \theta_k - a\dot{\theta}_k) - \sqrt{(\theta_d - \theta_k - a\dot{\theta}_k)^2 - \frac{\mu a^2(1+\gamma)}{2J}\dot{\theta}_k}}{\dot{\theta}_k} \tag{3.30}$$

Δ_k is obtained by combining (3.24), (3.26), and (3.30).

$$\Delta_k = \frac{1}{\dot{\theta}_k}\left[-\theta_d - \theta_k - a\dot{\theta}_k - \sqrt{(\theta_d - \theta_k - a\dot{\theta}_k)^2 - \frac{\mu a^2(1+\gamma)}{2J}\dot{\theta}_k}\right] \tag{3.31}$$

When this expression is substituted into the basic difference equation (3.3) the resultant state transition equation is

$$\theta_{k+1} = -\theta_d - a\dot{\theta}_k - \sqrt{(\theta_d - \theta_k - a\dot{\theta}_k)^2 - \frac{\mu a^2(1+\gamma)}{2J}\dot{\theta}_k} \qquad (3.32)$$

In Mode B, $e_o(\bar{t}_{k+1})$ is negative, so $\delta_k = +1$, and the second state transition equation is

$$\dot{\theta}_{k+1} = \dot{\theta}_k + \frac{\mu}{J} \qquad (3.33)$$

It is now necessary to separate Region I into two subregions--call them R_1 and R_4--such that $(\theta_k, \dot{\theta}_k) \in R_1$ leads to Mode A behavior, while $(\theta_k, \dot{\theta}_k) \in R_4$ leads to Mode B behavior. We note first that for $\dot{\theta}_k > 0$, a trajectory starting in I moves toward the right, away from the dead zone. Therefore, all points in that portion of the upper half of the state plane belonging to Region I also belong to R_1; R_4 must be in the lower half of the state plane. Further, R_4 must be adjacent to Region III, inasmuch as those $(\theta_k, \dot{\theta}_k)$ exhibiting Mode B behavior must be relatively close to the dead zone.

To find the boundary between R_1 and R_4, consider a point $(\theta_k, \dot{\theta}_k)$ located so that $e_o(t^*)$ is just equal to the integrator threshold (see Fig. 16). From the analysis described by (3.7) to (3.14), it is clear that the "horizontal" distance from this point to the edge of the dead zone is $\sqrt{[-\mu a^2(1+\gamma)/(2J)]}\,\dot{\theta}_k$. If $(\theta_k, \dot{\theta}_k)$ is taken slightly to the right of this point, Mode A will result. If it is taken slightly to the left, Mode B will prevail. Therefore, the boundary separating R_1 and R_4--call it B_4--is defined as follows, and it is depicted in Fig. 17.

$$B_4 = \left\{ (\theta, \dot{\theta}) : \dot{\theta} < 0 \quad \text{and} \quad \theta = \theta_d - a\dot{\theta} + \sqrt{\frac{-\mu a^2(1+\gamma)\dot{\theta}}{2J}} \right\} \qquad (3.34)$$

The slope of curve B_4 is zero at the point where it meets the θ axis, and the same is true for B_3. In some of the figures in later

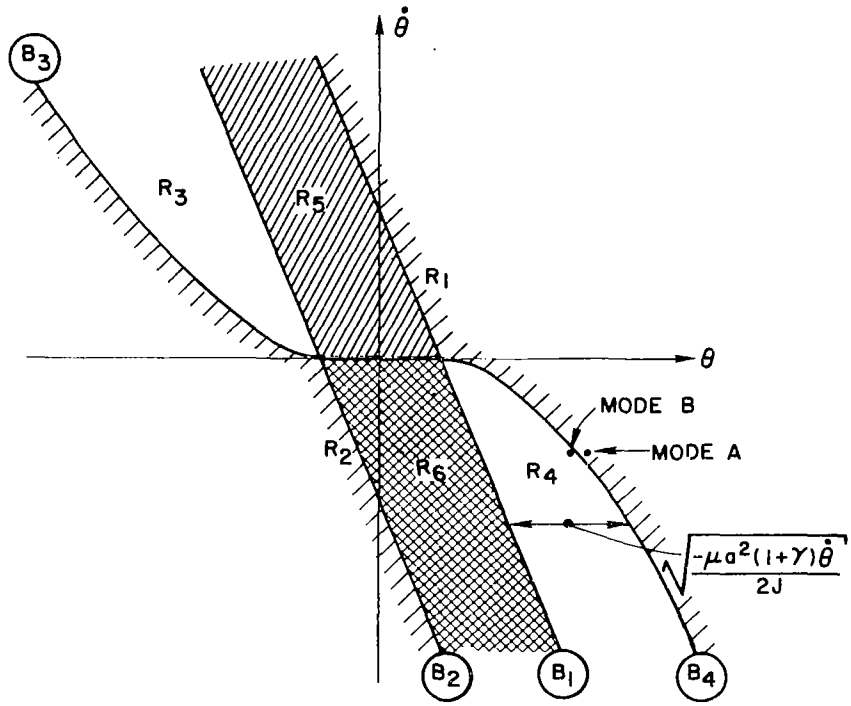

Fig. 17. SIX REGIONS OF THE STATE PLANE.

parts of this report, this fact may not be apparent because of the scale used.

Because of the symmetry of the system, Region II is also separated into two subregions--called R_2 and R_3--whose points are starting points for Mode A and Mode B behavior, respectively. These subregions are also shown in Fig. 17. Note also that Region III, the dead zone, is also subdivided into subregions R_5 (for $\dot{\theta}_k > 0$) and R_6 (for $\dot{\theta}_k < 0$).

Δ_k may be calculated for $(\theta_k, \dot{\theta}_k) \in R_2$ in exactly the same manner as it was for $(\theta_k, \dot{\theta}_k) \in R_1$. Mode A behavior prevails, and the state transition equations which result are

$$\dot{\theta}_{k+1} = \dot{\theta}_k + \frac{\mu}{J}$$

$$\theta_{k+1} = -\theta_d - a\dot{\theta}_k - \sqrt{(\theta_k + a\dot{\theta}_k + \theta_d)^2 - \frac{\mu a^2(1+\gamma)\dot{\theta}_k}{2J}} \qquad (3.35)$$

Similarly, the state transition equations for $(\theta_k, \dot{\theta}_k) \in R_3$ are derived from Mode B behavior

$$\dot{\theta}_{k+1} = \dot{\theta}_k - \frac{\mu}{J}$$

$$\theta_{k+1} = \theta_d - a\dot{\theta}_k + \sqrt{(\theta_k + a\dot{\theta}_k + \theta_d)^2 + \frac{\mu a^2(1 + \gamma)\dot{\theta}_k}{2J}} \qquad (3.36)$$

The boundary separating R_2 and R_3 is called B_3, and it is defined in the same manner as was B_4.

$$B_3 = \left\{ (\theta, \dot{\theta}) : \dot{\theta} > 0 \quad \text{and} \quad \theta = -\theta_d - a\dot{\theta} - \sqrt{\frac{\mu a^2(1 + \gamma)\dot{\theta}}{2J}} \right\} \qquad (3.37)$$

This section's objective has now been reached. The state transition equations have been found to consist of six different sets of difference equations, each set corresponding to the state $(\theta_k, \dot{\theta}_k)$ which exists at $t = t_k^+$. Table 1 identifies these six different sets of state transition equations.

Table 1

IDENTIFICATION OF STATE TRANSITION EQUATIONS

For $(\theta_k, \dot{\theta}_k)$ in Region	State Transition Equations Given by Equations
R_1	(3.20) and (3.21)
R_2	(3.35)
R_3	(3.36)
R_4	(3.32) and (3.33)
R_5	(3.11) and (3.13)
R_6	(3.14)

We complete this section with two remarks concerning the six sets of equations. In the degnerate case where $\dot{\theta}_k = 0$ and $-\theta_d < \theta_k < \theta_d$, the system is at rest in the dead zone and will remain there indefinitely. Δ_k will be infinite, and thus the state transition equations corresponding to R_5 and R_6 are not valid for $\dot{\theta}_k = 0$.

The symmetry of the state plane suggests that the state transition equations corresponding to R_1 should bear some form of similarity to those for R_2. R_3 and R_4 also should be paired in a like fashion, as should R_5 and R_6. Note that if the state plane is inverted, it resembles itself; R_1 is in the position formerly occupied by R_2, and R_3 and R_4 have also changed positions, as have R_5 and R_6. This suggests that, if θ is replaced by $-\theta$ and $\dot{\theta}$ by $-\dot{\theta}$ in the state transition equations for R_1, the result should be the equations for R_2. The same replacement in the equations for R_3 and R_5 should yield the equations for R_4 and R_6. This is indeed the case with the equations identified by Table 1.

In the following section, the state transition equations presented here are normalized for the sake of simplicity and convenience in computation. Each of the boundaries B_1, B_2, B_3, and B_4 is identified with one of the six regions, and all of the significant facts and equations developed so far are summarized in compact form.

C. The Normalized State Transition Equations

The state transition equations identified in Table 1 can be reduced to simpler forms that are convenient for analysis, if the state variables θ and $\dot{\theta}$ are normalized. For this, θ is normalized with respect to θ_d and $\dot{\theta}$ with respect to μ/J. x is the normalized state variable replacing θ, and y is the state variable replacing $\dot{\theta}$.

$$x = \frac{\theta}{\theta_d} \qquad y = \frac{\dot{\theta}J}{\mu} \tag{3.38}$$

If these substitutions are made in the state transition equations derived in Section III.B, the result is the set of normalized state transition

equations shown in Table 2. Here ℓ is a normalized version of the lead ratio

$$\ell = \frac{a\mu}{J\theta_d} \tag{3.39}$$

Table 2

STATE TRANSITION EQUATIONS

F_1:	$y_{k+1} = y_k - 1$ $x_{k+1} = \sqrt{(x_k + \ell y_k - 1)^2 + \frac{\ell^2(1+\gamma)}{2} y_k} + 1 - \ell y_k$
F_2:	$y_{k+1} = y_k + 1$ $x_{k+1} = -\sqrt{(x_k + \ell y_k + 1)^2 - \frac{\ell^2(1+\gamma)}{2} y_k} - 1 - \ell y_k$
F_3:	$y_{k+1} = y_k - 1$ $x_{k+1} = \sqrt{(x_k + \ell y_k + 1)^2 + \frac{\ell^2(1+\gamma)}{2} y_k} + 1 - \ell y_k$
F_4:	$y_{k+1} = y_k + 1$ $x_{k+1} = -\sqrt{(x_k + \ell y_k - 1)^2 - \frac{\ell^2(1+\gamma)}{2} y_k} - 1 - \ell y_k$
F_5:	$y_{k+1} = y_k - 1$ $x_{k+1} = \sqrt{\frac{\ell^2(1+\gamma)}{2} y_k} + 1 - \ell y_k$
F_6:	$y_{k+1} = y_k + 1$ $x_{k+1} = -\sqrt{-\frac{\ell^2(1+\gamma)}{2} y_k} - 1 - \ell y_k$

To define the six regions $R_1, \ldots, R_6$ illustrated in Fig. 17, the state vector z is introduced

$$z = (x,y) \tag{3.40}$$

The six regions of the (x,y) plane are described compactly by the expressions shown in Table 3, and the boundaries separating the six regions

Table 3

DEFINITION OF THE SIX REGIONS OF THE STATE PLANE

R_1	$\left\{ z = (x,y): \begin{array}{l} x > 1 - \ell y \quad \text{for} \quad y \geq 0 \\ x > 1 - \ell y + \ell \sqrt{-\frac{(1+\gamma)}{2} y} \quad \text{for} \quad y < 0 \end{array} \right\}$
R_2	$\left\{ z = (x,y): \begin{array}{l} x < -1 - \ell y - \ell \sqrt{\frac{(1+\gamma)}{2} y} \quad \text{for} \quad y > 0 \\ x < -1 - \ell y \quad \text{for} \quad y \leq 0 \end{array} \right\}$
R_3	$\left\{ z = (x,y): \begin{array}{l} y > 0 \\ -1 - \ell y - \ell \sqrt{\frac{(1+\gamma)}{2} y} \leq x \leq -1 - \ell y \end{array} \right\}$
R_4	$\left\{ z = (x,y): \begin{array}{l} y < 0 \\ 1 - \ell y \leq x \leq 1 - \ell y + \ell \sqrt{-\frac{(1+\gamma)}{2} y} \end{array} \right\}$
R_5	$\left\{ z = (x,y): \begin{array}{l} y > 0 \\ -1 - \ell y < x \leq 1 - \ell y \end{array} \right\}$
R_6	$\left\{ z = (x,y) \begin{array}{l} y < 0 \\ -1 - \ell y \leq x < 1 - \ell y \end{array} \right\}$

are defined in Table 4. Here that portion of the x axis lying in the dead zone is called B_5. For definiteness, each point on the boundaries is taken to be a member of one of the six regions. If Tables 3 and 4 are compared, it is clear that $B_3 \in R_3$, and $B_4 \in R_4$. That portion of B_1 which is above the x axis is in R_5 and that portion below is in R_4. The portion of B_2 which is above the x axis is in R_3, and the portion below is in R_6. The left end point of B_5 is also in B_2, and the right end point is in B_1. Thus it can be said that

$$\{z = (x,y)\} = \text{THE STATE PLANE} = \bigcup_{i=1}^{6} R_i \cup B_5 \tag{3.41}$$

Table 4

DEFINITION OF THE BOUNDARIES OF THE SIX REGIONS OF THE STATE PLANE

$B_1 = \{z = (x,y) : x = 1 - \ell y\}$
$B_2 = \{z = (x,y) : x = -1 - \ell y\}$
$B_3 = \left\{z = (x,y) : y > 0,\ x = -1 - \ell y - \ell\sqrt{\frac{(1+\gamma)}{2}}\, y\right\}$
$B_4 = \left\{z = (x,y) : y < 0,\ x = 1 - \ell y + \ell\sqrt{-\frac{(1+\gamma)}{2}}\, y\right\}$
$B_5 = \{z = (x,y) : y = 0,\ -1 \leq x \leq 1\}$

With the definitions made above, the dynamic characteristics of the attitude control system under study can be described by the compact state transition relationship

$$z_{k+1} = F(z_k) \tag{3.42}$$

where $z_k = (x_k, y_k) = [x(t_k), y(t_k^+)]$, and the mapping F is given by

$$F = \begin{cases} F_1 & \text{if } z_k \in R_1 \\ F_2 & \text{if } z_k \in R_2 \\ \cdot & \\ \cdot & \\ \cdot & \\ F_6 & \text{if } z_k \in R_6 \end{cases} \tag{3.43}$$

$F_1, F_2, \ldots, F_6$ are the state transition equations listed in Table 2. In the degenerate case $z_k \in B_5$, the system remains at rest indefinitely. Thus (3.42) is the basic mathematical model for the analysis given in Chapters IV and V where the stability of the two-pulse limit cycle oscillation is investigated, and the existence of higher order limit cycles is also determined.

The studies in Chapters IV and V consist of the analysis of the structure of the mapping (3.42) and of supplementary experimental results obtained from a digital simulation of that mapping. The digital simulation is described briefly in the following section.

D. Digital Simulation of Attitude Control System

The basic mathematical model of the attitude control system is the mapping (3.42) which is the set of six pairs of difference equations given in Table 2, together with the definitions of the regions $R_1, \ldots, R_6$ given in Table 3. These relationships are very naturally suited as algorithms for a digital computer program for computing successive values of z_k, starting from an initial condition $z_o = (x_o, y_o)$. Such a program has proven to be extremely useful as an experimental tool in discovering the intricate structure of the mapping (3.42) and, consequently, the limit cycle behavior of the system.

The way in which the program works is illustrated in the flow chart of Fig. 18. The input data are the values of γ and ℓ desired and the initial conditions. The program first determines in which region $z_o = (x_o, y_o)$ lies and then computes $z_1 = F_{jo}(z_o)$. F_{jo} is the algorithm

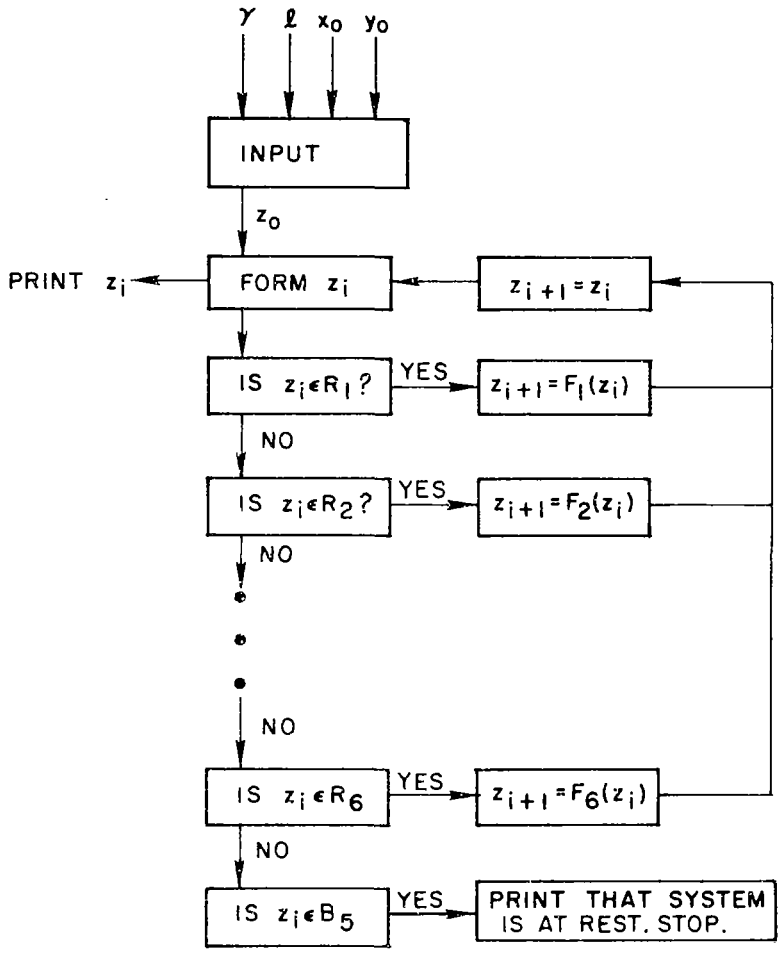

Fig. 18. FLOW CHART FOR BASIC COMPUTER ALGORITHM.

appropriate to the region R_j containing z_o. Then the region containing z_1 is determined, and z_2 is computed as $z_2 = F_{j1}(z_1)$, again using F_{j1}, the F algorithm appropriate to the region containing z_1. This process is continued for a preset number of iterations, and the successive values of z_k are printed out. A listing of the program statements and a sheet of typical readout data are contained in the Appendix.

A plot of z(t) may be constructed from this data by connecting the points (x_k, y_k) to the points (x_{k+1}, y_k) by straight lines. The result will be the "staircase" type of plot shown in Fig. 11. The height of each "step" in the y direction is 1 because of the normalization of

the $\dot{\theta}$ coordinate (3.38), and the total width of the dead zone, in the x direction, is 2, also because of the normalization of the θ coordinate.

A two-pulse limit cycle occurs whenever $z_{k+2} = z_k$ for all k larger than some integer.

Chapter IV

TWO-PULSE LIMIT CYCLE OSCILLATIONS

In Chapter II, the dynamic properties of the modulator which are necessary to sustain a symmetrical two-pulse limit cycle oscillation were determined. It was demonstrated that the common IPF modulator has these requisite characteristics if the threshold value $A(1+\gamma)$ is A, i.e., if $\gamma = 0$. In this chapter the transient characteristics of the system are studied with the objective of determining the conditions under which unsymmetrical two-pulse limit cycles exist, the stability of two-pulse limit cycles, and the convergence of the state trajectory to the two-pulse limit cycle from an arbitrary initial point in the state plane. The state transition equation (3.42), together with the detailed descriptions of the F function contained in (3.43), Tables 2, 3, and 4, and Fig. 17, constitute the basic mathematical model for the transient studies in this chapter.

A. Geometrical Approach

Limit cycle behavior of feedback systems having pulse-modulated controllers has been studied previously using modified Lyapunov theorems and point transformation techniques [2,7,12] and frequency domain methods [6,17,18]. An attempt to apply a Lyapunov-type approach to the system under study was also started but abandoned when an interesting geometrical structure of the state transition function was discovered. Subsequent pursuit of these geometrical properties revealed all of the dynamic characteristics of the system pertinent to its limit cycle oscillation behavior, as well as explicit conditions on the system parameters which must hold for the existence of stable two-pulse limit cycle oscillations. Beyond this, the conditions under which higher order limit cycles can occur were also revealed by this geometrical approach. The two-pulse limit cycle is discussed in this chapter, and the higher order limit cycles in Chapter V.

Two geometrical properties of the state transition equation (or map)

$$z_{k+1} = F(z_k) \tag{4.1}$$

form the basis for the studies described here. The first of these is that a state z_k in a given region of the state plane will lead to a z_{k+1} [through (4.1)] located only in certain regions. For example, if $z_k \in R_1$, then z_{k+1} will be in R_1, R_4, R_5, or R_6, but it cannot be in R_3 or R_2. Similarly, $z_k \in R_3$ implies z_{k+1} will be in R_1, R_4, R_5, or R_6, but not in R_2. The second geometrical property of significance here is that all points lying in the dead zone at a given value of y will map [through (4.1)] into a single point. The whole dead-zone area is mapped, therefore, onto a curve in the state plane.

B. Map of the Dead Zone

Consider a point $z_k \in R_5$, the upper half of the dead zone, as shown in Fig. 19. Then the state $z(t) = [x(t), y(t)]$ will progress from z_k at time t_k horizontally (at constant velocity y_k) until time t^-_{k+1}, at which instant it will have arrived on the dashed curve labelled B'_3. From the analysis in Chapter III, it is clear that points on B'_3 are the same horizontal distance from B_1, the right-hand edge of the dead zone, as are points on B_3 from B_2, the left-hand edge

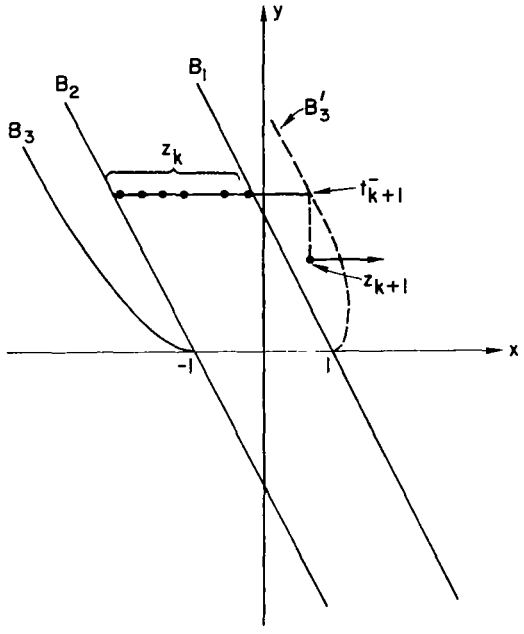

Fig. 19. STATE TRAJECTORY FOR z_k IN THE DEAD ZONE.

of the dead zone. Therefore, B_3' may be defined as

$$B_3' = \left\{ z = (x,y) : x = 1 - \ell y + \ell \sqrt{\frac{(1 + \gamma)y}{2}} , \quad y > 0 \right\} \tag{4.2}$$

At time t_{k+1}, the gas valve is fired so that $z(t)$ jumps vertically downward by 1 unit, placing z_{k+1} as shown. We note that any z_k, located on the horizontal line between the edges of the dead zone, will map into the same z_{k+1}, so that the single point z_{k+1} is the domain of the map F where the range of F is taken to be the horizontal line segment lying in the dead zone. The coordinates of z_{k+1} are easily established from the formula describing B_3'. From this formula, (4.2) becomes

$$x_{k+1} = 1 - \ell y_k + \ell \sqrt{\frac{(1 + \gamma)}{2} y_k} \tag{4.3}$$

and the y coordinate of z_{k+1} is obviously (from F_5 in Table 2)

$$y_{k+1} = y_k - 1 \tag{4.4}$$

If all the points in R_5 are mapped into their corresponding z_{k+1} points, the mapping will form a curve [the equation of which may be determined by combining Eqs. (4.3) and (4.4)] which may be taken to represent the mapping of the general point $z_k \in R_5$ into z_{k+1}. This curve is called $F(R_5)$ and is defined as

$$F(R_5) = \left\{ z = (x,y) : x = 1 - \ell - \ell y + \ell \sqrt{\frac{(1 + \gamma)}{2} (y + 1)} , \quad y > -1 \right\} \tag{4.5}$$

The anatomy of this curve is quite important in what follows, so it is displayed in Fig. 20 where it is drawn to an exaggerated scale and is shown for $\gamma > 1$. The coordinates of particular points are indicated on

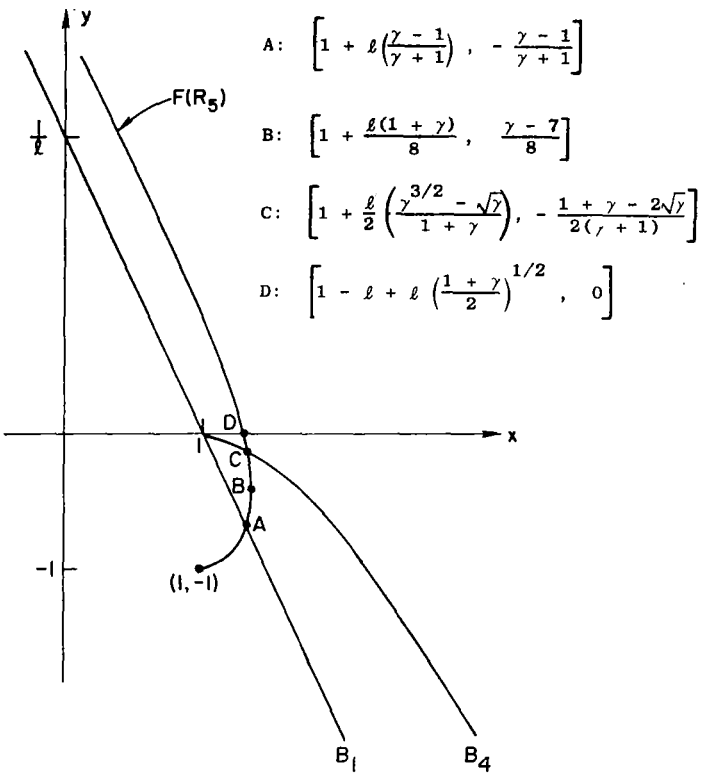

Fig. 20. STATE TRANSITION MAP OF THE DEAD ZONE. Coordinates of the points A, B, C, and D are also shown.

the figure. The slope of $F(R_5)$ is calculated from (4.5) to be

$$\frac{dy}{dx} = \frac{1}{\ell}\left[\frac{2\sqrt{y+1}}{\left(\frac{1+\gamma}{2}\right)^{1/2} - 2\sqrt{y+1}}\right] \tag{4.6}$$

At the point $(1,-1)$ the slope of $F(R_5)$ is zero. Point A is the point at which $F(R_5)$ intersects B_1, the edge of the dead zone. Point B is the rightmost point of $F(R_5)$ and the slope dy/dx is infinite there. Notice that the x coordinate of point B is greater than 1 for all $\gamma > -1$. B lies below the x axis for $\gamma < 7$ and above it for $\gamma > 7$. Point C is the point at which $F(R_5)$ intersects B_4, the boundary separating R_1 from R_4. Note that if $\gamma = 1$, point C lies at $(1,0)$.

Point D is the intersection of $F(R_5)$ with the x axis. The slope of $F(R_5)$ at point D is

$$\frac{1}{\ell}\left[\frac{2}{\left(\frac{1+\gamma}{2}\right)^{1/2} - 2}\right]$$

Note that for $\gamma = 7$ point B coincides with point D, and the slope is infinite at that point. The slope of $F(R_5)$ approaches $-1/\ell$, the slope of B_1, as $y \to \infty$.

Figure 21 shows $F(R_5)$, drawn approximately to scale for $\ell = 1/2$, and for three different values for γ : $\gamma = 0$, $\gamma = 1$, and $\gamma = 7$.

It is clear from the symmetry of the phase plane that the mapping of R_6, the lower portion of the dead zone, is similar to the mapping of R_5. The map $F(R_6)$ is just the image, through the origin, of $F(R_5)$. $F(R_6)$ is not shown in Figs. 20 and 21, but it will be used and shown in later figures.

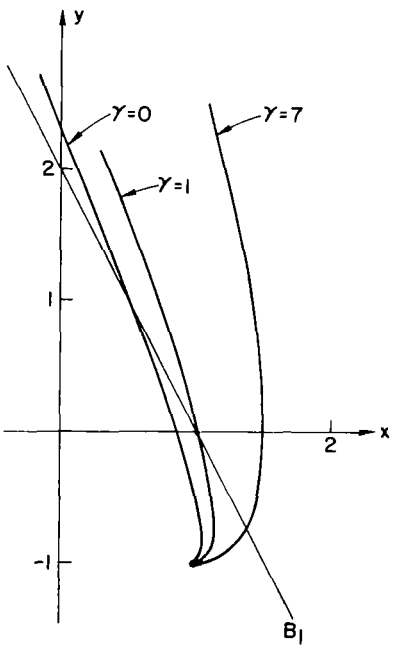

Fig. 21. STATE TRANSITION MAP OF THE DEAD ZONE $F(R_5)$ FOR $\ell = 1/2$ AND THREE DIFFERENT VALUES OF γ.

C. Two-Pulse Limit Cycles

A two-pulse limit cycle, if it exists, must lie in the phase plane between the limits $y = 1$ and $y = -1$, because the amplitude of the limit cycle in the y direction can be at most 1. Therefore, we begin our determination of the stability of two pulse limit cycles by observing the transient behavior of the system for starting states z_o in the dead zone and in the strip lying between $y = 1$ and $y = -1$. Because of the symmetry of the system we need consider only those starting points in the upper half of this strip.

We trace the trajectory of $z(t)$, using the mapping of the dead zone derived in the previous section. As the first example take $\gamma > 1$, then the two maps $F(R_5)$ and $F(R_6)$ appear (not to exact scale) as in Fig. 22; z_o is taken at a point slightly above the line $y = 1/2$, as shown. The trajectory emanating from this initial state will be horizontal until it strikes the curve B_3' (see Fig. 19) at time t_1^-, and then it will drop abruptly by 1 unit in the y direction; this drop corresponds to the sudden change in angular velocity of the satellite brought about by the firing of the gas valve at $t = t_1$. The state at $t = t_1^+$, z_1, lies on the map $F(R_5)$ because $z_o \in R_5$; this is shown

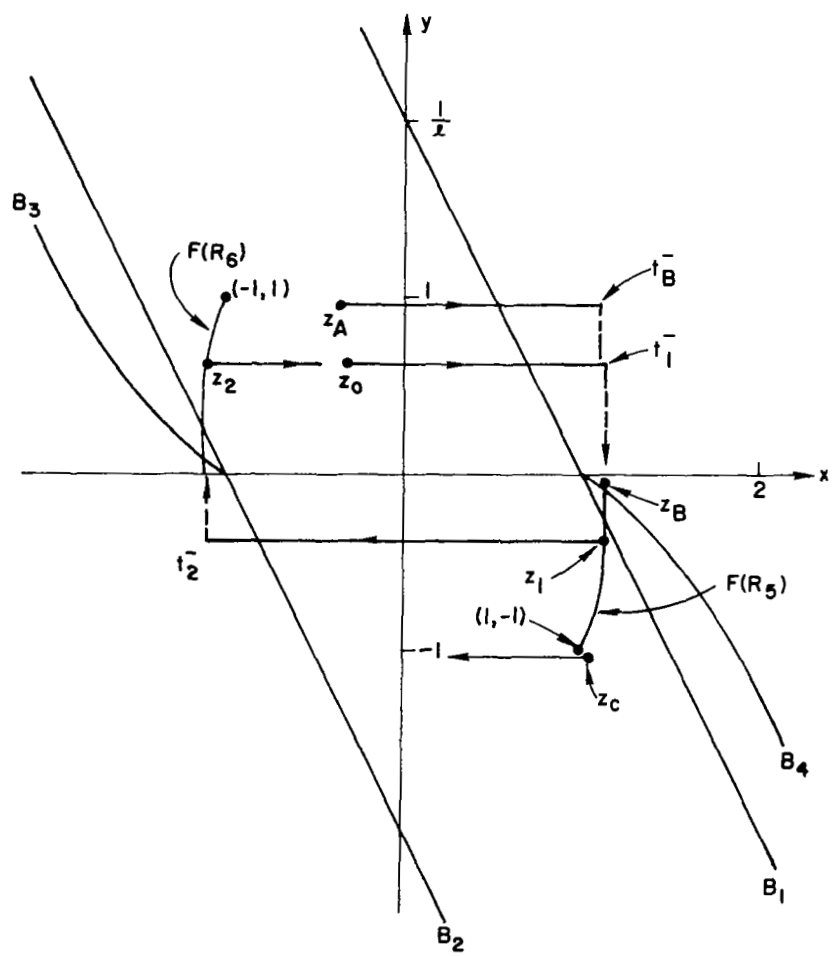

Fig. 22. STATE TRANSITIONS FOR POINTS IN THE DEAD ZONE, $\gamma > 1$.

in Fig. 22. The trajectory from z_1 is again horizontal, moving toward the left. Now, since z_1 lies in the dead zone, in R_6, the valve will fire at $t = t_2$ so as to put z_2 on the map $F(R_6)$, at the same y coordinate as that of the initial state z_o, as shown. But z_2 is also in the dead zone so it will be mapped into the same point of $F(R_5)$ as was z_o, namely the point indicated by z_1. That a two-pulse limit cycle has been established is clear because each successive state is mapped into the dead zone. This limit cycle is slightly unsymmetrical because the trajectory does not pass through the $y = 1/2$ and $y = -1/2$ lines. Peak to peak amplitude of the $x(t)$ oscillation will be slightly greater than 2; this means the $\theta(t)$ oscillation will have a peak-to-peak value of slightly more than $2\theta_d$ or approximately that established as the design goal in the design of the modulator (Chapter II).

Notice that the two-pulse limit cycle established here is "neutrally stable" in that a small change in z_o in the y direction will lead to a two-pulse limit cycle adjacent to the original one. Because of the finite, constant strength, torque impulse imparted to the system at each firing instant, the trajectory cannot return to the original limit cycle after a small perturbation in the y direction. It will return, however, for a small perturbation in the x direction. Hence, "neutral stability" of the limit cycles, as illustrated here, is the best one can ask for in this system.

Consider next a trajectory starting in the dead zone but at a different level of velocity, as indicated by z_A in Fig. 22. We ask if this trajectory will lead to a two-pulse limit cycle. y_A is slightly less than 1, so that z_A will map into a point on $F(R_5)$ just slightly below the x axis, shown as z_B. Now, z_B is in region R_1 which means that the horizontal trajectory leaving z_B, toward the left, will be very short and the switch instant t_C will occur before the trajectory strikes B_1. Therefore, z_B will map into $z_C = F(z_B)$ and, although it appears that z_C will be in the dead zone, its y coordinate will be slightly <u>less than</u> $y = -1$, as shown. Therefore, $z_D = F(z_C)$ will lie <u>below</u> the x axis. $z_E = F(z_D)$ will be back at the same y level as the original state z_A, and if z_E lies in the dead zone, the trajectory emanating from it will coincide with the original portion of the trajectory,

and the system will be in a limit cycle oscillation, but it will be a four-pulse limit cycle oscillation. It is now clear that, because z_B is in region R_1, there cannot be a two-pulse limit cycle with a trajectory passing through point z_A. It is also clear that the same holds true for points displaced slightly in the y direction from z_A.

In Chapter V, the higher order limit cycles, starting from points such as z_A, are considered in detail. Now, however, we turn to the question of eliminating the conditions under which they can occur.

In Fig. 22, the trajectory starting at z_o converged, in a single step, to a two-pulse limit cycle, while that starting from z_A did not. The apparent difference between the two trajectories is that z_1 lies on $F(R_5)$ in the dead zone, while z_B lies on $F(R_5)$ in region R_1. Figures 20 and 21 show that if $\gamma \leq 1$, $F(R_5)$, in the strip bounded by $y = 0$ and $y = -1$, will lie completely within the dead zone, therefore, any z_o in R_5 (below $y = 1$) will map into a z_1 in R_6. And, if $z_1 \in R_6$, then z_1 will map onto that portion of $F(R_6)$ which lies completely within R_5. Hence, for $\gamma \leq 1$, any z_o in the dead zone lying between $y = 1$ and $y = -1$ will be the starting point for a trajectory that quickly converges to a stable (neutrally so!) two-pulse limit cycle. Figure 23 illustrates three such two-pulse limit cycles shown for $\gamma = 0.9$, $\ell = 1/2$. The digital simulation described in Chapter III and in the Appendix was employed to calculate some of these trajectories. The results of two such calculations are given in Table 5. These results verify the exact behavior to be expected from the geometrical relationship shown in Fig. 23.

If z_o lies on $y = 1$, $y = 0$, or $y = -1$, the trajectory will come to rest on B_5 and will remain there indefinitely. This degenerate case is not discussed further here.

D. Convergence of Trajectories From Arbitrary Initial States

It was shown in Section IV.C, that $\gamma \leq 1$ is a necessary and sufficient condition for the convergence of the state trajectory to a stable two-pulse limit cycle starting from any initial point in the dead zone lying between the limits $y = 1$ and $y = -1$. In this section, the fates of these trajectories that start from initial points outside this small

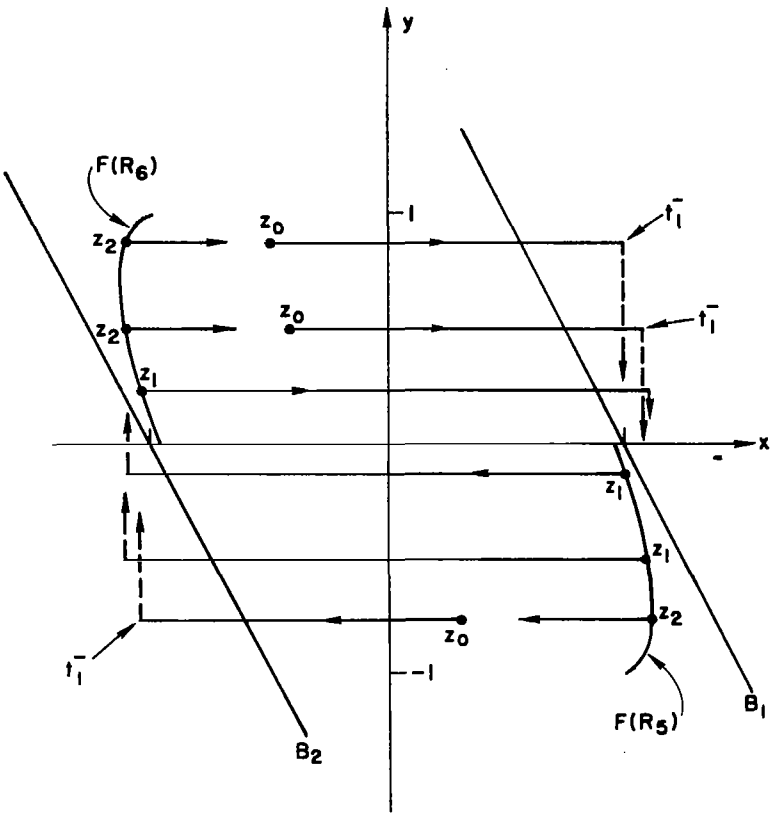

Fig. 23. THREE TRAJECTORIES THAT START IN THE DEAD ZONE AND IMMEDIATELY CONVERGE TO TWO-PULSE LIMIT CYCLES, $\gamma < 1$.

trapezoidal region are determined, and the conditions under which they converge to a stable two-pulse limit cycle oscillation are revealed.

At the outset, it is clear that $\gamma \leq 1$ is a necessary condition for all trajectories to converge to two-pulse limit cycles. For if $\gamma > 1$, then any trajectory leading to a point such as z_A in Fig. 22 cannot converge to a two-pulse limit cycle. It is also clear that $\ell > 0$ is also a necessary condition for such convergence. If $\ell = 0$ (the dead-zone boundaries parallel to the y axis), a trajectory starting at any integer value of y, or an integer plus 1/2 from inside the dead zone, will immediately enter an "undamped" multipulse limit cycle oscillation. A negative ℓ corresponds to negative damping, and the oscillations will diverge.

Assuming $\ell > 0$ and $\gamma \leq 1$, we now investigate the trajectories for initial points at arbitrary locations in the state plane. Note

Table 5

TRAJECTORIES CONVERGING TO TWO-PULSE LIMIT CYCLES, $\gamma = 0.9$, $\ell = 0.5$

k	x_k	y_k
0	0.985	0.01
1	1.044	-0.99
2	-0.990	0.01
3	1.044	-0.99
4	-0.990	0.01
0	1.093	-0.40
1	-1.108	0.60
2	1.077	-0.40
3	-1.108	0.60
4	1.077	-0.40

first that if $\gamma < 1$ (see Fig. 21), there will be points on $F(R_5)$ above the x axis, as high as $y = (1-\gamma)/(1+\gamma)$, which lie in R_5 itself. Therefore, any z_o in R_5 lying below a y level of $1 + (1-\gamma)/(1+\gamma) = 2/(1+\gamma)$ will map into the dead zone and hence will eventually enter a two-pulse limit cycle oscillation like one of those shown in Fig. 23. Hence, the region of the dead zone lying between the limits $y = -2/(1+\gamma)$ and $y = 2/(1+\gamma)$ may be considered to be a "capture zone" (CZ) in that any trajectory which eventually has a state z_k in this zone will converge to a two-pulse limit cycle. The CZ is illustrated in Fig. 24.

Because of the symmetry of the state plane, a trajectory starting from a given point z_o in R_1 will be similar to the trajectory starting from the point in R_2 which is the image of z_o through the origin. The same is true of points in R_4 corresponding to initial points in R_3 and also for corresponding points in R_5 and R_6. Therefore, only initial points in R_1, R_3, and R_5 need be considered.

Consider next those initial points lying in R_3, R_5, and R_1 above the x axis. The fates of the trajectories emanating from all these points are subject to the following argument. Because the state vector $z(t)$ is never at rest in these regions, and because it always progresses

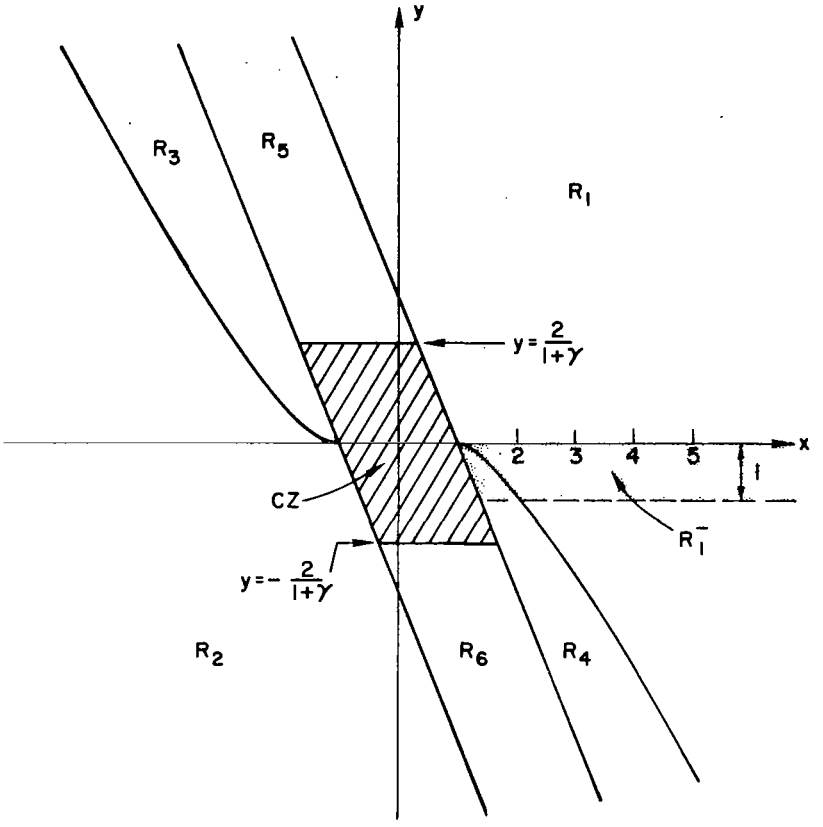

Fig. 24. R_1^- AND THE CAPTURE-ZONE CZ.

toward the right and downward, only one of two possible things can happen to $z(t)$. It may pass into CZ and be in CZ at a firing instant t_k, in which case $z(t)$ will converge to a two-pulse limit cycle. Or, $z(t)$ may cross the x axis to the right of the point $(1,0)$, headed downward. In the latter case, a firing instant t_k must occur somewhere in the strip of unit width just below the x axis (shaded area shown in Fig. 24 as R_1^-). Therefore, all of the trajectories starting in R_3, R_5, and R_1 (above the x axis) that do not enter CZ will have state points $z_k \in R_1^-$. Furthermore, any initial state lying in R_1 below the strip R_1^- can be considered to be a point on some trajectory which emanated from an initial state lying in R_1^-. Therefore, we need only consider trajectories starting from points in R_1^- and, if these can all be shown

to converge to two-pulse limit cycles, then the same is true for all points in the state plane, except, of course, for the degenerate points in B_5.

Before proceeding with the convergence proof, it is of interest to note the nature of the trajectories starting from initial points in $\bar{R}_1$. Three of these, for initial states having large magnitudes, are shown in Fig. 25, and three for small initial states are shown in Fig. 26. These

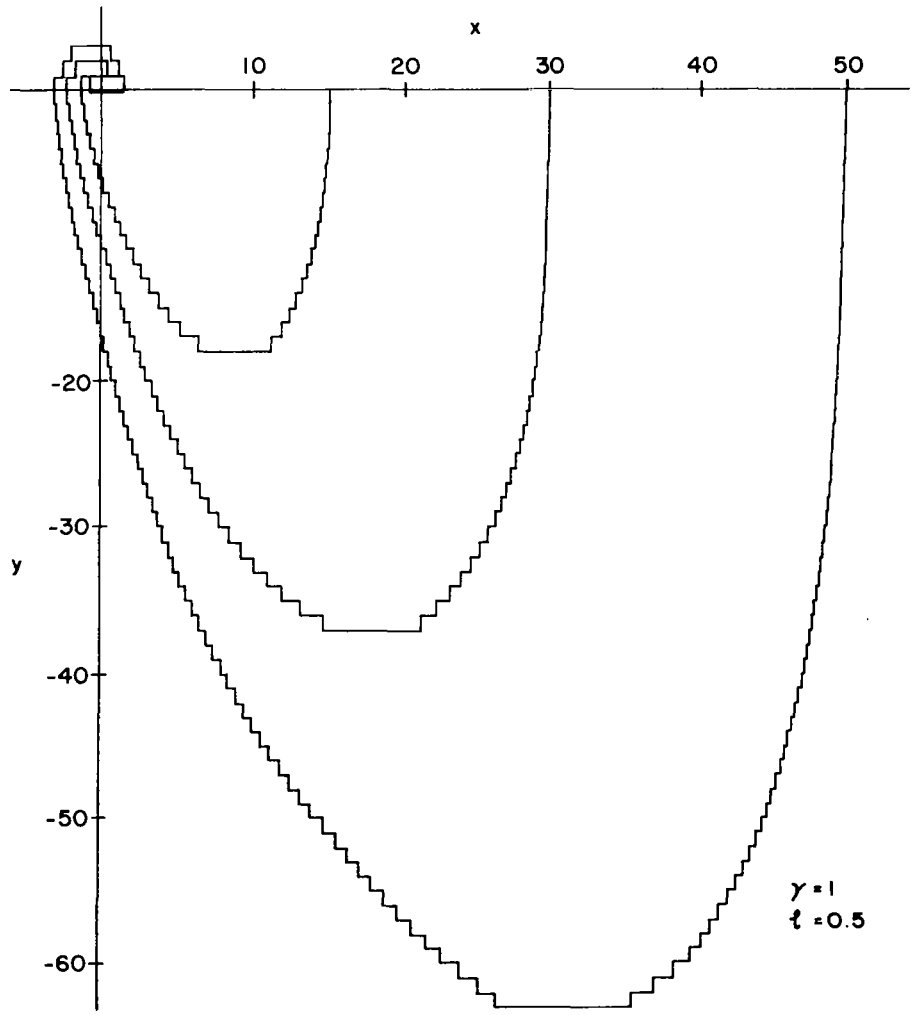

Fig. 25. TYPICAL TRAJECTORIES CONVERGING TO UNSYMMETRICAL TWO-PULSE LIMIT CYCLE FROM REMOTE INITIAL POINTS, $\gamma = 1$ AND $\ell = 0.5$.

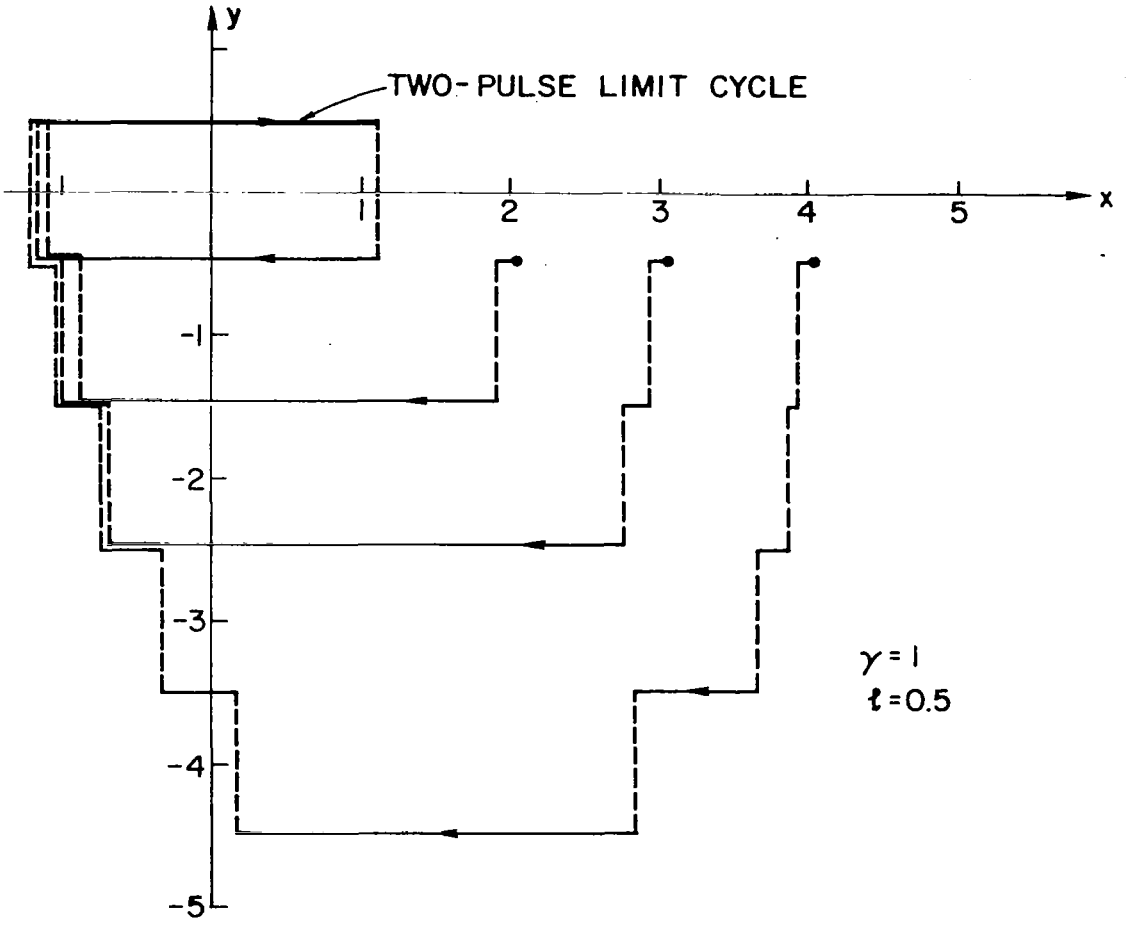

Fig. 26. TYPICAL TRAJECTORIES CONVERGING TO SYMMETRICAL TWO-PULSE LIMIT CYCLE.

trajectories were obtained from the digital simulation of the system described in Chapter III and in the Appendix. These computer runs were made for $\ell = 0.5$ and $\gamma = 1$. Other runs for ℓ as small as 0.01 showed convergence to CZ nearly as abrupt as that shown here. The two-pulse limit cycle in Fig. 26 is symmetrical because the initial value of the y coordinate is -1/2. The limit cycle shown in Fig. 25 is not symmetrical because the initial value of the y coordinate is -0.1, which requires all subsequent y coordinates to have values differing from -0.1

by integer terms only. Hence the y coordinates of the limit cycle are +0.9 and -0.1.

A proof that the trajectories will converge from any initial point in $\bar{R}_1$ can be based on an argument which depends on the "staircase" nature of the trajectories which is so evident in Figs. 25 and 26. Figure 27 represents the staircase characteristic schematically (not to scale). We can show that the point z_{2k+3}, lying on the trajectory which emanates from $z_o \in \bar{R}_1$, is closer to the y axis, by a positive amount δ bounded away from zero, than is z_o itself. That portion of the trajectory subsequent to z_{2k+3} will either lead into the CZ, or cross the positive x axis and have a state point at the same y level as z_o, but closer to the y axis. Hence the trajectory will eventually converge to the CZ.

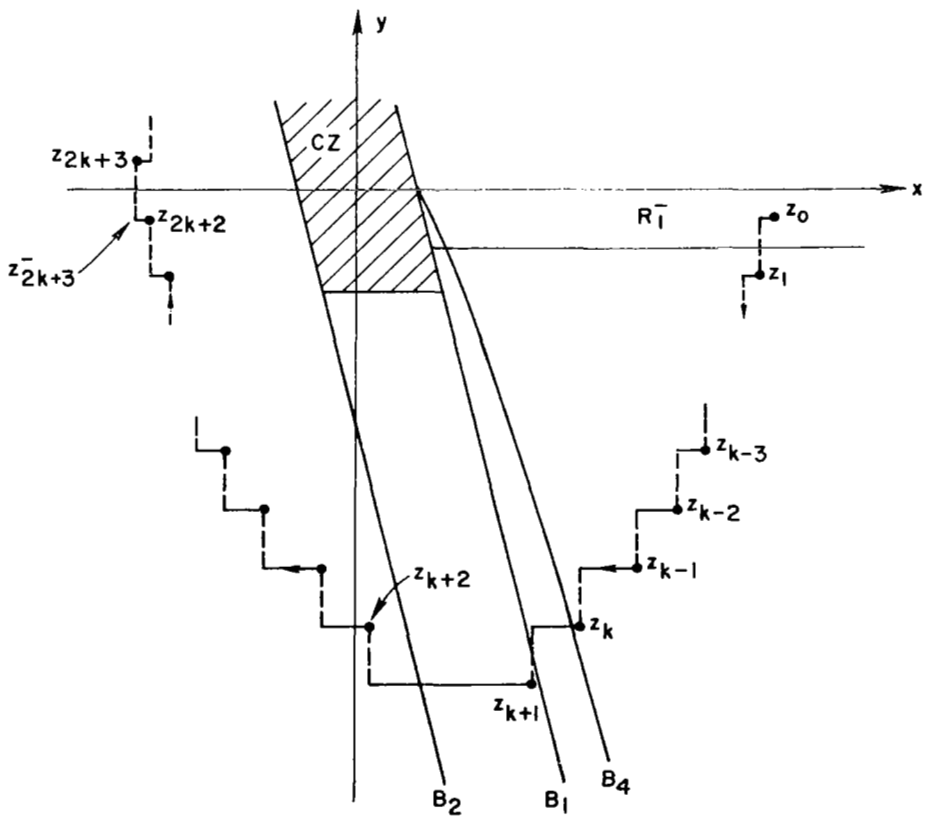

Fig. 27. STAIRCASE NATURE OF THE STATE TRAJECTORY.

If the total width of the (k+1) steps leading downward from z_o to z_{k+1} were exactly equal to the total width of the (k+1) steps leading upward from $\bar{z}_{k+2}$ to $\bar{z}_{2k+3}$, then a simple demonstration that $|x_{k+2}| < x_{k+1}$ would be sufficient to prove that z_{2k+3} is closer to the y axis than is z_o. It is difficult to calculate the total width of the (k+1) steps in question. Furthermore, a comparison of individual step widths shows that in some cases an ascending step can actually be wider than its counterpart (at the same y level) in the descending staircase. However, in our proof, it is not necessary that each ascending stair be narrower than (or equal to) its descending counterpart, nor is it necessary that the total widths of the staircases be equal. The total width of the ascending stairs can, in fact, be the wider of the two, as shown by the trajectories in Fig. 25.

Instead of comparing the descending staircase with the ascending one, let us compare the width of a step on the descending path to a step lying at the same y level but on the ascending path of a fictitious trajectory whose terminal point has an x coordinate which is less in magnitude, by a finite amount, than the x coordinate of the starting point of the step on the descending path. This situation is illustrated in Fig. 28. The magnitude of the x coordinate of the

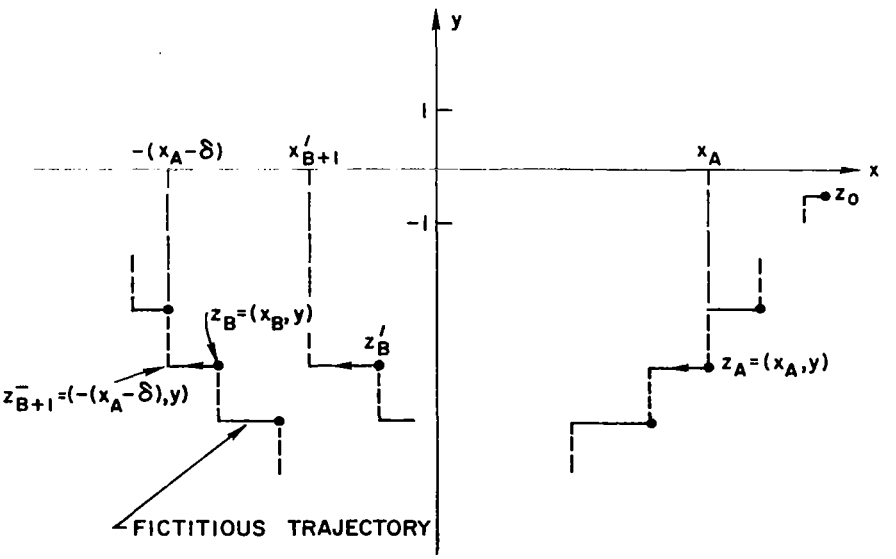

Fig. 28. FICTITIOUS TRAJECTORIES FOR USE IN CONVERGENCE PROOF, $y_o < -1/2$.

terminal point of step z_B is $(x_A-\delta)$, where δ is a positive quantity, independent of x_A and y, and is to be suitably chosen. x_A is the x coordinate of the initial point of step z_A. We will show that the width of step z_B is less than that of step z_A. Then we can make use of the fact that, for a given value of y, the width of a step on a trajectory becomes smaller as the initial point is moved farther from the dead zone. (This is simply a result of the faster charging time of the integrator for larger input voltages.) To compare the widths of steps z_A and z_B, we simply need to compare $\triangle_A = (t_{A+1}-t_A)$ and $\triangle_B = (t_{B+1}-t_B)$, because the two steps are at the same y (velocity) level.

To calculate $\triangle_A$ and $\triangle_B$ in terms of the normalized coordinates, we use the expressions for $e(t)$, developed in Chapter III, along with the relationships

$$\ell = \frac{\mu a}{J\theta_d} \qquad A = \frac{K\mu a^2}{4J}$$

$$\theta = \theta_d x \qquad \dot{\theta} = \frac{\mu}{J} y \qquad \dot{x} = \frac{\ell}{a} y \tag{4.7}$$

For $z_A \in R_1$, the voltage into the integrator is

$$e_A(t) = K(\theta + a\dot{\theta} - \theta_d) \tag{4.8}$$

and, for $z_B \in R_2$, it is

$$e_B(t) = K(\theta + a\dot{\theta} + \theta_d) \tag{4.9}$$

Now, in each case $\dot{\theta} = (\mu/J)\, y$. For z_A, we have

$$\theta(\tau_1) = \theta_A + \dot{\theta}\tau_1 \tag{4.10}$$

where $\tau_1 = t-t_A$ and

$$\theta_A = \theta_d x_A \tag{4.11}$$

For z_B, we have

$$\theta(\tau_2) = \theta_B + \dot{\theta}\tau_2 \tag{4.12}$$

where $\tau_2 = t - t_B$, and θ_B is the initial point of the step z_B and is related to θ_A by

$$\theta_B = -(\theta_A - \delta_\theta) - \dot{\theta}\Delta_B \tag{4.13}$$

where $\delta_\theta = \delta\theta_d$.

Now, combining Eqs. (4.10) to (4.13) with Eqs. (4.7) to (4.9) yields

$$e_A(\tau_1) = K\theta_d\left[x_A + \ell y - 1 + \left(\frac{\ell y}{a}\right)\tau_1\right]$$

$$e_B(\tau_2) = K\theta_d\left[1 - (x_A - \delta) + \ell y - \left(\frac{\ell y}{a}\right)\Delta_B + \left(\frac{\ell y}{a}\right)\tau_2\right] \tag{4.14}$$

To calculate Δ_A and Δ_B we evaluate the following integrals at the instants of firing

$$\int_0^{\Delta_A} e_A(\tau_1)\, d\tau_1 = A(1 + \gamma)$$

$$\int_0^{\Delta_B} e_B(\tau_2)\, d\tau_2 = -A(1 + \gamma) \tag{4.15}$$

These integrals yield the following quadratic formulas which must be solved for their least positive roots.

$$\left(\frac{\ell y}{2a}\right)\Delta_A^2 + (x_A + \ell y - 1)\Delta_A - \frac{a\ell(1 + \gamma)}{4} = 0$$

$$\left(\frac{\ell y}{2a}\right)\Delta_B^2 + (x_A - \delta - \ell y - 1)\Delta_B - \frac{a\ell(1 + \gamma)}{4} = 0 \tag{4.16}$$

We note that y is negative, so the least positive roots of these expressions are

$$\Delta_A = \frac{(x_A + \ell y - 1) - \sqrt{(x_A + \ell y - 1)^2 + \frac{\ell^2(1+\gamma)}{2} y}}{-\left(\frac{\ell y}{a}\right)}$$

$$\Delta_B = \frac{(x_A - \delta - \ell y - 1) - \sqrt{(x_A - \delta - \ell y - 1)^2 + \frac{\ell^2(1+\gamma)}{2} y}}{-\left(\frac{\ell y}{a}\right)} \tag{4.17}$$

We form the difference $\Delta_A - \Delta_B$ as

$$\frac{2\ell y + \delta - \sqrt{(x_A + \ell y - 1)^2 + \frac{\ell^2(1+\gamma)}{2} y} + \sqrt{(x_A - \delta - \ell y - 1)^2 + \frac{\ell^2(1+\gamma)}{2} y}}{-\left(\frac{\ell y}{a}\right)} \tag{4.18}$$

Now, the conditions on δ to insure (4.18) being positive and thus step z_A being wider than step z_B (Fig. 28) must be found. In the condition under consideration, y is negative, so we consider only the numerator of (4.18). We also note that for $y = 0$, (4.18) is invalid, and that steps z_A and z_B are equal in width, but that the width is zero. The numerator of (4.18) is rearranged as

$$\sqrt{(x_A - \delta - \ell y - 1)^2 + \beta^2 y} - \sqrt{(x_A + \ell y - 1)^2 + \beta^2 y} + (2\ell y + \delta) \tag{4.19}$$

where $\beta^2 = [\ell^2(1+\gamma)]/2$ is used to simplify the expression.

We now pose the question of (4.18) being positive by forming an inequality out of the three terms in (4.19)

$$\sqrt{(x_A - \delta - \ell y - 1)^2 + \beta^2 y} \overset{?}{>} \sqrt{(x_A + \ell y - 1)^2 + \beta^2 y} - (2\ell y + \delta) \tag{4.20}$$

The symbol $\overset{?}{>}$ means that if δ is such that the left side of (4.20) is greater than the right side, then (4.18) is positive. The left side of (4.20) is positive, and the right side is also positive, provided the following inequality is satisfied

$$\sqrt{(x_A + \ell y - 1)^2 + \beta^2 y} > (2\ell y + \delta) \tag{4.21}$$

We accept (4.21) as a constraint on δ, so both sides of (4.20) may be squared without losing the validity of the question indicated by the $\overset{?}{>}$ symbol. If both sides of (4.20) are squared and terms common to both sides are eliminated, the question posed by (4.20) is reduced to

$$-2\ell y(x_A - 1) - \ell y\delta - \left[\delta(x_A - 1) + 2\ell^2 y^2\right] \overset{?}{>} -(2\ell y + \delta)\sqrt{(x_A + \ell y - 1)^2 + \beta^2 y} \tag{4.22}$$

If the following condition is met, the right side of (4.22) will be positive

$$2\ell y + \delta < 0 \tag{4.23}$$

The left side will be positive if

$$-2\ell y(x_A - 1) - \ell y\delta > \delta(x_A - 1) + 2\ell^2 y^2 \tag{4.24}$$

We accept both conditions (4.23) and (4.24), and we square both sides of (4.22). Many common terms appear on each side of the $\overset{?}{>}$ sign. This allows the question to be resolved to the simple form of

$$0 \overset{?}{>} 4\ell^2 y^3 + 4\delta\ell y^2 + \delta^2 y \tag{4.25}$$

Note that (4.25) can be written as

$$0 \overset{?}{>} y[\delta + 2\ell y]^2 \tag{4.26}$$

which is clearly satisfied for $y < 0$ and for any δ. Thus, if we can find a positive δ to satisfy the three conditions, (4.21), (4.23), and (4.24), and not depend upon x_A or y, the positivity of (4.18) will be assured.

Consider the case $\delta = \ell$. With this condition (4.21) becomes

$$\sqrt{(x_A + \ell y - 1)^2 + \beta^2 y} > \ell(2y + 1) \tag{4.27}$$

If y is restricted to the range of

$$y < -\frac{1}{2} \tag{4.28}$$

then (4.21) is satisfied. Condition (4.23), with $\delta = \ell$ and $y < -1/2$, is also satisfied, so (4.28) replaces both (4.21) and (4.23) as the condition for the positivity of (4.18). Finally, condition (4.24), with $\delta = \ell$, becomes

$$-\ell(x_A - 1)(2y + 1) > \ell^2 y(2y + 1) \tag{4.29}$$

For $y < -1/2$, both sides of (4.29) may be divided by $-\ell(2y + 1)$, thus reducing the condition to

$$x_A > 1 - \ell y \tag{4.30}$$

This is obviously satisfied because $z_A \in R_1$, which puts z_A well to the right of the boundary of the dead zone. Therefore, with $\delta = \ell$ for $y < -1/2$, the width of step z_B in Fig. 28 is less than the width of the corresponding step z_A. The proof of convergence is completed by the following argument.

Consider a state point z'_B, lying to the right of z_B but at the same y level on a second fictitious trajectory, as shown in Fig. 28. Because z'_B is closer to the dead zone than is z_B, the "step" z'_B is wider than the step z_B and $|x'_{B+1}| < |-x_A|$, as shown. Now, if z'_B happens to lie on the "real" trajectory (the same trajectory

containing z_A), then the step Z'_B can be wider than the step z_A. (It can also be narrower.) Thus, if a step on the ascending staircase is wider than its counterpart on the descending staircase, then that step must lie to the right of the fictitious step z_B, whose terminal point z^-_{B+1} is known to be closer to the y axis by an amount at least $\delta = \ell$ than is the starting point of step z_A. This is true for all the steps having y levels less than -1/2, so the point z_{2k+3} (see Fig. 27) lies closer to the y axis, by the positive amount δ, than does z_o, provided $-1/2 > y_o \geq -1$. Hence, the trajectory will eventually converge to a point $z_k \in CZ$.

For z_o lying in the strip $0 > y_o \geq -1/2$, convergence is guaranteed under the following argument. [Refer to Fig. 29, which shows a trajectory starting at $z_o = (x_A, y_o)$.] The width of the initial step of this

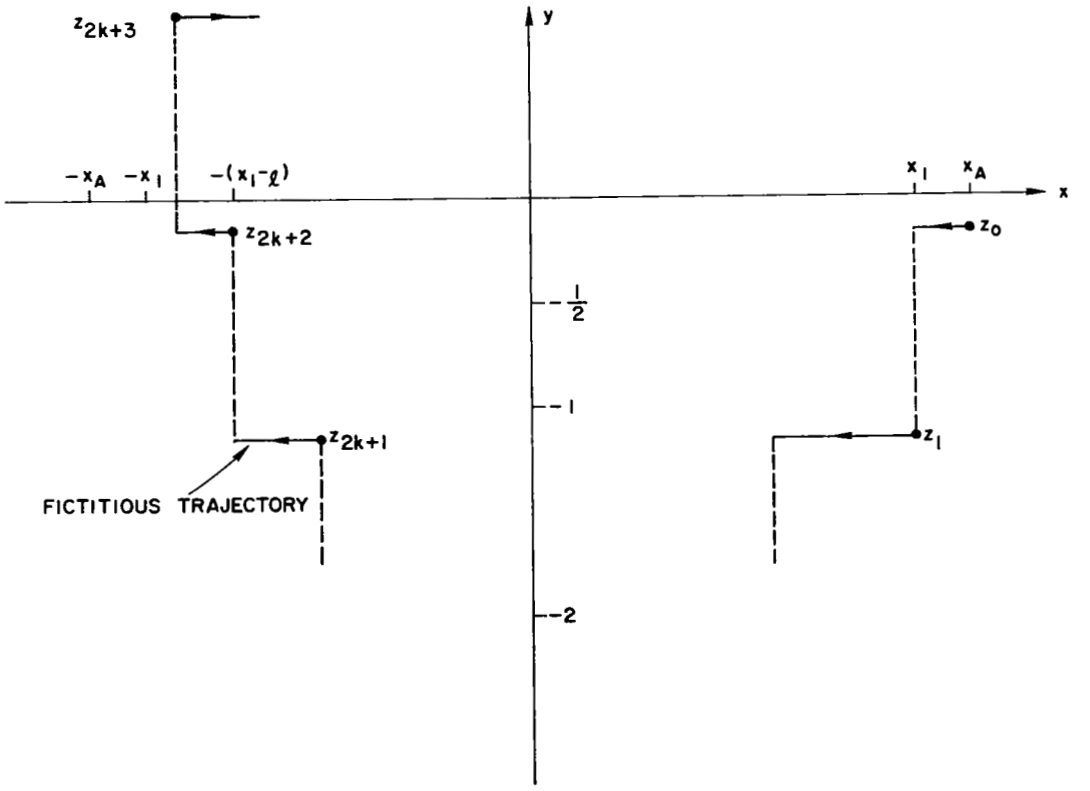

Fig. 29. FICTITIOUS TRAJECTORY FOR USE IN CONVERGENCE PROOF, $0 > y_o \geq -1/2$.

of this trajectory is $(x_A - x_1)$, as shown. By the argument developed above, the terminal point of step z_{2k+1} must lie to the right of the line $x = -(x_1 - \ell)$. Figure 29 shows the fictitious trajectory which bounds all possible real trajectories (starting from z_o) on the left.

The width of the initial step may be determined by combining (4.7) and (4.17)

$$(x_A - x_1) = (x_A + \ell y_o - 1) - \sqrt{(x_A + \ell y_o - 1)^2 + \frac{\ell^2(1+\gamma)}{2} y_o} \qquad (4.31)$$

Similarly, the width of step z_{2k+2} is determined for $\delta = \ell$, as

$$|x_{2k+3} - x_{2k+2}| = (x_A - \ell - \ell y_o - 1) - \sqrt{(x_A - \ell - \ell y_o - 1)^2 + \frac{\ell^2(1+\gamma)}{2} y_o} \qquad (4.32)$$

From Fig. 29, it is apparent that convergence is assured, if

$$(x_1 - \ell) + |x_{2k+3} - x_{2k+2}| < x_A \qquad (4.33)$$

From (4.31) and (4.32), the left side of (4.33) may be calculated in terms of x_A

$$(x_1 - \ell) + |x_{2k+3} - x_{2k+2}| = x_A - 2\ell(1+y_o) - \sqrt{(x_A - \ell - \ell y_o - 1)^2 + \frac{\ell^2(1+\gamma)}{2} y_o} + \sqrt{(x_A + \ell y_o - 1)^2 + \frac{\ell^2(1+\gamma)}{2} y_o} \qquad (4.34)$$

From this expression, it is apparent that (4.33) will hold, provided that the following inequality is valid

$$2\ell(1+y_o) + \sqrt{(x_A - \ell - \ell y_o - 1)^2 + \frac{\ell^2(1+\gamma)}{2} y_o} \overset{?}{>} \sqrt{(x_A + \ell y_o - 1)^2 + \frac{\ell^2(1+\gamma)}{2} y_o} \qquad (4.35)$$

In proving the validity of (4.35), the following notational changes are convenient

$$y_o = -\alpha \qquad \left(\frac{1 - \alpha}{1 - 2\alpha}\right)^2 = b$$

$$\frac{x_A - 1}{\ell} = k \qquad \frac{1 + \gamma}{2} = \zeta \tag{4.36}$$

Both ℓ and $(x_A - 1)$ are positive, and γ is less than or equal to unity, so the conditions on the newly defined parameters α, k, b, and ζ under which (4.35) is to be valid

$$0 < \alpha \leq \frac{1}{2} \qquad b \geq 1$$

$$k > 0 \qquad \zeta \leq 1 \tag{4.37}$$

Equation (4.35), expressed in the simplified notation of (4.36), is

$$2(1 - \alpha) + \sqrt{(k - 1 + \alpha)^2 - \zeta\alpha} \overset{?}{\geq} \sqrt{(k - \alpha)^2 - \zeta\alpha} \tag{4.38}$$

Each term in (4.38) is positive under the conditions (4.37), so both sides of (4.38) may be squared without changing the validity of the $\overset{?}{\geq}$ symbol. Squaring both sides and rearranging the terms yields

$$1\alpha^2 + 4(1 - \alpha)\sqrt{(k - 1 + \alpha)^2 - \zeta\alpha} \overset{?}{\geq} (1 - 2\alpha)(2k - 5) \tag{4.39}$$

The left side of (4.39) is positive for all allowable combinations of α, ζ, and k, and the right side is negative for $k < 5/2$. Therefore, (4.39) (without the ?) is valid for $k < 5/2$, and we need be concerned only about the case $k \geq 5/2$.

We note at this point that (4.39) must be proved valid for $\alpha = 0$. Therefore, the term $4\alpha^2$ may be dropped and (4.39) reduced to

$$4(1 - \alpha)\sqrt{(k - 1 + \alpha)^2 - \zeta\alpha} \overset{?}{>} (1 - 2\alpha)(2k - 5) \qquad (4.40)$$

Now, (4.40) [without the ? for $k > 5/2$ and for α, b, and ζ, as in (4.36)] is a sufficient condition for the validity of (4.35) and hence for the convergence of all trajectories to the CZ.

Using the notation introduced in (4.36), (4.40) may be written as

$$4b^{1/2}\sqrt{(k - 1 + \alpha)^2 - \zeta\alpha} \overset{?}{>} (2k - 5) \qquad (4.41)$$

Both sides of (4.41) are positive, so both sides may be squared

$$16b\,[(k - 1 + \alpha)^2 - \zeta\alpha] \overset{?}{>} 4k^2 - 20k + 25 \qquad (4.42)$$

Expanding the left side of (4.42) and rearranging the terms yields

$$4k^2[3b + (b - 1)] + 5(4k - 5) + 16b[1 + \alpha^2 + 2\alpha k] \overset{?}{>} 16b[2k + 2\alpha + \zeta\alpha] \qquad (4.43)$$

Now the following inequalities hold because of the conditions (4.37)

$$\begin{aligned} 16b &\geq 32b\alpha \\ 32bk\alpha &\geq 32b\zeta\alpha \end{aligned} \qquad (4.44)$$

Therefore, (4.43) may be reduced to

$$4k^2[3b + (b - 1)] + 5(4k - 5) + 16b\alpha^2 + 16b\alpha k \overset{?}{>} 32bk \qquad (4.45)$$

where the = sign must be included because of the $\geq$ signs in (4.44). However, the = sign holds in (4.44) only for $\alpha = 1/2$. Therefore, since $b \geq 1$, if the term $16b\alpha^2$ is dropped from the left side of (4.45), the = sign may also be dropped. Equation (4.45) must also hold for $\alpha = 0$, so the term $16b\alpha k$ can be dropped. This reduces (4.45) to

$$4k^2[3b + (b-1)] + 5(4k-5) \overset{?}{>} 32bk \tag{4.46}$$

which must hold for $b > 1$ and $k > 5/2$.

It is convenient to rearrange (4.46) to

$$bk[12k-32] + 4k^2(b-1) + 5(4k-5) \overset{?}{>} 0 \tag{4.47}$$

where $k \geq 5/2$ and $b \geq 1$. We note that, for any value of b, the minimum value of the left side of (4.47) occurs for $k = 5/2$. Thus, if (4.47) holds for $k = 5/2$ and for all $b \geq 1$, the proof will be complete. Substituting $k = 5/2$ into (4.47) yields

$$20b \overset{?}{>} 0 \tag{4.48}$$

which obviously holds for $b \geq 1$. Thus the original inequality (4.33) is proved to be valid, and the convergence of all trajectories starting at points $z_o \in \bar{R}_1$ to the CZ is assured.

E. Summary

In this chapter, it has been shown that the necessary and sufficient conditions on the system parameters for the existence of stable two-pulse limit cycles, and no other limit cycles, are $\ell > 0$ and $\gamma \leq 1$. These conditions imply that a, the lead ratio of the rate network, must be positive and the setting of the integrator threshold must be

$$(\text{Integrator Threshold}) \leq \frac{K\mu a^2}{2J}$$

This means the threshold can be set as much as 100 percent higher than its nominal value.

Chapter V

HIGHER ORDER LIMIT CYCLES

It has been shown that, if $\gamma \leq 1$ and $\ell > 0$, a trajectory starting from any $z_o \notin B_5$ will converge to a stable two-pulse limit cycle. Those results constitute the principal part of this dissertation in that they solve three of the four questions set forth in Chapter I. In this chapter the fourth question, the dynamic properties of the system for $\gamma > 1$, is investigated. The practical importance of the case $\gamma > 1$ can be questioned inasmuch as it represents an error in the integrator threshold setting of more than 100 percent from the nominal value which was chosen on the basis of the desired amplitude of the two-pulse limit cycle. Nevertheless, the results described here have revealed some very interesting dynamic behavior for the case $\gamma > 1$, and some practical information on the ultimate limits of γ has also been derived.

Sufficient conditions on γ and z_o, for the existence and stability of two-pulse limit cycles, are derived analytically here, and these are verified experimentally by trajectories obtained from the digital simulator. Certain other sufficient conditions on γ and z_o for the nonexistence of two-pulse limit cycles are derived; these too are verified experimentally. The trajectories in these cases are observed to converge to four-pulse limit cycles, six-pulse limit cycles, and higher order limit cycles, depending upon γ and z_o. Attention is confined to initial states z_o in the region surrounding the origin of the z plane for the analytical work, but it is not so restricted, of course, for the experimental work.

A. The (γ, y_o) Plane

In the analytical work described here, the intial point z_o will lie in the dead zone between the limits $-1 < y_o < 1$. Because of the symmetry of the state plane trajectories starting from z_o, points above the x axis are similar to trajectories starting from corresponding z_o points below the x axis, so we need only consider the case $0 < y_o < 1$. We assume that $\ell > 0$, and it turns out that, if

this condition is satisfied, ℓ does not influence the qualitative properties of limit cycle behavior (existence and stability) under study. In the graphical work, ℓ is taken to be 0.5 because this represents a practical value for ℓ, and the slope of B_1 is such that the geometrical features of the important curves in the state plane are evident. γ and the initial state z_o are the only parameters having influence on this behavior, so that results of the analysis may be displayed on the (γ, y_o) plane where $0 < y_o < 1$, and $\gamma > 1$. (It is understood that $\ell > 0$ and $z_o \in R_5$). We find boundary lines in (γ, y_o) that separate regions of two-pulse limit cycle behavior from regions of "non-two-pulse limit cycle" behavior; the latter regions are identified experimentally as four-pulse, six-pulse, etc. regions. It is convenient to study the (γ, y_o) plane by pieces because the geometrical structure of the state transition equation depends on γ. This structure is based upon the $F(R_5)$ curve described earlier in Figs. 20, 21, and 22 for the case $\gamma > 1$.

B. The Case $1 < \gamma \leq 3$

An accurate plot of the curve $F(R_5)$ [see Eq. (4.5)] for $\gamma = 3$ and $\ell = 0.5$ appears in Fig. 30. This curve is representative of the entire range of $1 < \gamma \leq 3$. Consider first z_o lying in the small strip just below the line $y = 1$ so that $1 < y_o < (\gamma+1+2\sqrt{\gamma})/[2(\gamma+1)]$. (Note that the width of this strip is $[(1/2 - \sqrt{\gamma}/(1+\gamma)]$ and that this width approaches zero as $\gamma \longrightarrow 1$.) Then, $z_1 = F_5(z_o)$ will lie on $F(R_5)$, but at a point just below the x axis and in R_1. Hence, $z_2 = F_1(z_1)$ will lie at some point <u>below</u> $y = -1$, and two additional pulses will be required subsequent to $t = t_2$ to bring the state z back up to the level y_o. Thus, z_o cannot be the initial state of a trajectory that converges to a two-pulse limit cycle. It can converge to a higher order limit cycle, and in fact, the experiments show it converging to a four-pulse limit cycle oscillation.

Consider next the fate of the trajectory starting at z_o, in the small strip of width $[1/2 - \sqrt{\gamma}/(1+\gamma)]$, just above the x axis. $z_1 = F_5(z_o)$ will lie in R_6, at a point on $F(R_5)$ <u>in the narrow strip</u> of width $[1/2 - \sqrt{\gamma}/(1+\gamma)]$, just above the line $y = -1$. Now the trajectory subsequent to $t = t_1$ will suffer the same fate as that in the

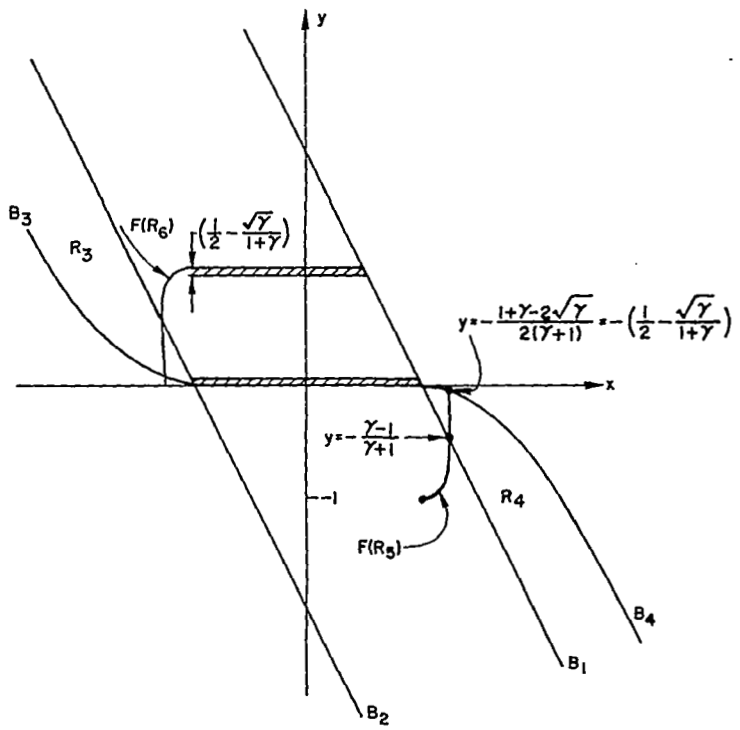

Fig. 30. $F(R_5)$ FOR $\gamma = 3$.

previous example because z_1 is in the strip in R_6, the counterpart to the strip in R_5, adjacent to the line $y = 1$. $z_2 = F_6(z_1)$ will lie in R_2, just above the x axis, so the trajectory cannot converge to a two-pulse limit cycle. Experiments show that it converges to a four-pulse limit cycle, similar to the one in the previous example, but is not the same one.

Consider next $z_o \in R_5$, lying below the line $y = 1 - (\gamma-1)/(\gamma+1)$ (thus $y_o \geq 1/2$ for $1 < \gamma \leq 3$), but not in the narrow strip adjacent to the x axis. $z_1 = F_5(z_o)$ now lies on $F(R_5)$ in R_6, so that $z_2 = F_6(z_1)$ will lie on $F(R_6)$ <u>at a point in</u> R_5, at the same y level as z_o. The trajectory subsequent to $t = t_1$ will therefore be in a two-pulse limit cycle oscillation.

Finally, we consider the initial condition $z_o \in R_5$, below the narrow strip adjacent to $y = 1$ but <u>above</u> the line $y = 1 - (\gamma-1)/(\gamma+1)$. Now, $z_1 = F_5(z_o)$ will lie on $F(R_5)$ <u>at a point in</u> R_4, in the strip

bounded above by $y = (1+\gamma-2\sqrt{\gamma})/[2(\gamma+1)]$ and below by $y = -(\gamma-1)/(\gamma+1)$. Now since $z_1 \in R_4$, z_2 will not lie on $F(R_6)$ but at a point to the left of $F(R_6)$, and at a y level the same as y_o. If $z_2 \in R_5$, then the trajectory will enter a two-pulse limit cycle, but if z_2 lies in R_3 it might not enter a two-pulse limit cycle (although it might do so). We may determine all possible locations of z_2 by calculating $F_4(B_4)$. z_2 must lie at y_o, between $F(R_6)$ and $F_4(B_4)$.

y_1 is (y_o-1), so B_4 may be represented by

$$B_4 = \left\{ z = (x,y) : x = 1 + \ell - \ell y_o + \left(\frac{1+\gamma}{2}\right)^{1/2} \ell\sqrt{1-y_o} \right\} \quad (5.1)$$

so that $F_4(B_4)$ is

$$F_4(B_4) = \left\{ z = (x,y_o) : x = \ell - 1 - \ell y_o - \sqrt{2}\,\ell \left(\frac{1+\gamma}{2}\right)^{1/2} \sqrt{1-y_o} \right\} \quad (5.2)$$

It is of interest to note that the intersection of $F_4(B_4)$ with B_2 occurs for $y = \gamma/(1+\gamma)$. These curves are shown schematically in Fig. 31, which is not drawn to scale.

From Fig. 31 it is clear that if $\gamma = 2$ the lower boundary of the strip containing z_o is at the same y level as the point of intersection of B_2 and $F_4(B_4)$. z_2 then lies in R_5, and we have a stable two-pulse limit cycle. If $\gamma < 2$, then the intersection point lies <u>below</u> the level of the least y_o, so again z_2 will definitely be in R_5. If $2 < \gamma < 3$, we need to show that z_2 lies in R_5, although it is fairly obvious from Fig. 31 that it does lie there. All possible points z_1 for the case under consideration here are the elements of the set defined as

$$z_1 = \left\{ z = (x,y) : x = 1 - \ell y - \ell + \left(\frac{1+\gamma}{2}\right)^{1/2} \ell\sqrt{y+1}\ ; \right.$$
$$\left. -\left(\frac{1}{2} - \frac{\sqrt{\gamma}}{1+\gamma}\right) > y > -\frac{\gamma-1}{\gamma+1} \right\} \quad (5.3)$$

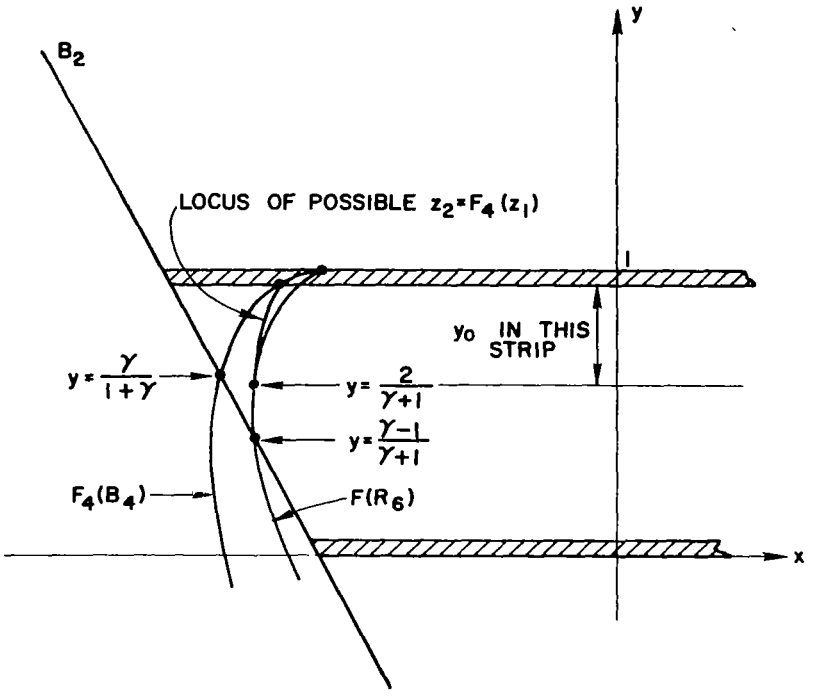

Fig. 31. INTERSECTION OF $F(R_6)$ AND $F_4(B_4)$ WITH B_2.

$z_2 = F_4(z_1)$, so all possible points z_2 are the elements of the set

$$z_2 = \left\{ z = (x,y) \;:\; x = \ell - \ell y - 1 - \ell\sqrt{1 + \frac{1+\gamma}{2} - 2\left(\frac{1+\gamma}{2}\right)^{1/2}\sqrt{y}}\;; \right.$$

$$\left. \left(\frac{1}{2} + \frac{\sqrt{\gamma}}{1+\gamma}\right) < y < \frac{2}{\gamma+1} \right\} \qquad (5.4)$$

We need simply to consider the difference between the x coordinate of z_2 and that of B_2, which is $x = -1 - \ell y$ for $2 < \gamma < 3$ and for y_o, in the strip of interest. This difference is

$$x_2 - x_B = \ell \left[1 - \sqrt{1 + \frac{1+\gamma}{2} - 2\left(\frac{1+\gamma}{2}\right)^{1/2}\sqrt{y}} \right] \tag{5.5}$$

which is positive for y and γ in the ranges of interest. This proves $z_2 \in R_5$, and the trajectory enters a two-pulse limit cycle oscillation.

One may then conclude that for $1 < \gamma \leq 3$ all the trajectories starting from z_o points in R_5, between the narrow strips shown in Fig. 31, will converge to stable two-pulse limit cycles. Those trajectories starting from any point within the strips will not converge to two-pulse limit cycles. We may now plot a boundary in the (γ, y_o) plane showing the demarcation between the two-pulse and non-two-pulse (known experimentally to be four-pulse) zones. This is done, not to scale, in Fig. 32. The equation for the left-hand branch of this boundary is

$$y = \frac{1}{2} - \frac{\sqrt{\gamma}}{1+\gamma} \tag{5.6}$$

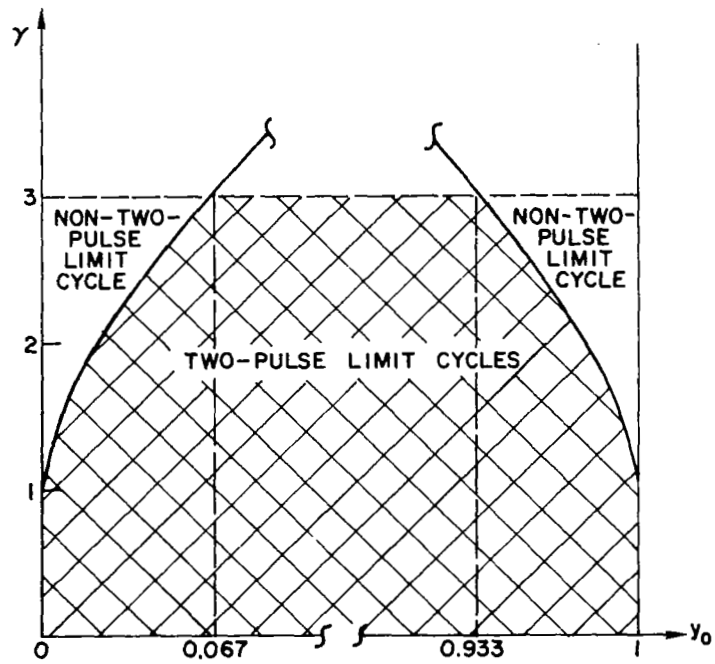

Fig. 32. $\gamma - y_o$ PLANE FOR $\gamma < 3$.

C. The Case $3 < \gamma < 5.8285$

An accurate plot of the significant curves in the region of the origin, for $\gamma = 5$ and $\ell = 0.5$, appears in Fig. 33. This is representative of the situation for γ lying in the range $3 < \gamma < 5.8285$. (The significance of this odd number is disclosed at the end of this section.) Consider first trajectories starting from initial states z_o, lying in the two shaded strips shown in Fig. 33. These are defined by the ranges

$$1 > y > \frac{1}{2} + \frac{\sqrt{\gamma}}{1+\gamma} \qquad \text{(UPPER STRIP)}$$

$$\frac{1}{2} - \frac{\sqrt{\gamma}}{1+\gamma} > y > 0 \qquad \text{(LOWER STRIP)} \tag{5.7}$$

and are the same as the strips shown in Fig. 31; the only difference being that they are a little wider because γ is larger. For $z_o \in$ (UPPER STRIP), z_1 will lie on $F(R_5)$ but in R_1; hence the trajectory cannot converge to a two-pulse limit cycle for the reasons described in

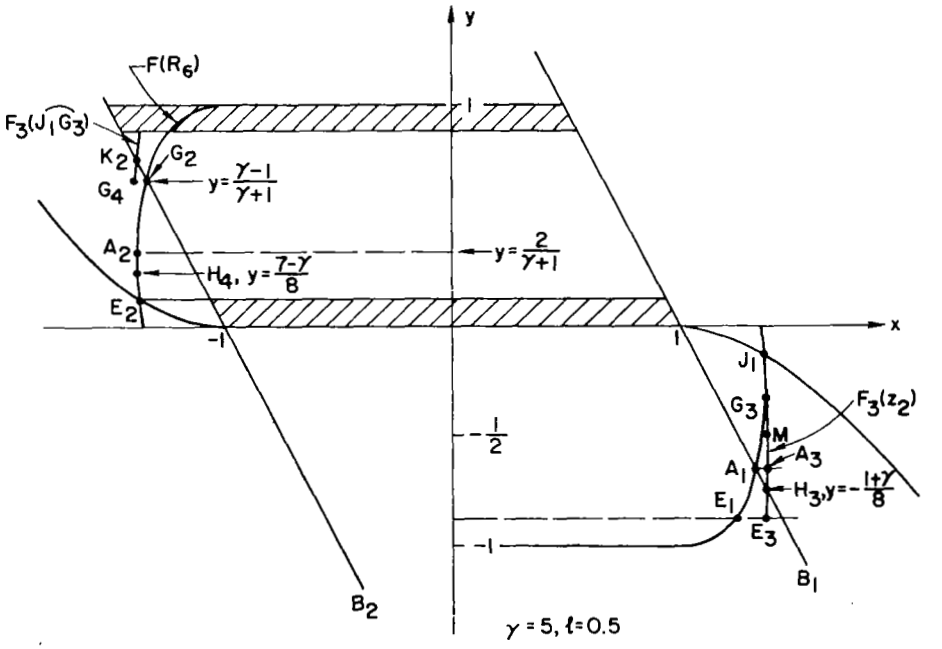

Fig. 33. REGION NEAR THE ORIGIN FOR $\gamma = 5$, $\ell = 0.5$.

Section V.B. Similarly if $z_o \in$ (LOWER STRIP), the trajectory cannot converge to a two-pulse limit cycle.

Consider next initial states z_o, lying in the strip, just above the lower shaded strip, defined by the range

$$\frac{1}{2} - \frac{\sqrt{\gamma}}{1+\gamma} < y < \frac{2}{\gamma+1} \tag{5.8}$$

From points in this strip, $z_1 = F_5(z_o)$ will lie on $F(R_5)$ in R_6, and between the points A_1 and E_1 in Fig. 33. $z_2 = F_6(z_1)$ will then lie on $F(R_6)$ somewhere between the points A_2 and E_2. Note that $z_2 \in R_3$, so now there is an element of doubt as to whether the trajectory will converge to a two-pulse limit cycle. The doubt may be resolved by calculating the positions of z_3, z_4, etc. z_3 is calculated simply as $F_3(z_2)$. For z_2, lying between A_2 and E_2, z_3 will lie on $F_3(z_2)$, between the points A_3 (which is at the same y level as A_1) and E_3; $F_3(z_2)$ itself will lie slightly to the right of $F(R_5)$. $F_3(z_2)$ is calculated as follows.

Let z_2 lie on $F(R_6)$, defined as the set

$$F(R_6) = \left\{ z = (x,y) : x = \ell - 1 - \ell y - \ell\left(\frac{1+\gamma}{2}\right)^{1/2}\sqrt{1-y} \; ; \; 0 < y < 1 \right\} \tag{5.9}$$

Thus, $z_3 = F_3(z_2)$ is calculated from the state transition equations (Table 2) as

$$z_3 = \left\{ z = (x,y) : x = 1 - \ell y - \ell + \ell\sqrt{1 + \frac{1+\gamma}{2} - 2\left(\frac{1+\gamma}{2}\right)^{1/2}\sqrt{-y}} \; ; \right.$$
$$\left. -\frac{2}{\gamma+1} > y > -\left(\frac{1}{2} + \frac{\sqrt{\gamma}}{1+\gamma}\right) \right\} \tag{5.10}$$

Note here that this expression is valid for z_3 lying between the points G_3 and E_3 although our attention at the moment if focused only on those points lying between A_3 and E_3. $F_3(z_2)$ intersects B_1 at point H_3, which has the y coordinate

$$H_3 \; : \; y = -\frac{1+\gamma}{8} \tag{5.11}$$

The points on $F_3(z_2)$, lying between E_3 and H_3, are in R_6. Therefore, they will map into the segment E_2H_4 in R_3, and the system will be in a two-pulse limit cycle, oscillating between a point in R_3 and one in R_6. Simulator experiments confirm this expectation, as is indicated in Table 6.

Table 6

TRAJECTORY FOR $\gamma = 5$, $x_o = 0$, $y_o = 0.2$

x(0) = 0.0000	y(0) = 0.2000	z(0) $\in R_5$
x(1) = 1.2873	y(1) = -0.8000	z(1) $\in R_6$
x(2) = -1.3746	y(2) = 0.2000	z(2) $\in R_3$
x(3) = 1.3748	y(3) = -0.8000	z(3) $\in R_6$
x(4) = -1.3746	y(4) = 0.2000	z(4) $\in R_3$
x(5) = 1.3748	y(5) = -0.8000	z(5) $\in R_6$
x(6) = -1.3746	y(6) = 0.2000	z(6) $\in R_3$

We have now accounted for all of the initial points in $R_5^+(0<y_o<1)$, lying below the level of H_4, whose y coordinate is $(7-\gamma)/8$, and those lying in the upper strip. Before proceeding with those points that remain, it is useful to observe the symmetry of this situation about the line $y = 1/2$.

Consider a point starting in the unshaded region above the level of G_2. This point will map onto $F(R_5)$ in R_4 between J_1 and G_3, which is similar to the segment E_2A_2 in R_3. Thus we can expect similar subsequent behavior from these points. The mapping $F_4(J_1G_3)$ will cross B_2 at a point K_2, similar to point H_3, at a level $y = (1+\gamma)/8$. Thus all points in R_5^+ above the level of K_2 will also produce trajectories that quickly enter two-pulse limit cycles similar to the one described in Table 6.

The remaining strip, centered in R_5^+ and lying between the levels of H_4 and K_2, may now be investigated by considering only half of them, say those below $y = 1/2$ but above the level of H_4. If these are represented by z_o, then z_3 lies on $F_3(z_2)$ between the points H_3 and M; M has a y coordinate of -1/2. A mapping of this segment is shown in Fig. 34 (which is not drawn to exact scale) where it

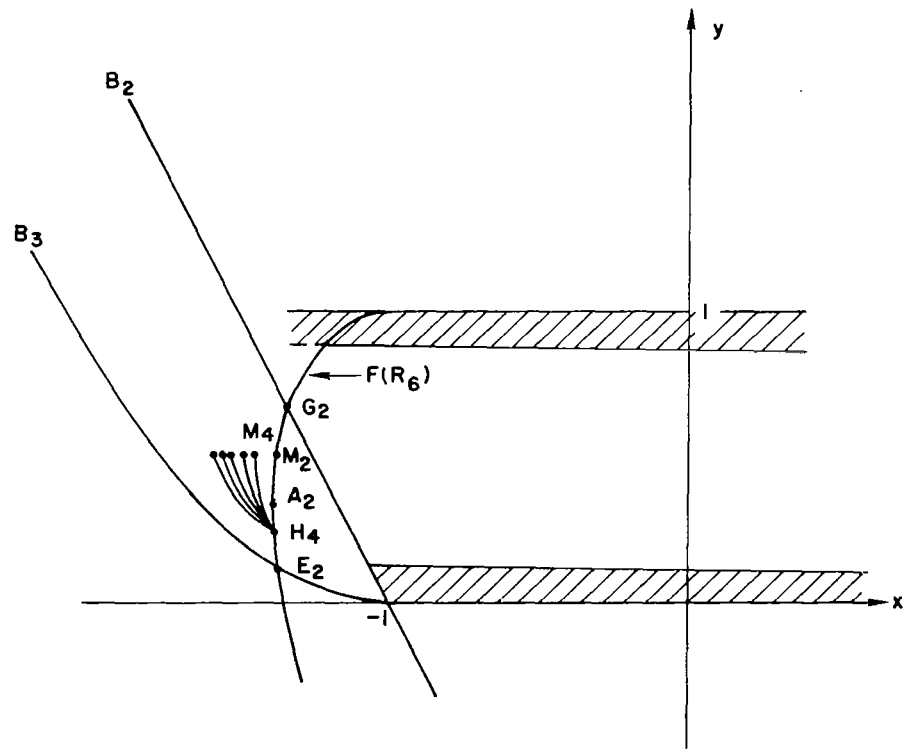

Fig. 34. SEQUENCE OF STATE TRANSITION MAPPINGS SUBSEQUENT TO $z_o \in R_5^+$.

is labelled H_4M_4. Now, H_4M_4 will map into R_4 onto a segment lying slightly to the right of H_3M, and this in turn will map into a segment in R_3 just to the left of H_4M_4. Subsequent mappings will lie on segments anchored in H_4 but are increasing steadily to the left of H_4M_4. This sequence of segments is indicated in Fig. 34 by the fan-like structure emanating from H_4. This fan-shaped behavior is greatly exaggerated in the figure, as is evidenced by the trajectory calculation in Table 7 that traces the leftward migration of the point M_2. The increasing sequence of segments is seen to converge rapidly to a point that is rather close to M_2, and it enters a two-pulse limit cycle at $t = t_6$. A similar fan-like structure (not shown) is attached to H_3 and lies in R_4.

Table 7

TRAJECTORY FOR $\gamma = 5$, $x_o = 0$, $y_o = 0.5$

x(0) = 0.00000	y(0) = 0.5	z(0) $\in R_5$
x(1) = 1.36237	y(1) = -0.5	z(1) $\in R_4$
x(2) = -1.37260	y(2) = 0.5	z(2) $\in R_3$
x(3) = 1.37452	y(3) = -0.5	z(3) $\in R_4$
x(4) = -1.37490	y(4) = 0.5	z(4) $\in R_3$
x(5) = 1.37498	y(5) = -0.5	z(5) $\in R_4$
x(6) = -1.37500	y(6) = 0.5	z(6) $\in R_3$
x(7) = 1.37500	y(7) = -0.5	z(7) $\in R_4$
x(8) = -1.37500	y(8) = 0.5	z(8) $\in R_3$
.	.	.
.	.	.
.	.	.
x(50) = -1.37500	y(50) = 0.5	z(50) $\in R_3$

It is of interest to obtain an analytical expression for the increasing sequence just described and to calculate the limit of the sequence. This is done by taking a point $z_o \in R_3$, mapping it into $z_1 \in R_4$, and in turn mapping into $z_2 \in R_3$. y_2 will be the same as y_o, so the sequence is simply the sequence of x coordinates x_o, x_2, x_4, ... It is convenient to look at the displacement of z_i from the boundary B_2 and to use the absolute value of that difference as the sequential variable. This difference is called Δx and is written as

$$\Delta x_k = -1 - \ell y - x_k \tag{5.12}$$

Application of the state transition equations to z_o and then to z_1 gives

$$\Delta x_2 = \sqrt{(\Delta x_o)^2 + \ell^2\left(1 + \frac{1+\gamma}{2}\right) - 2\ell\sqrt{(\Delta x_o)^2 + \ell^2\left(\frac{1+\gamma}{2}\right)y}} - \ell \tag{5.13}$$

If Δx is normalized with respect to the horizontal width of R_3 at the level y, and if the indexing is changed from $0,2,4,6,\ldots$ to $1,2,3,4,\ldots$ through the following definitions

$$M_1 = \frac{\Delta x_2}{\ell\left(\frac{1+\gamma}{2}\right)^{1/2}\sqrt{y}} \quad ; \quad M_o = \frac{\Delta x_o}{\ell\left(\frac{1+\gamma}{2}\right)^{1/2}\sqrt{y}} \tag{5.14}$$

then the sequence may be represented by the recursive formula relating M_{i+1} to M_i

$$M_{i+1} = \sqrt{M_i^2 - \left[\frac{8}{(1+\gamma)y}\right]^{1/2}\sqrt{M_i^2 + 1} + \frac{(3+\gamma)}{(1+\gamma)y}} - \left[\frac{2}{(1+\gamma)y}\right]^{1/2} \tag{5.15}$$

We note that ℓ has dropped out of the picture, and the properties of the sequence depend only on γ and y, each of which is constant for any

given trajectory. If a term M_j in the sequence should exceed 1, then the trajectory point z_{2j} will not lie in R_3, and the system will not go into a two-pulse limit cycle oscillation.

We can calculate the limit of the sequence (5.15) by setting $M_{i+1} = M_i$ and solving for $M = M_i$; this yields

$$M = \frac{1 + \gamma - 8y}{8\left(\frac{1+\gamma}{2}\right)^{1/2}\sqrt{y}} \tag{5.16}$$

If the data shown in Table 7 is used in (5.16), M turns out to be $1/(2\sqrt{6})$, $\ell\left[(1+\gamma)/2\right]^{1/2}\sqrt{y}$ is $\sqrt{6}/4$, so that the limit of Δx is 1/8. The sequence limit predicts an ultimate x coordinate in R_3 of $-1 - \ell y - 1/8 = -1.375$. This checks exactly with the observed values.

It is clear from (5.16) that for γ in the range $3 < \gamma \leq 5.8285$, and y in the strip bounded by the levels of H_4 and M_2, M will not exceed 1, so that every z_o outside the shaded strips but inside R_5^+ will generate trajectories which converge to two-pulse limit cycles. The boundary in the γ, y_o plane, started in Fig. 32, may now be extended up to $\gamma = 5.8285$, using formula (5.6).

We now turn our attention to the case $\gamma > 5.8285$ by noting first the origin of this odd number. In Fig. 33, which is drawn for $\gamma = 5$, it can be seen that if γ is increased, point A_1 will move downward and E_1 will move upward, and they will meet when their y coordinates are equal--that is, for that γ satisfying

$$\frac{1 - \gamma}{1 + \gamma} = -\left[\frac{\sqrt{\gamma}}{1 + \gamma} + \frac{1}{2}\right] \tag{5.17}$$

or, for $\gamma = 9$. Further, point H_3 will meet E_3, i.e., $F_3(z_2)$ will be completely outside of R_6 when the y coordinate of H_3 is the same as that of E_3

$$-\frac{1 + \gamma}{8} = -\left[\frac{\sqrt{\gamma}}{1 + \gamma} + \frac{1}{2}\right] \tag{5.18}$$

This equation is satisfied for $\gamma \cong 5.8285$.

The meeting of H_3 and E_3 produces a significant qualitative change in the behavior of the system, because with $F_3(z_2)$ detached from R_6, the fan-like structure shown in Fig. 34 loses its anchor point H_4, and the pattern of increasing segments produces a wave-like pattern in place of the fan-like pattern. We now turn to this interesting situation.

D. The Case $\gamma > 5.8285$

The region of the origin, for $\gamma = 7$, $\ell = 0.5$, is drawn accurately in Fig. 35. This example is representative of all the cases $\gamma > 5.8285$. Consider first the trajectories starting from z_o points, in the shaded strips adjacent to the lines $y = 0$ and $y = 1$. For z_o in the lower strip, z_1 will be in R_6, so that z_2 will lie on $F(R_6)$ but in R_2; hence, the trajectory cannot converge to a two-pulse limit cycle. For z_o in the upper strip, z_1 will lie on $F(R_5)$ but will be in R_1, so this trajectory too will suffer a fate similar to that of the one starting in the lower strip. Note that what happened to the first trajectory at $t = t_2$ is the same thing that happened to the second trajectory at $t = t_1$.

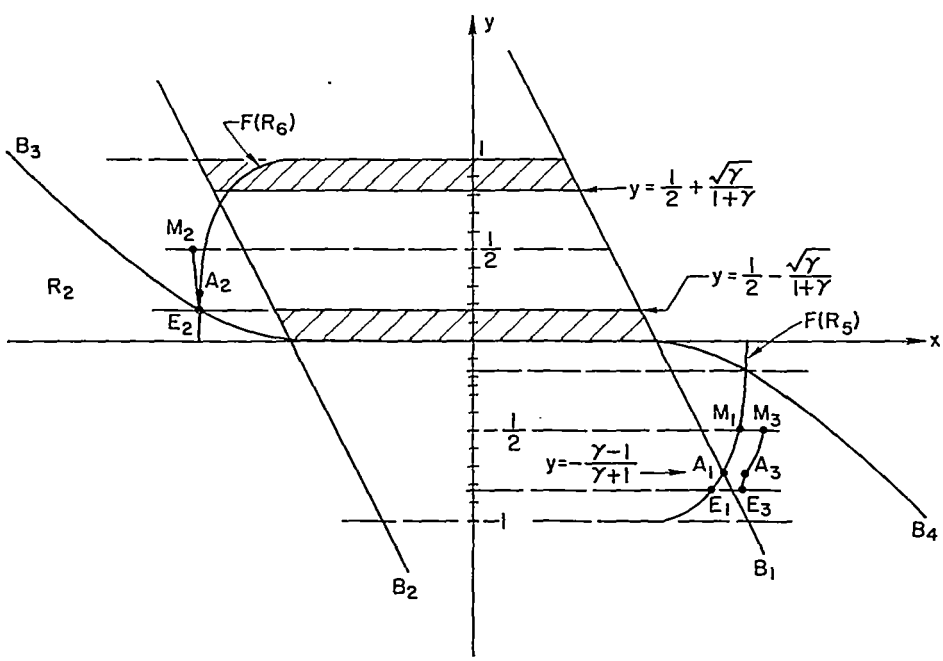

Fig. 35. REGION NEAR THE ORIGIN FOR $\gamma = 7$, $\ell = 0.5$.

given trajectory. If a term M_j in the sequence should exceed 1, then the trajectory point z_{2j} will not lie in R_3, and the system will not go into a two-pulse limit cycle oscillation.

We can calculate the limit of the sequence (5.15) by setting $M_{i+1} = M_i$ and solving for $M = M_i$; this yields

$$M = \frac{1 + \gamma - 8y}{8\left(\frac{1+\gamma}{2}\right)^{1/2}\sqrt{y}} \tag{5.16}$$

If the data shown in Table 7 is used in (5.16), M turns out to be $1/(2\sqrt{6})$, $\ell\left[(1+\gamma)/2\right]^{1/2}\sqrt{y}$ is $\sqrt{6}/4$, so that the limit of Δx is 1/8. The sequence limit predicts an ultimate x coordinate in R_3 of $-1 - \ell y - 1/8 = -1.375$. This checks exactly with the observed values.

It is clear from (5.16) that for γ in the range $3 < \gamma \leq 5.8285$, and y in the strip bounded by the levels of H_4 and M_2, M will not exceed 1, so that every z_o outside the shaded strips but inside R_5^+ will generate trajectories which converge to two-pulse limit cycles. The boundary in the γ, y_o plane, started in Fig. 32, may now be extended up to $\gamma = 5.8285$, using formula (5.6).

We now turn our attention to the case $\gamma > 5.8285$ by noting first the origin of this odd number. In Fig. 33, which is drawn for $\gamma = 5$, it can be seen that if γ is increased, point A_1 will move downward and E_1 will move upward, and they will meet when their y coordinates are equal--that is, for that γ satisfying

$$\frac{1 - \gamma}{1 + \gamma} = -\left[\frac{\sqrt{\gamma}}{1 + \gamma} + \frac{1}{2}\right] \tag{5.17}$$

or, for $\gamma = 9$. Further, point H_3 will meet E_3, i.e., $F_3(z_2)$ will be completely outside of R_6 when the y coordinate of H_3 is the same as that of E_3

$$-\frac{1 + \gamma}{8} = -\left[\frac{\sqrt{\gamma}}{1 + \gamma} + \frac{1}{2}\right] \tag{5.18}$$

This equation is satisfied for $\gamma \cong 5.8285$.

Consider next the trajectories starting from z_o, lying in R_5^+ between $1/2 < y < [1/2 - \sqrt{\gamma}/(1+\gamma)]$. z_1 then lies on $F(R_5)$ between the points E_1 and M_1. Therefore, z_2 will lie on a curve entirely in R_3, a portion of which (the mapping of segment E_1A_1) is coincident with $F(R_6)$, the remainder of it (the mapping of A_1M_1) lies to the left of $F(R_6)$. This is shown in Fig. 35.

The segment A_2M_2 is drawn out of scale for clarity. z_3 lies on the mapping $F_3(E_2M_2)$, and because γ is greater than 5.8285, this mapping, denoted as E_3M_3 in the figure, lies entirely within R_4. (E_3M_3 is also drawn out of scale.)

The behavior of the trajectory subsequent to $t = t_3$ may be studied from the qualitative sketch of the iterative mappings of E_3M_3 in the region near E_2. This region is shown in exaggerated scale in Fig. 36. Here E_4M_4 is the mapping of E_3M_3. Note that E_4M_4 intersects B_4 at a point I_4. Those state points z_4, lying on the segment E_4I_4, will not lead to a two-pulse limit cycle because they are in R_2; hence, they are eliminated from further consideration. I_4M_4 is mapped into R_4, on a segment (not shown) lying just to the right of E_3M_3, and

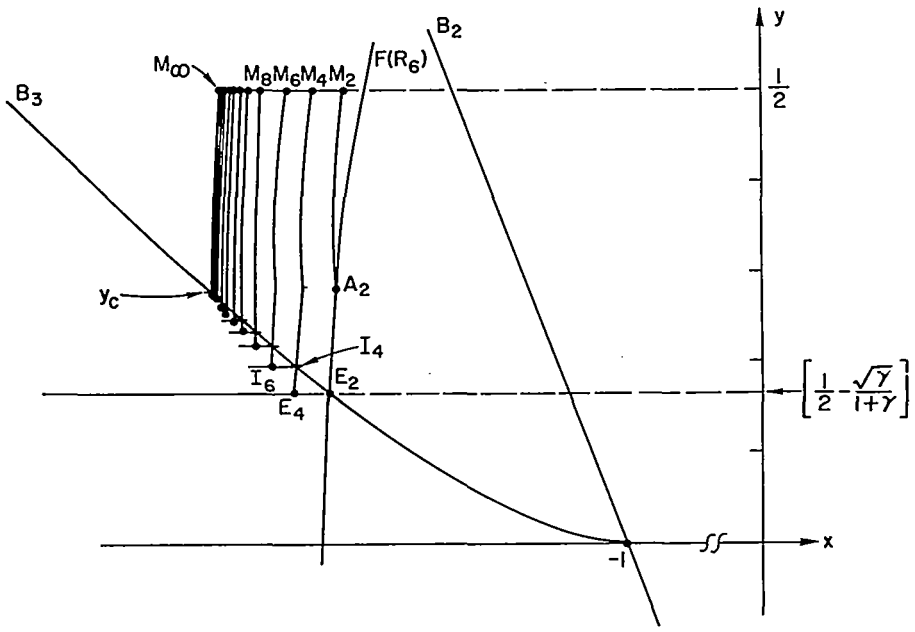

Fig. 36. SEQUENCE OF STATE TRANSITION MAPPINGS LEADING TO TWO-PULSE AND NON-TWO-PULSE OSCILLATIONS.

that segment is mapped again into I_6M_6. I_6M_6 must lie slightly to the left of I_4M_4, so that a small portion of it projects into R_2, and the points on this small portion are lost as candidates for states leading subsequently to two-pulse limit cycles. The sequence of mappings M_6, M_8, M_{10}, ... continues until it converges to the curve shown as $M_\infty y_c$ in Fig. 36. This sequence of mappings which resembles a "wave motion" may be described in terms of the recursive formula derived in Section V.C. The point y_c may be determined from this formula by setting $M_{i+1} = M_i = M_\infty = 1$. This yields

$$y_c = \frac{1 + \gamma}{8(3 + 2\sqrt{2})} \tag{5.19}$$

which is the formula separating the (γ, y_o) plane into two-pulse and non-two-pulse regions. A dramatic demonstration of the converging sequence of segments is given if two trajectories, each starting in R_5^+ at $t = 0$ but with slightly different y_o coordinates, one just slightly above y_c and the other just slightly below y_c, are calculated. This is done here for $\gamma = 16$. Equation (5.19) gives $y_c = 0.36459$ as the boundary separating the two-pulse and non-two-pulse regions. Simulation runs with $z_o = (0, 0.36460)$ and $z_o = (0, 0.36458)$ were made, and the results are shown in Tables 8 and 9. Note in Table 8 that the sequence converges on the 26th step to an x coordinate of -2.06250, and that in Table 9, on the 22nd step, the x coordinate is -2.06249, exactly the same as $x(22)$ in Table 8. This slight difference (0.00002) in the y coordinates of the two trajectories is enough to place $z(22)$ in R_3 on the first trajectory but in R_2 on the second! It is also interesting to note that the second trajectory, having entered R_2 for the first time at $t = t_{22}$, converges eventually to a four-pulse limit cycle at $t = t_{32}$.

The fate of trajectories starting in the upper half of R_5^+ is similar to those starting in the lower half of R_5^+, except, of course, they converge to different limit cycles.

We can now complete the portrait of the (γ, y_o) plane started in Fig. 37. The boundary separating the two-pulse limit cycle inital points

that segment is mapped again into I_6M_6. I_6M_6 must lie slightly to the left of I_4M_4, so that a small portion of it projects into R_2, and the points on this small portion are lost as candidates for states leading subsequently to two-pulse limit cycles. The sequence of mappings M_6, M_8, M_{10}, ... continues until it converges to the curve shown as $M_\infty y_c$ in Fig. 36. This sequence of mappings which resembles a "wave motion" may be described in terms of the recursive formula derived in Section V.C. The point y_c may be determined from this formula by setting $M_{i+1} = M_i = M_\infty = 1$. This yields

$$y_c = \frac{1 + \gamma}{8(3 + 2\sqrt{2})} \tag{5.19}$$

which is the formula separating the (γ, y_o) plane into two-pulse and non-two-pulse regions. A dramatic demonstration of the converging sequence of segments is given if two trajectories, each starting in R_5^+ at $t = 0$ but with slightly different y_o coordinates, one just slightly above y_c and the other just slightly below y_c, are calculated. This is done here for $\gamma = 16$. Equation (5.19) gives $y_c = 0.36459$ as the boundary separating the two-pulse and non-two-pulse regions. Simulation runs with $z_o = (0, 0.36460)$ and $z_o = (0, 0.36458)$ were made, and the results are shown in Tables 8 and 9. Note in Table 8 that the sequence converges on the 26th step to an x coordinate of -2.06250, and that in Table 9, on the 22nd step, the x coordinate is -2.06249, exactly the same as $x(22)$ in Table 8. This slight difference (0.00002) in the y coordinates of the two trajectories is enough to place $z(22)$ in R_3 on the first trajectory but in R_2 on the second! It is also interesting to note that the second trajectory, having entered R_2 for the first time at $t = t_{22}$, converges eventually to a four-pulse limit cycle at $t = t_{32}$.

The fate of trajectories starting in the upper half of R_5^+ is similar to those starting in the lower half of R_5^+, except, of course, they converge to different limit cycles.

We can now complete the portrait of the (γ, y_o) plane started in Fig. 37. The boundary separating the two-pulse limit cycle inital points

GAMMA(AMPLIFIER FIRING THRESHOLD)= 16.0000 L=0.5000

K= 0	X(K)= 0.00000	Y(K)= 0.36460	REGION= 5
K= 1	X(K)= 1.69791	Y(K)= -0.63540	REGION= 4
K= 2	X(K)= -1.90491	Y(K)= 0.36460	REGION= 3
K= 3	X(K)= 1.95653	Y(K)= -0.63540	REGION= 4
K= 4	X(K)= -2.00832	Y(K)= 0.36460	REGION= 3
K= 5	X(K)= 2.02480	Y(K)= -0.63540	REGION= 4
K= 6	X(K)= -2.04252	Y(K)= 0.36460	REGION= 3
K= 7	X(K)= 2.04845	Y(K)= -0.63540	REGION= 4
K= 8	X(K)= -2.05497	Y(K)= 0.36460	REGION= 3
K= 9	X(K)= 2.05719	Y(K)= -0.63540	REGION= 4
K= 10	X(K)= -2.05964	Y(K)= 0.36460	REGION= 3
K= 11	X(K)= 2.06048	Y(K)= -0.63540	REGION= 4
K= 12	X(K)= -2.06141	Y(K)= 0.36460	REGION= 3
K= 13	X(K)= 2.06173	Y(K)= -0.63540	REGION= 4
K= 14	X(K)= -2.06208	Y(K)= 0.36460	REGION= 3
K= 15	X(K)= 2.06220	Y(K)= -0.63540	REGION= 4
K= 16	X(K)= -2.06234	Y(K)= 0.36460	REGION= 3
K= 17	X(K)= 2.06238	Y(K)= -0.63540	REGION= 4
K= 18	X(K)= -2.06244	Y(K)= 0.36460	REGION= 3
K= 19	X(K)= 2.06245	Y(K)= -0.63540	REGION= 4
K= 20	X(K)= -2.06247	Y(K)= 0.36460	REGION= 3
K= 21	X(K)= 2.06248	Y(K)= -0.63540	REGION= 4
K= 22	X(K)= -2.06249	Y(K)= 0.36460	REGION= 3
K= 23	X(K)= 2.06249	Y(K)= -0.63540	REGION= 4
K= 24	X(K)= -2.06249	Y(K)= 0.36460	REGION= 3
K= 25	X(K)= 2.06249	Y(K)= -0.63540	REGION= 4
K= 26	X(K)= -2.06250	Y(K)= 0.36460	REGION= 3
K= 27	X(K)= 2.06250	Y(K)= -0.63540	REGION= 4
K= 28	X(K)= -2.06250	Y(K)= 0.36460	REGION= 3
K= 29	X(K)= 2.06250	Y(K)= -0.63540	REGION= 4
K= 30	X(K)= -2.06250	Y(K)= 0.36460	REGION= 3
K= 31	X(K)= 2.06250	Y(K)= -0.63540	REGION= 4
K= 32	X(K)= -2.06250	Y(K)= 0.36460	REGION= 3
K= 33	X(K)= 2.06250	Y(K)= -0.63540	REGION= 4
K= 34	X(K)= -2.06250	Y(K)= 0.36460	REGION= 3
K= 35	X(K)= 2.06250	Y(K)= -0.63540	REGION= 4
K= 36	X(K)= -2.06250	Y(K)= 0.36460	REGION= 3
K= 37	X(K)= 2.06250	Y(K)= -0.63540	REGION= 4
K= 38	X(K)= -2.06250	Y(K)= 0.36460	REGION= 3
K= 39	X(K)= 2.06250	Y(K)= -0.63540	REGION= 4
K= 40	X(K)= -2.06250	Y(K)= 0.36460	REGION= 3
K= 41	X(K)= 2.06250	Y(K)= -0.63540	REGION= 4
K= 42	X(K)= -2.06250	Y(K)= 0.36460	REGION= 3
K= 43	X(K)= 2.06250	Y(K)= -0.63540	REGION= 4
K= 44	X(K)= -2.06250	Y(K)= 0.36460	REGION= 3
K= 45	X(K)= 2.06250	Y(K)= -0.63540	REGION= 4
K= 46	X(K)= -2.06250	Y(K)= 0.36460	REGION= 3
K= 47	X(K)= 2.06250	Y(K)= -0.63540	REGION= 4
K= 48	X(K)= -2.06250	Y(K)= 0.36460	REGION= 3
K= 49	X(K)= 2.06250	Y(K)= -0.63540	REGION= 4
K= 50	X(K)= -2.06250	Y(K)= 0.36460	REGION= 3

Table 8

TRAJECTORY FOR $\gamma = 16$, $\ell = 0.5$, $x_o = 0$, $y_o = 0.36460$

GAMMA(AMPLIFIER FIRING THRESHOLD)= 16.0000 L=0.5000

K= 0	X(K)= 0.00000	Y(K)= 0.36458	REGION= 5
K= 1	X(K)= 1.69790	Y(K)= -0.63542	REGION= 4
K= 2	X(K)= -1.90491	Y(K)= 0.36458	REGION= 3
K= 3	X(K)= 1.95653	Y(K)= -0.63542	REGION= 4
K= 4	X(K)= -2.00832	Y(K)= 0.36458	REGION= 3
K= 5	X(K)= 2.02480	Y(K)= -0.63542	REGION= 4
K= 6	X(K)= -2.04252	Y(K)= 0.36458	REGION= 3
K= 7	X(K)= 2.04845	Y(K)= -0.63542	REGION= 4
K= 8	X(K)= -2.05497	Y(K)= 0.36458	REGION= 3
K= 9	X(K)= 2.05719	Y(K)= -0.63542	REGION= 4
K= 10	X(K)= -2.05964	Y(K)= 0.36458	REGION= 3
K= 11	X(K)= 2.06048	Y(K)= -0.63542	REGION= 4
K= 12	X(K)= -2.06141	Y(K)= 0.36458	REGION= 3
K= 13	X(K)= 2.06173	Y(K)= -0.63542	REGION= 4
K= 14	X(K)= -2.06208	Y(K)= 0.36458	REGION= 3
K= 15	X(K)= 2.06220	Y(K)= -0.63542	REGION= 4
K= 16	X(K)= -2.06234	Y(K)= 0.36458	REGION= 3
K= 17	X(K)= 2.06238	Y(K)= -0.63542	REGION= 4
K= 18	X(K)= -2.06244	Y(K)= 0.36458	REGION= 3
K= 19	X(K)= 2.06245	Y(K)= -0.63542	REGION= 4
K= 20	X(K)= -2.06247	Y(K)= 0.36458	REGION= 3
K= 21	X(K)= 2.06248	Y(K)= -0.63542	REGION= 4
K= 22	X(K)= -2.06249	Y(K)= 0.36458	REGION= 2
K= 23	X(K)= -1.18620	Y(K)= 1.36458	REGION= 5
K= 24	X(K)= 2.02057	Y(K)= 0.36458	REGION= 1
K= 25	X(K)= 2.30821	Y(K)= -0.63542	REGION= 4
K= 26	X(K)= -2.20917	Y(K)= 0.36458	REGION= 2
K= 27	X(K)= -1.71120	Y(K)= 1.36458	REGION= 3
K= 28	X(K)= 2.02081	Y(K)= 0.36458	REGION= 1
K= 29	X(K)= 2.30841	Y(K)= -0.63542	REGION= 4
K= 30	X(K)= -2.20930	Y(K)= 0.36458	REGION= 2
K= 31	X(K)= -1.71145	Y(K)= 1.36458	REGION= 3
K= 32	X(K)= 2.02082	Y(K)= 0.36458	REGION= 1
K= 33	X(K)= 2.30841	Y(K)= -0.63542	REGION= 4
K= 34	X(K)= -2.20930	Y(K)= 0.36458	REGION= 2
K= 35	X(K)= -1.71145	Y(K)= 1.36458	REGION= 3
K= 36	X(K)= 2.02082	Y(K)= 0.36458	REGION= 1
K= 37	X(K)= 2.30841	Y(K)= -0.63542	REGION= 4
K= 38	X(K)= -2.20930	Y(K)= 0.36458	REGION= 2
K= 39	X(K)= -1.71145	Y(K)= 1.36458	REGION= 3
K= 40	X(K)= 2.02082	Y(K)= 0.36458	REGION= 1
K= 41	X(K)= 2.30841	Y(K)= -0.63542	REGION= 4
K= 42	X(K)= -2.20930	Y(K)= 0.36458	REGION= 2
K= 43	X(K)= -1.71145	Y(K)= 1.36458	REGION= 3
K= 44	X(K)= 2.02082	Y(K)= 0.36458	REGION= 1
K= 45	X(K)= 2.30841	Y(K)= -0.63542	REGION= 4
K= 46	X(K)= -2.20930	Y(K)= 0.36458	REGION= 2
K= 47	X(K)= -1.71145	Y(K)= 1.36458	REGION= 3
K= 48	X(K)= 2.02082	Y(K)= 0.36458	REGION= 1
K= 49	X(K)= 2.30841	Y(K)= -0.63542	REGION= 4
K= 50	X(K)= -2.20930	Y(K)= 0.36458	REGION= 2

Table 9

TRAJECTORY FOR $\gamma = 16$, $\ell = 0.5$, $x_o = 0$, $y_o = 0.36458$

from the rest of the plane is given by (5.6) and (5.19) as

$$y_o = \frac{1}{2} - \frac{\sqrt{\gamma}}{1+\gamma} \qquad (1 < \gamma \leq 5.8258)$$

$$y_o = \frac{1+\gamma}{8(3+2\sqrt{2})} \qquad \begin{pmatrix} 5.8258 < \gamma \\ y_o \leq 0.5 \end{pmatrix} \tag{5.20}$$

These expressions give the boundary for $0 \leq y_o \leq 0.5$. The boundary itself is symmetrical about the $y_o = 0.5$ line, and so the complete curve is approximately that shown in Fig. 37.

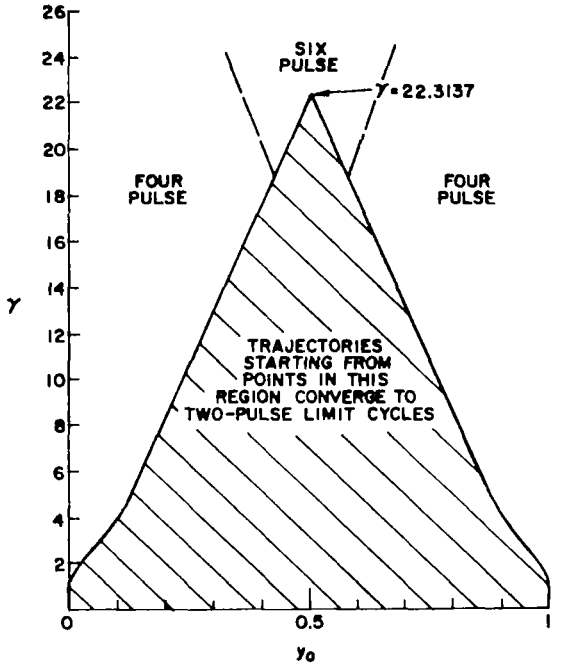

Fig. 37. $\gamma - y_o$ PLANE FOR $\gamma < 23$.

It is interesting to note that (5.20) implies that for $\gamma > 22.3137$ there can be no two-pulse limit cycles. This point was verified experimentally by running two trajectories, each starting at $y_o = 0.5$ but one for $\gamma = 22.31$ and the other for $\gamma = 22.32$. The results of these runs are listed in Tables 10 and 11. The trajectory for $\gamma = 22.31$ converges,

GAMMA(AMPLIFIER FIRING THRESHOLD)= 22.31 L=0.5000

K= 0	X(K)= 0.00000	Y(K)= 0.50000	REGION= 5
K= 1	X(K)= 1.95701	Y(K)= -0.50000	REGION= 4
K= 2	X(K)= -2.14883	Y(K)= 0.50000	REGION= 3
K= 3	X(K)= 2.25492	Y(K)= -0.50000	REGION= 4
K= 4	X(K)= -2.32058	Y(K)= 0.50000	REGION= 3
K= 5	X(K)= 2.36339	Y(K)= -0.50000	REGION= 4
K= 6	X(K)= -2.39210	Y(K)= 0.50000	REGION= 3
K= 7	X(K)= 2.41171	Y(K)= -0.50000	REGION= 4
K= 8	X(K)= -2.42524	Y(K)= 0.50000	REGION= 3
K= 9	X(K)= 2.43466	Y(K)= -0.50000	REGION= 4
K=10	X(K)= -2.44124	Y(K)= 0.50000	REGION= 3
K=11	X(K)= 2.44585	Y(K)= -0.50000	REGION= 4
K=12	X(K)= -2.44910	Y(K)= 0.50000	REGION= 3
K=13	X(K)= 2.45138	Y(K)= -0.50000	REGION= 4
K=14	X(K)= -2.45300	Y(K)= 0.50000	REGION= 3
K=15	X(K)= 2.45413	Y(K)= -0.50000	REGION= 4
K=16	X(K)= -2.45494	Y(K)= 0.50000	REGION= 3
K=17	X(K)= 2.45550	Y(K)= -0.50000	REGION= 4
K=18	X(K)= -2.45591	Y(K)= 0.50000	REGION= 3
K=19	X(K)= 2.45619	Y(K)= -0.50000	REGION= 4
K=20	X(K)= -2.45639	Y(K)= 0.50000	REGION= 3
K=21	X(K)= 2.45653	Y(K)= -0.50000	REGION= 4
K=22	X(K)= -2.45663	Y(K)= 0.50000	REGION= 3
K=23	X(K)= 2.45670	Y(K)= -0.50000	REGION= 4
K=24	X(K)= -2.45675	Y(K)= 0.50000	REGION= 3
K=25	X(K)= 2.45679	Y(K)= -0.50000	REGION= 4
K=26	X(K)= -2.45681	Y(K)= 0.50000	REGION= 3
K=27	X(K)= 2.45683	Y(K)= -0.50000	REGION= 4
K=28	X(K)= -2.45684	Y(K)= 0.50000	REGION= 3
K=29	X(K)= 2.45685	Y(K)= -0.50000	REGION= 4
K=30	X(K)= -2.45686	Y(K)= 0.50000	REGION= 3
K=31	X(K)= 2.45686	Y(K)= -0.50000	REGION= 4
K=32	X(K)= -2.45687	Y(K)= 0.50000	REGION= 3
K=33	X(K)= 2.45687	Y(K)= -0.50000	REGION= 4
K=34	X(K)= -2.45687	Y(K)= 0.50000	REGION= 3
K=35	X(K)= 2.45687	Y(K)= -0.50000	REGION= 4
K=36	X(K)= -2.45687	Y(K)= 0.50000	REGION= 3
K=37	X(K)= 2.45687	Y(K)= -0.50000	REGION= 4
K=38	X(K)= -2.45687	Y(K)= 0.50000	REGION= 3
K=39	X(K)= 2.45687	Y(K)= -0.50000	REGION= 4
K=40	X(K)= -2.45687	Y(K)= 0.50000	REGION= 3
K=41	X(K)= 2.45687	Y(K)= -0.50000	REGION= 4
K=42	X(K)= -2.45687	Y(K)= 0.50000	REGION= 3
K=43	X(K)= 2.45687	Y(K)= -0.50000	REGION= 4
K=44	X(K)= -2.45687	Y(K)= 0.50000	REGION= 3
K=45	X(K)= 2.45687	Y(K)= -0.50000	REGION= 4
K=46	X(K)= -2.45687	Y(K)= 0.50000	REGION= 3
K=47	X(K)= 2.45687	Y(K)= -0.50000	REGION= 4
K=48	X(K)= -2.45687	Y(K)= 0.50000	REGION= 3
K=49	X(K)= 2.45687	Y(K)= -0.50000	REGION= 4
K=50	X(K)= -2.45687	Y(K)= 0.50000	REGION= 3

Table 10

TRAJECTORY CONVERGING TO TWO-PULSE LIMIT CYCLE FOR $\gamma = 22.31$

GAMMA(AMPLIFIER FIRING THRESHOLD)= 22.32 L=0.5000

K= 0	X(K)= 0.00000	Y(K)= 0.50000	REGION= 5
K= 1	X(K)= 1.95727	Y(K)= -0.50000	REGION= 4
K= 2	X(K)= -2.14919	Y(K)= 0.50000	REGION= 3
K= 3	X(K)= 2.25534	Y(K)= -0.50000	REGION= 4
K= 4	X(K)= -2.32105	Y(K)= 0.50000	REGION= 3
K= 5	X(K)= 2.36389	Y(K)= -0.50000	REGION= 4
K= 6	X(K)= -2.39264	Y(K)= 0.50000	REGION= 3
K= 7	X(K)= 2.41226	Y(K)= -0.50000	REGION= 4
K= 8	X(K)= -2.42581	Y(K)= 0.50000	REGION= 3
K= 9	X(K)= 2.43524	Y(K)= -0.50000	REGION= 4
K=10	X(K)= -2.44183	Y(K)= 0.50000	REGION= 3
K=11	X(K)= 2.44646	Y(K)= -0.50000	REGION= 4
K=12	X(K)= -2.44971	Y(K)= 0.50000	REGION= 3
K=13	X(K)= 2.45200	Y(K)= -0.50000	REGION= 4
K=14	X(K)= -2.45361	Y(K)= 0.50000	REGION= 3
K=15	X(K)= 2.45475	Y(K)= -0.50000	REGION= 4
K=16	X(K)= -2.45556	Y(K)= 0.50000	REGION= 3
K=17	X(K)= 2.45613	Y(K)= -0.50000	REGION= 4
K=18	X(K)= -2.45653	Y(K)= 0.50000	REGION= 3
K=19	X(K)= 2.45681	Y(K)= -0.50000	REGION= 4
K=20	X(K)= -2.45701	Y(K)= 0.50000	REGION= 3
K=21	X(K)= 2.45716	Y(K)= -0.50000	REGION= 4
K=22	X(K)= -2.45726	Y(K)= 0.50000	REGION= 3
K=23	X(K)= 2.45733	Y(K)= -0.50000	REGION= 1
K=24	X(K)= 1.26172	Y(K)= -1.50000	REGION= 6
K=25	X(K)= -2.34105	Y(K)= -0.50000	REGION= 2
K=26	X(K)= -2.74723	Y(K)= 0.50000	REGION= 2
K=27	X(K)= -2.13556	Y(K)= 1.50000	REGION= 3
K=28	X(K)= 2.37630	Y(K)= 0.50000	REGION= 1
K=29	X(K)= 2.77543	Y(K)= -0.50000	REGION= 1
K=30	X(K)= 2.18243	Y(K)= -1.50000	REGION= 4
K=31	X(K)= -2.38530	Y(K)= -0.50000	REGION= 2
K=32	X(K)= -2.78266	Y(K)= 0.50000	REGION= 2
K=33	X(K)= -2.19421	Y(K)= 1.50000	REGION= 3
K=34	X(K)= 2.38771	Y(K)= 0.50000	REGION= 1
K=35	X(K)= 2.78460	Y(K)= -0.50000	REGION= 1
K=36	X(K)= 2.19737	Y(K)= -1.50000	REGION= 4
K=37	X(K)= -2.38837	Y(K)= -0.50000	REGION= 2
K=38	X(K)= -2.78513	Y(K)= 0.50000	REGION= 2
K=39	X(K)= -2.19822	Y(K)= 1.50000	REGION= 3
K=40	X(K)= 2.38855	Y(K)= 0.50000	REGION= 1
K=41	X(K)= 2.78528	Y(K)= -0.50000	REGION= 1
K=42	X(K)= 2.19846	Y(K)= -1.50000	REGION= 4
K=43	X(K)= -2.38860	Y(K)= -0.50000	REGION= 2
K=44	X(K)= -2.78532	Y(K)= 0.50000	REGION= 2
K=45	X(K)= -2.19852	Y(K)= 1.50000	REGION= 3
K=46	X(K)= 2.38861	Y(K)= 0.50000	REGION= 1
K=47	X(K)= 2.78533	Y(K)= -0.50000	REGION= 1
K=48	X(K)= 2.19854	Y(K)= -1.50000	REGION= 4
K=49	X(K)= -2.38862	Y(K)= -0.50000	REGION= 2
K=50	X(K)= -2.78533	Y(K)= 0.50000	REGION= 2

TRAJECTORY APPARENTLY CONVERGING TOWARD A SIX-PULSE LIMIT CYCLE FOR $\gamma = 22.32$

as expected, to a two-pulse limit cycle on the 32nd step. For $\gamma = 22.32$, the trajectory follows a path which appears to be close to one which converges to a two-pulse limit cycle, z_k jumping back and forth between R_3 and R_4, up to the 23rd step. At this point, z enters R_1, and the trajectory diverges away from a two-pulse limit cycle; it appears to be converging toward a six-pulse limit cycle at the end of the run.

It is also interesting to note that at the point where the two boundary sections meet ($\gamma = 5.8285$, $y \cong 0.14645$), (5.20) indicates that the slope of the boundary curve for $y_o = 0.14645^-$ [derived from the first equation of (5.20)] is the same as the slope for $y = 0.14645^+$ [derived from the second equation of (5.20)].

Numerous experimental runs were made to verify the boundary shown in Fig. 37, and these all indicated that (5.20) was valid to within the accuracy of the computer (five decimal places). Many other runs were made to determine the nature of the trajectory for starting points outside the two-pulse region. Four-pulse, six-pulse, eight-pulse, and ten-pulse limit cycle oscillations were observed. (The eight- and ten-pulse oscillations were observed only for extreme values of γ, in the range of 50 to 100.) Approximate boundaries between the two-pulse, four-pulse, and six-pulse regions were established and are shown in the dashed lines of Fig. 37.

It should further be noted that the studies described in this chapter, the results of which are essentially summarized in Fig. 37, are concerned solely with trajectories that start from points within the dead zone between the limits $-1 < y < 1$. (The γ, y_o portrait for $-1 < y_o < 0$ is the same as that in Fig. 37 because of the symmetry of the system.) Several experimental runs were made for initial points outside the dead zone; some of these converged to two-pulse limit cycles and some to four-pulse limit cycles. Further study of the convergence properties of such trajectories is suggested in Section E of Chapter VII.

Chapter VI

SUMMARY OF RESEARCH RESULTS

The principal result of the work described in the earlier chapters of this report has been the discovery of the geometrical properties of the state transition equations; and, these equations lead to the solution of the basic question regarding the existence, stability, and convergence properties of two-pulse limit cycles. This solution is summarized by the two conditions

$$\begin{aligned} \ell &> 0 \\ \gamma &\leq 1 \end{aligned} \tag{6.1}$$

described in Chapter IV. An equally important application of the geometrical properties of the state transition equations uncovered the intricate structure of the region near the origin of the state plane that exists for $\gamma > 1$ and that explain the fascinating dynamic behavior of the system as it diverges from the two-pulse limit cycle toward the higher order limit cycles. The necessary conditions for existence of two-pulse limit cycles are

$$\gamma < 8\left(3 + 2\sqrt{2}\right) y_o - 1 \qquad \left(y_o \leq \frac{1}{2}\right) \tag{6.2}$$

derived in Chapter V. These conditions are also typical of the practical information resulting from the application of this geometrical approach to analysis.

The describing-function-like approach used in Chapter II, to determine the necessary steady-state characteristics of the modulator, appears to be new--at least it is not a widely known technique and it yielded very useful results in this study.

Other information, produced by this work and not previously available, includes the state transition equations for the specific class of attitude control system with a dead-band element. Only equations for

the case $\theta_d = 0$ (no dead band) are available [2], as far as the author is aware. The computer program based on these equations (see Appendix) makes convenient experimental work possible on this system.

Other by-products of the principal results reported are some ideas for future research work. This work might yield a better understanding of some other practical problems associated with the design of attitude control systems. These suggestions for future work are listed and described briefly in the following chapter.

Chapter VII

FUTURE WORK

A. Different Modulators

The IPF modulator used in the system described here is only one of a class of modulators having the specific steady-state characteristics determined in Chapter II to be necessary for the existence of two-pulse limit cycles. Several other commonly used modulators, such as the increasingly important "derived rate" modulator [4,5], could probably be studied using the geometrical properties of the state transition equations for the systems in which they are used.

Modulators which produce unbalanced impulses, uniform for clockwise torques, and also uniform, but of different magnitude, for counterclockwise torques, might also be studied using this approach.

Modulators in which the threshold error γ is not constant but fluctuates randomly might produce important variations in the regular limit cycle behavior of attitude control systems. This work has shown that if γ is constant, two-pulse limit cycles will occur for γ anywhere in the range $-1 < \gamma \leq 1$. This result gives grounds for believing that γ could fluctuate by small amounts from time to time without upsetting the desired two-pulse limit cycle. If this is true, what are the limitations on the fluctuations which are allowed?

B. Torque Disturbances

If a small constant torque is applied to the satellite body by some external agent such as aerodynamic drag, radiation pressure, or gravity gradients, a "one-pulse" limit cycle oscillation is possible. The constant disturbance torque causes a small acceleration in one direction which must be countered occasionally by an impulse from the controller. It seems that the limit cycle oscillations of such a system could be studied by making modifications to the state transition equations derived here.

C. Different Controlled Bodies

The controlled body studied here is the simplest model of a rigid satellite. It is a second order system, and although the modulator itself is a first order system, it is a "degenerate" one. This allows the dynamic nature of the entire system to be represented by second order difference equations (see Chapter III). If some "damping" is added to the body, making its transfer function

$$\frac{\theta(s)}{M(s)} = \frac{1}{Js^2 + fs} \tag{7.1}$$

the whole system may still be represented by second order difference equations, which will be slightly more complex than those treated here. The trajectories will no longer be segments of horizontal lines and the limit cycle behavior might be different from that exhibited here, especially for large values of f.

Bodies which are not rigid will have transfer functions of an order higher than two. It seems unlikely that any significant dynamic properties of such a system could be determined from studies on the plane. If a geometrical approach were to be used, it would be a higher dimensional approach and therefore much more obscure if a graphical treatment were attempted. This indicates a more abstract approach, as discussed briefly in Section F below.

D. Sensor Noise

Attitude sensors always contain some noise on their output signals. For this reason rate circuits, in systems of the type studied here, have higher order transfer functions such as

$$\frac{e_N(s)}{e_s(s)} = \frac{1 + as}{(1 + Ts)^2} \tag{7.2}$$

where the time constant T is chosen to diminish the ill effects of the noise content of $e_N(t)$ as much as possible without seriously altering

the fidelity of the $Ka\dot{\theta}(t)$ term in $e_N(t)$. An exact analysis of the system containing a rate network with $T \neq 0$ would require a higher dimension state space. It might be possible to model the noise properties of the sensor by using the same system as that shown in Fig. 1 and adding an "equivalent noise" at the output of the simple lead circuit. This might lead to a detailed study similar to those which would result from allowing γ to fluctuate randomly with time, or from incorporating a disturbance torque into the system as suggested above.

E. Stability and Convergence Properties of Higher Order Limit Cycles

The work described in Chapter V establishes conditions under which two-pulse limit cycles will not occur, but it does not prove analytically what will happen to the system under those conditions. One expects, on intuitive grounds, that higher order limit cycles will occur, and many such oscillations were, in fact, observed from the computer experiments. However, it remains to be shown analytically, for example, what conditions must be met for a stable four-pulse limit cycle to exist, and what the convergence properties of that limit cycle are. The same questions can be asked about six-pulse, eight-pulse, etc. limit cycles. It seems these questions can be approached using the same techniques developed here for the two-pulse limit cycle. The computer simulation of the system can be very helpful, not only in verifying analytical results but also in discovering dynamic facts about the system which themselves suggest modifications and improvements in the analytical techniques used.

F. Abstract Studies

The geometrical properties of the second order state transition equations treated here suggest that higher order systems might be analyzed in a similar manner if topological methods of mathematics can be brought to bear on the higher order equations. A recently published book by O. Hajek [19] offers an excellent starting point for anyone who is interested in extending the work in this direction. Hajek introduces the topological notions in two-dimensional systems.

Aside from the purely intellectual excitement offered by such an abstract study, it might lead to some practical insight into how multiple

nonlinear feedbacks from the state variables could be used to drive multiple pulse-modulators, each providing an impulse input to the multivariable plant. It seems that it would be exceedingly difficult to obtain practical results from such an abstract analysis, but it also seems that many exceedingly efficient control systems, such as biological mechanisms, operate precisely in the manner described above. Therefore, the prize of such a research effort is worthy of the challenge.

REFERENCES

1. Forney, R. G., S. Z. Szirmay, and H. K. Bouvier. "Mariner 4 Manuever and Attitude Control." Aeron. and Astronaut., Oct 1965.

2. Farrenkopf, R. L., A. E. Sabroff, and P. C. Wheeler. "Integral Pulse Frequency On-Off Control." Guidance and Control--II, Academic Press, New York (1964).

3. Lange, B. "The Drag-Free Satellite." AIAA Journal 2, 9, pp. 1590-1606, Sep 1964.

4. Nicklas, J. C., and H. C. Vivan. "Derived-Rate Increment Stabilization: Its Application to the Attitude Control Problem." ASME Journal of Basic Engineering 84, 1, pp. 54-59, Mar 1962.

5. Scott, E. D. "Pseudo-Rate Sawtooth-Pulse Reset Control System Analysis and Design," Proc. of AIAA/JACC Guidance and Control Conference, pp. 208-214, Aug 1966.

6. Jones, R. W., and C. C. Li. "Integral Pulse Frequency Modulated Control Systems." Proc. of Second IFAC Congress. Butterworth and Co. (Publishers) Ltd., London (1963).

7. Clark, J. P. C., and E. Noges. "The Stability of Pulse Frequency Modulated Closed Loop Control Systems." Proc. of IEEE Convention Record, Part 6, 1966.

8. Hinson, J. L., and M. D. Sarles. "Nonlinear Pulse Modulation." IEEE Eleventh Annual East Coast Conference on Aerospace and Navigational Electronics (preprint volume), Baltimore, Md., Oct 1964.

9. Hinson, J. L., and M. D. Sarles. "Optimal Design of Several Jet Switching Techniques." IEEE Wescon Convention Record, Aug 1964.

10. Kuntsevich, V. M., and Y. N. Chekhovoi. "Stability of Control Systems with Double Modulation." Automation and Remote Control, Jul 1967.

11. LaSalle, J., and S. Lefchetz. Stability by Liapunov's Direct Method with Applications. Academic Press, New York (1961).

12. Alex, F. R. "A Study of Russian Feedback Control Theory." WADD Technical Report No. 61-32, 5, Part II, Feb 1961.

13. Cunningham, W. J. Nonlinear Analysis. McGraw-Hill Book Co., New York (1958).

14. Graham, D., and D. McRuer. Analysis of Nonlinear Control Systems. John Wiley and Sons, Inc., New York (1961).

15. Flügge-Lotz, I. Discontinuous and Optimal Control. McGraw-Hill Book Co., New York (1968).

16. Ragazzini, J. R., and G. F. Franklin. Sampled-Data Control Systems. McGraw-Hill Book Co., New York, (1958).

17. Monopoli, R. V., and B. K. Wylie. "Finite Pulse Width Models for Pulse Frequency Modulated Feedback Systems." Engineering Research Inst., University of Massachusetts. Project NGR-22-010-018. Report No. 5, Jun 1968.

18. Fitzgerald, J. F. "Frequency Domain Techniques for Pulse Modulated Feedback Systems." Engineering Research Inst., University of Massachusetts. Project NGR-22-010-018, Report No. 2, Jul 1967.

19. Hájek, O. Dynamical Systems in the Plane, Academic Press, New York (1968).

Appendix

DIGITAL SIMULATION

The digital computer program which constitutes the simulation of the attitude control system through the solution of the basic mapping function

$$z_{k+1} = F(z_k)$$

is listed here. Enough comments are included in the program to make it self-explanatory to anyone with some knowledge of Fortran programming. A master deck of cards, from which this program was printed, is on file with the author, and a copy deck may be obtained from him upon request to the Electrical Engineering Department, University of Washington, Seattle, Washington, 98105.

The input information for a trajectory calculation is simply (x_o, y_o) and the desired values for ℓ and γ. The program is set up so that a whole series of different trajectories, each for a different combination of (x_o, y_o), ℓ, and γ, may be computed on one run of the computer. The program copy shown here is the one used to obtain the data listed in Tables 8 and 9.

Included in this program, but not used in the work described in the earlier chapters, is the calculation of an expression

$$V_k = x_k^2 + Cx_k y_k + By_k^2$$

This is called a Lyapunov function, and values for the two constants B and C must be supplied to the computer. V(k) is printed out along with x(k) and y(k).

Also included here is a readout sheet illustrating the format in which the trajectories are listed. This one, for $x_o = 15$, $y_o = -0.1$ $\gamma = 1$, and $\ell = 0.5$, lists the data plotted in the smallest curve of Fig. 25. Note here that the two-pulse limit cycle is entered on step number 40.

```
$WATFOR        RUN=FREE                                                    5.
C R.N.CLARK LIMIT CYCLE OSCILLATION STUDY                                  6.
30     FORMAT)-1-,-GAMMA) AMPLIFIER FIRING THRESHOLD *=-,F8.4,6X,-L=-,     7.
     1       F6.4,5X,- LYAPUNOV CONSTANTS     C= -,F4.2,-    B= -,F4.2,/*  8.
31     FORMAT)- -,6X,-K=-,I3,4X,-X)K*=-,F11.5,4X,-Y)K*=-,F11.5,            9.
     15X,-REGION=-,I2,9X,-V=-,F10.3*                                       10.
32     FORMAT)-0-,-  THE SYSTEM IS AT REST IN THE DEAD ZONE)Y=0-,F8.4,     11.
     1-)X)-,F7.4,-*-*                                                      12.
       INTEGER REGION                                                      13.
       REAL   X)251*,Y)251*,V)251*                                         14.
       REAL L)1*/.5/                                                       15.
       REAL YY)2*/10.171,10.172/                                           16.
       REAL XX)1*/0.0/                                                     17.
       REAL GG)1*/7.0/                                                     18.
C*****BB AND C ARE THE LYAPUNOV CONSTANTS                                  19.
       BB=1.                                                               20.
       C=1.0                                                               21.
C*****A -DO LOOP- SHOULD REPLACE THE FOLLOWING STATEMENT WHEN              22.
C      THERE EXISTS MORE THAN ONE VALUE IN THE GG ARRAY.                   23.
       N=1                                                                 24.
C*****A -DO LOOP- SHOULD REPLACE THE FOLLOWING STATEMENT WHEN              25.
C      THERE EXISTS MORE THAN ONE VALUE IN THE L ARRAY.                    26.
       J=1                                                                 27.
       SQL=L)J**L)J**)1..GG)N**/2.0                                        28.
C*****THE FOLLOWING DO LOOP ITERATIONS SHOULD COINCIDE WITH                29.
C      NUMBER ON VALUES IN THE X AND/OR Y ARRAYS.                          30.
       DO 9999 KK=1,2                                                      31.
C*****IN THIS POSITION CONTROL STATEMENTS)IF* ARE PLACED TO                32.
C      MANIPULATE THE MANNER INWHICH X AND Y ARRAYS ARE RUN TOGETHER.      33.
                                                                           34.
C*****THE FOLLOWING DO LOOP CONTROLS THE NUMBER OF ITERATIONS              35.
C      MINUS ONE.                                                          35.1
       DO 1000 K=1,51                                                      36.
C*****THE FOLLOWING IF STATEMENTS CONTROL THE INITIAL VALUES               37.
C      OF X AND Y AT THE COMMENCEMENT OF EACH SERIES OF ITERATION.         38.
       IF)K .EQ. 1* Y)K*=YY)KK*                                            39.
       IF)K .EQ. 1* X)K*=XX)1*                                             40.
C NOW FIND X FOR EACH BOUNDARY                                             41.
                                                                           42.
       X1=1. - L)J**Y)K*                                                   43.
       X2=-1. -L)J**Y)K*                                                   44.
       IF)Y)K*.GT.0.0*X3=-)1.. L)J**Y)K*. L)J**SQRT))1..GG)N***Y)K*/2.**   45.
       IF)-Y)K*.GT.0.0*X4=1.-L)J**Y)K* . L)J**SQRT)-)1..GG)N***Y)K*/2.*    46.
                                                                           47.
C NOW WE JUMP TO THE BOUNDARY SET FOR Y=0,GT 0 + LT 0                      48.
       IF)Y)K* .GT. 0.0* GO TO 666                                         49.
       IF)Y)K* .LT. 0.0* GO TO 777                                         50.
       IF)Y)K* .EQ. 0.0* GO TO 888                                         51.
C NOW WE FIND THE REGION OF OCCUPATION                                     52.
666    IF)X)K* .GT. X1*REGION=1                                            53.
       IF)X)K* .LE. X1 .AND. X)K* .GE. X2*REGION=5                         54.
       IF)X)K* .LE. X2 .AND. X)K* .GE. X3*REGION=3                         55.
       IF)X)K* .LT. X3*REGION=2                                            56.
       GO TO 900                                                           57.
777    IF)X)K* .GT. X4*REGION=1                                            58.
       IF)X)K* .LE. X4 .AND. X)K* .GE. X1*REGION=4                         59.
```

PROGRAM STATEMENTS

```
      IF)X)K* .LE. X1 .AND. X)K* .GE. X2*REGION=6                        60.
      IF)X)K* .LT. X2*REGION=2                                           61.
      GO TO 900                                                          62.
                                                                         63.
888   IF)X)K* .GE. X1*REGION=1                                           64.
      IF)X)K* .GE. X1*GO TO 900                                          65.
                                                                         66.
      IF)X)K* .LE. X2*REGION=2                                           67.
      IF)X)K* .LE. X2*GO TO 900                                          68.
      WRITE)6,32*X2,X1                                                   69.
      GO TO 9999                                                         70.
900   CONTINUE                                                           71.
C KNOWING THE OCCUPIED REGION WE NOW FIND THE NEXT STEP                  72.
      IF)K .EQ. 1*WRITE)6,30*GG)N*,L)J*,C,BB                             73.
      IF)REGION .EQ. 1*GO TO 11                                          74.
      IF)REGION .EQ. 2*GO TO 22                                          75.
      IF)REGION .EQ. 3*GO TO 33                                          76.
      IF)REGION .EQ. 4*GO TO 44                                          77.
      IF)REGION .EQ. 5*GO TO 55                                          78.
      IF)REGION .EQ. 6*GO TO 66                                          79.
11    D=-1.                                                              80.
       ZZ=)X)K* .L)J**Y)K* .D***2 -D*SQL*Y)K*                            81.
       X)K.1*=-D*SQRT)ZZ*-D -L)J**Y)K*                                   82.
      GO TO 950                                                          83.
22    D=.1.0                                                             84.
       ZZ=)X)K* .L)J**Y)K* .D***2 -D*SQL*Y)K*                            85.
       X)K.1*=-D*SQRT)ZZ*-D -L)J**Y)K*                                   86.
      GO TO 950                                                          87.
33    D=-1.0                                                             88.
       ZZ=)X)K* .L)J**Y)K* -D***2 -D*SQL*Y)K*                            89.
       X)K.1*=-D*SQRT)ZZ*-D -L)J**Y)K*                                   90.
      GO TO 950                                                          91.
44    D=1.0                                                              92.
       ZZ=)X)K* .L)J**Y)K* -D***2 -D*SQL*Y)K*                            93.
       X)K.1*=-D*SQRT)ZZ*-D -L)J**Y)K*                                   94.
      GO TO 950                                                          95.
55    D=-1.0                                                             96.
      ZZ=-D*SQL*Y)K*                                                     97.
      X)K.1*=-D*SQRT)ZZ* -D -L)J**Y)K*                                   98.
      GO TO 950                                                          99.
66    D=.1.0                                                            100.
      ZZ=-D*SQL*Y)K*                                                    101.
      X)K.1*=-D*SQRT)ZZ* -D -L)J**Y)K*                                  102.
                                                                        103.
950   CONTINUE                                                          104.
      Y)K.1*=Y)K* . D                                                   105.
      V)K*=X)K***2 .C*X)K**Y)K* .BB*Y)K***2                             106.
      I=K-1                                                             107.
      WRITE)6,31*I,X)K*,Y)K*,REGION,V)K*                                108.
1000  CONTINUE                                                          109.
9999  CONTINUE                                                          110.
19999 CONTINUE                                                          111.
      RETURN                                                            112.
      END                                                               113.
$DATA                                                                   114.
$STOP                                                                   115.
```

PROGRAM STATEMENTS (cont)

GAMMA(AMPLIFIER FIRING THRESHOLD)= 1.0000 L=0.5000

K= 0	X(K)=	15.00000	Y(K)=	-0.10000	REGION= 1
K= 1	X(K)=	14.99910	Y(K)=	-1.10000	REGION= 1
K= 2	X(K)=	14.98887	Y(K)=	-2.10000	REGION= 1
K= 3	X(K)=	14.96856	Y(K)=	-3.10000	REGION= 1
K= 4	X(K)=	14.93732	Y(K)=	-4.10000	REGION= 1
K= 5	X(K)=	14.89413	Y(K)=	-5.10000	REGION= 1
K= 6	X(K)=	14.83779	Y(K)=	-6.10000	REGION= 1
K= 7	X(K)=	14.76687	Y(K)=	-7.10000	REGION= 1
K= 8	X(K)=	14.67963	Y(K)=	-8.10000	REGION= 1
K= 9	X(K)=	14.57391	Y(K)=	-9.10000	REGION= 1
K= 10	X(K)=	14.44696	Y(K)=	-10.09999	REGION= 1
K= 11	X(K)=	14.29524	Y(K)=	-11.09999	REGION= 1
K= 12	X(K)=	14.11397	Y(K)=	-12.09999	REGION= 1
K= 13	X(K)=	13.89651	Y(K)=	-13.09999	REGION= 1
K= 14	X(K)=	13.63302	Y(K)=	-14.09999	REGION= 1
K= 15	X(K)=	13.30786	Y(K)=	-15.09999	REGION= 1
K= 16	X(K)=	12.89307	Y(K)=	-16.09999	REGION= 1
K= 17	X(K)=	12.32783	Y(K)=	-17.09999	REGION= 1
K= 18	X(K)=	11.40509	Y(K)=	-18.09999	REGION= 4
K= 19	X(K)=	5.52784	Y(K)=	-17.09999	REGION= 2
K= 20	X(K)=	4.65792	Y(K)=	-16.09999	REGION= 2
K= 21	X(K)=	3.92797	Y(K)=	-15.09999	REGION= 2
K= 22	X(K)=	3.28656	Y(K)=	-14.09999	REGION= 2
K= 23	X(K)=	2.70910	Y(K)=	-13.09999	REGION= 2
K= 24	X(K)=	2.13166	Y(K)=	-12.09999	REGION= 2
K= 25	X(K)=	1.69555	Y(K)=	-11.09999	REGION= 2
K= 26	X(K)=	1.24502	Y(K)=	-10.09999	REGION= 2
K= 27	X(K)=	0.82619	Y(K)=	-9.09999	REGION= 2
K= 28	X(K)=	0.43646	Y(K)=	-8.09999	REGION= 2
K= 29	X(K)=	0.07417	Y(K)=	-7.09999	REGION= 2
K= 30	X(K)=	-0.26154	Y(K)=	-6.09999	REGION= 2
K= 31	X(K)=	-0.57072	Y(K)=	-5.09999	REGION= 2
K= 32	X(K)=	-0.85260	Y(K)=	-4.09999	REGION= 2
K= 33	X(K)=	-1.10520	Y(K)=	-3.09999	REGION= 2
K= 34	X(K)=	-1.32475	Y(K)=	-2.09999	REGION= 2
K= 35	X(K)=	-1.50400	Y(K)=	-1.09999	REGION= 2
K= 36	X(K)=	-1.62725	Y(K)=	-0.09999	REGION= 2
K= 37	X(K)=	-1.64546	Y(K)=	0.90001	REGION= 3
K= 38	X(K)=	1.06303	Y(K)=	-0.09999	REGION= 4
K= 39	X(K)=	-1.10865	Y(K)=	0.90001	REGION= 5
K= 40	X(K)=	1.02434	Y(K)=	-0.09999	REGION= 6
K= 41	X(K)=	-1.10811	Y(K)=	0.90001	REGION= 5
K= 42	X(K)=	1.02434	Y(K)=	-0.09999	REGION= 6
K= 43	X(K)=	-1.10811	Y(K)=	0.90001	REGION= 5
K= 44	X(K)=	1.02434	Y(K)=	-0.09999	REGION= 6
K= 45	X(K)=	-1.10811	Y(K)=	0.90001	REGION= 5
K= 46	X(K)=	1.02434	Y(K)=	-0.09999	REGION= 6
K= 47	X(K)=	-1.10811	Y(K)=	0.90001	REGION= 5
K= 48	X(K)=	1.02434	Y(K)=	-0.09999	REGION= 6
K= 49	X(K)=	-1.10811	Y(K)=	0.90001	REGION= 5
K= 50	X(K)=	1.02434	Y(K)=	-0.09999	REGION= 6
K= 51	X(K)=	-1.10811	Y(K)=	0.90001	REGION= 5
K= 52	X(K)=	1.02434	Y(K)=	-0.09999	REGION= 6
K= 53	X(K)=	-1.10811	Y(K)=	0.90001	REGION= 5
K= 54	X(K)=	1.02434	Y(K)=	-0.09999	REGION= 6
K= 55	X(K)=	-1.10811	Y(K)=	0.90001	REGION= 5
K= 56	X(K)=	1.02434	Y(K)=	-0.09999	REGION= 6
K= 57	X(K)=	-1.10811	Y(K)=	0.90001	REGION= 5

TYPICAL READOUT DATA